BURNING RATE AND FLAME HEAT FLUX FOR PMMA IN THE CONE CALORIMETER

Brian T. Rhodes

University of Maryland
College Park, MD 20742

Notice

This report was prepared for the Building and Fire Research Laboratory of the National Institute of Standards and Technology under grant number 60NA2D1266. The statement and conclusions contained in this report are those of the authors and do not necessarily reflect the views of the National Institute of Standards and Technology or the Building and Fire Research Laboratory.

ABSTRACT

Title of Thesis:	Burning Rate and Flame Heat Flux for PMMA in the Cone Calorimeter
Degree candidate:	Brian T. Rhodes
Degree and Year:	Master of Science in Fire Protection Engineering, 1994
Thesis directed by:	Dr. James G. Quintiere, Professor, Department of Fire Protection Engineering, College of Engineering, University of Maryland at College Park

Ignition and burning rate data are developed for thick (25 mm.) black Polycast PMMA in a Cone Calorimeter heating assembly. The objective is to establish a testing protocol that will lead to the prediction of ignition and burning rate from Cone data. This is done for a thermoplastic like PMMA. For black PMMA, ignition temperatures of 250 to 350 °C and vaporization temperatures of approximately 325 to 380 °C were measured over irradiance levels of 15 to 65 kW/m². The incident flame heat flux, for irradiation levels of 0 to 75 kW/m², is found to be approximately 37 kW/m² for black PMMA. Its constancy is shown due to the geometry of the Cone flame. Also, this flame is shown to be nearly transparent for Cone irradiance (> 90%). The heat of gasification of the black PMMA used is found to be approximately 2.8 kJ/g; higher than other values reported for PMMA. This is believed to be due to differences in molecular structure or pigmentation effects and the types of PMMA tested. A burning rate model is demonstrated to yield good accuracy (> 80%) in comparison to measured transient values.

Keywords: burning rate, Cone Calorimeter, flame heat flux, PMMA

Burning Rate and Flame Heat Flux for PMMA in the Cone Calorimeter

by

Brian T. Rhodes

Thesis submitted to the Faculty of the Graduate School
of The University of Maryland in partial fulfillment
of the requirements for the degree of
Master of Science
May, 1994

Advisory Committee:

Dr. James G. Quintiere, Chairman/Advisor
Dr. James A. Milke
Dr. Frederick W. Mowrer

ACKNOWLEDGMENT

TABLE OF CONTENTS

LIST OF TABLES

LIST OF FIGURES

Zone models and other methods currently used to evaluate materials and products for their contribution toward fire growth and life safeties generate results using specified fire data. Therefore, the heat release rate, total energy, and flame spread characteristics of the fire must be known in order to accurately determine the effects of the fire on its surroundings and the hazard to occupants. In general, it is difficult to predict how a fire will grow and spread under realistic conditions. As a result, many of the current fire modeling methods utilize inadequate fire source information.

Given a particular fuel load configuration, it is desirable to describe the fire growth and spread rate in terms of measurable material properties. In order to do this, a general model for predicting the burning rate of materials is needed. Quintiere presents one such model [1]. Quintiere's model includes charring, vaporization, extinction, flame and heat conduction effects. It is one dimensional and assumes that vaporization occurs at a specified temperature in an infinitesimal plane. However, unsteady solutions for the burning rate were not determined. Steckler et al. [2] presents an analytical model for the one dimensional transient gasification of a non-charring thermoplastic material subjected to an external heat flux. However, their model considers only the non-flaming case in a nitrogen atmosphere. Quintiere and Iqbal [3] provide a model similar to that of Steckler et al. [2]. Their model consists of solving the one dimensional unsteady heat transfer equations during the pre-heating and gasification periods using an integral method. They assume a polynomial temperature profile within the solid which satisfies the heat transfer boundary conditions. However, their model considers only gasification of the thermoplastic and does not address the effects of the flame in its solution. Delichatsios et al. [4] and Chen, Delichatsios and Motevalli [5] present a similar approach consistent with the more complete formulation for charring materials developed by Quintiere [1]. They adopt the same governing equations, but their methodology employs two moments

of the energy equation with an assumed exponential temperature profile for a finite solid. As a result, two ordinary differential equations must be solved numerically rather than one ordinary differential equation and one algebraic equation resulting from an assumed polynomial temperature profile [3]. However, their solution comparisons with exact computations suggest that an integral method can give excellent accuracy for the burning rate problem.

Iqbal [6] extended the approach presented by Quintiere [1], but for non-charring thermoplastic materials. His model includes flame radiative and convective effects, transient heat conduction effects, turbulent and laminar burning. In Iqbal's model, the flame radiation to the pool surface is calculated from the experimental steady state mass loss rate results of Modak and Croce [7]. Modak and Croce investigated burning behavior of laminar and turbulent horizontal PMMA pool fires of varying sizes. They found flame radiation to be a dominant factor affecting the burning rate of horizontal pools, particularly for the turbulent fires. However, accurate methods to predict the flame radiation in such fires are not currently available. Knowledge of the flame heat flux is crucial to any attempts at developing methods to predict the burning rate of real materials.

The objective of the present research is to develop transient burning models from data derived from the Cone Calorimeter [8]. The models will be dependent on the class of materials; namely, thermoplastic, charring, dripping, and laminated. However, before a complex, inclusive model is formulated, the methodology for such a solution is tested by investigating simpler models. Initially, thermoplastics, thick enough not to be affected by their substrate and large enough to be considered approximately one-dimensional in behavior, are considered. Black Polycast PMMA (25 mm thick) is chosen as representative of this class and is used in the present study.

Mass loss data in addition to flame heat flux and surface temperature results have been measured for irradiances ranging from 0 to 75 kW/m^2 under a Cone Calorimeter heater assembly. Experimentally measured steady state mass loss rates are used to calculate the flame radiation to the PMMA surface. The steady state mass loss rate results

2

allow the extrapolation of an effective heat of gasification, L_g, for the PMMA. Transient burning rates are calculated using the derived material properties from the Cone heater experiments.

Ultimately, these burning rate models will be incorporated into fire growth simulations [e.g. 9, 10, 11, 12] to give more accurate predictions of hazard. The first step is to succeed, for at least thick thermoplastic and charring materials, in developing a viable strategy for using the Cone data for transient burning rate predictions.

Several studies are seeking to address this objective with modeling strategies that differ from that to be presented [2, 5, 13]. A very similar and successfully applied pyrolysis model for PMMA has been presented by Agrawal and Atreya [14]. The present approach is believed to be the simplest in form and the most reasonable to practically implement, without sacrificing phenomenological significance. The model is based on the integral formulation outlined by Quintiere [1], and implemented by Quintiere and Iqbal [3] for non-flaming pyrolysis of a thermoplastic.

2.1 Introduction

The Cone Calorimeter is a device widely used to measure the unit mass loss rate

$(\dot{m}'')$ and energy release rate $(\dot{Q}'')$ under a specified external radiative heat flux. The ratio

of these two quantities $(\dot{Q}''/\dot{m}'')$ gives the instantaneous heat of combustion (ΔH_c) relative

to the gaseous fuel produced during flaming combustion. During flaming combustion
this heat of combustion is approximately constant for the material. In the least, it can be
measured, and is expected to be scale independent, i.e. not change as a larger area of fuel
is burned. Also, except for multi-dimensional effects involving seams, joints, edges,
etc., the thermal and chemical properties of the decomposing material are also

independent of scale. In contrast, the heat flux $(\dot{q}'')$ to the material's surface depends on

fire scale or on test conditions as in the Cone Calorimeter. Hence, it follows that under
these one dimensional burning conditions,

$$\dot{m}'' = f(\dot{q}'', \text{thermo-chemical properties}) \qquad (2.1)$$

and, $$\dot{Q}'' = \dot{m}'' \Delta H_c. \qquad (2.2)$$

Equation (2.1) symbolically represents a model to predict the transient burning rate
involving the surface heat flux and needed properties. A specific model for a vaporizing,
non-charring thermoplastic-like material is examined. Experimentally, black PMMA is
considered.

2.2 Burning Rate Experiment

The purpose of these experiments was to measure the mass loss rate, flame heat flux, ignition time, and surface temperature for black PMMA. A cone heater apparatus (see Section 3.2) was used with a continuous mass loss measurement. The processes of ignition and burning rate were examined for imposed heat fluxes between 0 and 75 kW/m^2. In order to assess the total heat flux required by Eq. (2.1), both the external radiant heat flux and the flame heat flux were monitored. This was done with a small diameter (3 mm) water cooled heat flux gage. Measurements were conducted until steady burning. These measurements give two methods for determining the incident flame heat flux (convection plus radiation). The first is from the gage measurements directly; the second from steady burning in which Eq. (2.1) reverts to,

$$\dot{m}'' = \frac{\dot{q}''}{L} \qquad (2.3)$$

where, $\dot{q}''$ is the net surface heat flux,

and, L is the effective heat of gasification.

At steady burning, the incident flame heat flux is deduced from the net surface heat flux in Eq. (2.3). Results from both methods suggest that the total flame heat flux is approximately constant for PMMA burned in the Cone Calorimeter. The results of these measurements and analyses are discussed.

2.3 Flame Heat Transfer

Additional study was done to measure the flame heat flux and calculate the flame emission-absorption for the Cone Calorimeter assembly. In order to assess the effects of flame absorption on the external radiant flux imposed from the cone heater, two methods

are used. The first employs a simulated sample; the second calculates the flame emissivity using existing correlations. The simulated sample consisted of a glass bead burner matrix with a center slot for the heat flux meter. Methane was supplied at fixed rates in a standard horizontal cone mounting. The energy release rate of the methane was regulated to correspond to the energy release rates of the PMMA tested in the Cone. The net surface heat flux was measured using the heat flux gage from the PMMA experiments.

Analysis of both methods suggest that the flame is transparent (> 91%); therefore, approximately all of the external heat flux imposed by the Cone reaches the surface of the PMMA.

2.4 Application of Models

Experimental data are examined in conjunction with ignition and burning rate models designed to elucidate the needed thermochemical properties, i.e. the thermal conductivity, density, specific heat and heat of gasification. Although these properties are model dependent, they are not devoid of physical significance nor in extreme conflict with their more precisely derived counterparts. The derived properties are used to predict the transient burning rate of the PMMA under various external fluxes. Calculated results are found to be within 20 percent of the measured experimental burning rates. It is believed that the simplicity of these models will increase their potential utility and application to other materials.

The experimental and modeling details are discussed and their results presented in the following chapters. A recommended testing protocol for thermoplastics is presented in Chapter 6. Its usefulness will be assessed in the future by examining its applicability to other materials.

CHAPTER 3   EXPERIMENTAL APPARATUS AND PROCEDURE

3.1 Experimental System

Burning rate experiments were conducted using a cone heater apparatus consisting of a radiant cone heater, load cell, pilot igniter, and a data acquisition system. Figures 3.1 and 3.2 show the schematic layout of the cone heater apparatus. A photograph of the system is shown in Figure 3.3. A scanner and voltmeter were used to monitor the thermocouples, load cell and heat flux meters. A computer was used as the data acquisition system. The voltage measurements for temperatures, mass, and heat fluxes were converted to the appropriate metric units before the data was displayed and recorded. The program, written in HP Basic, is provided in Appendix A, although explanation of the program is not provided. As the data were being measured, they were transferred to a second computer, using a communication software, where it was recorded.

3.2 Burning Rate Apparatus

The mass loss of the PMMA was measured using a load cell. The load cell moved freely on the platform and was guided by steel bars secured to the platform in order to maintain proper alignment of the load cell under the cone. Removing the entire load cell from the Cone exposure prior to the test was necessary because a heat flux gage was located within the sample and was mounted to the load cell. Because of this configuration, the sample needed to be positioned on the load cell and the heat flux gage inserted prior to test.

Using the guidebars, the load cell could be slid into position once the sample and heat flux gage were properly mounted and the external irradiance became steady. Because sliding the entire load cell caused the sample to bounce slightly, fluctuations in the mass measurements are evident during the first couple of seconds. However, even at the
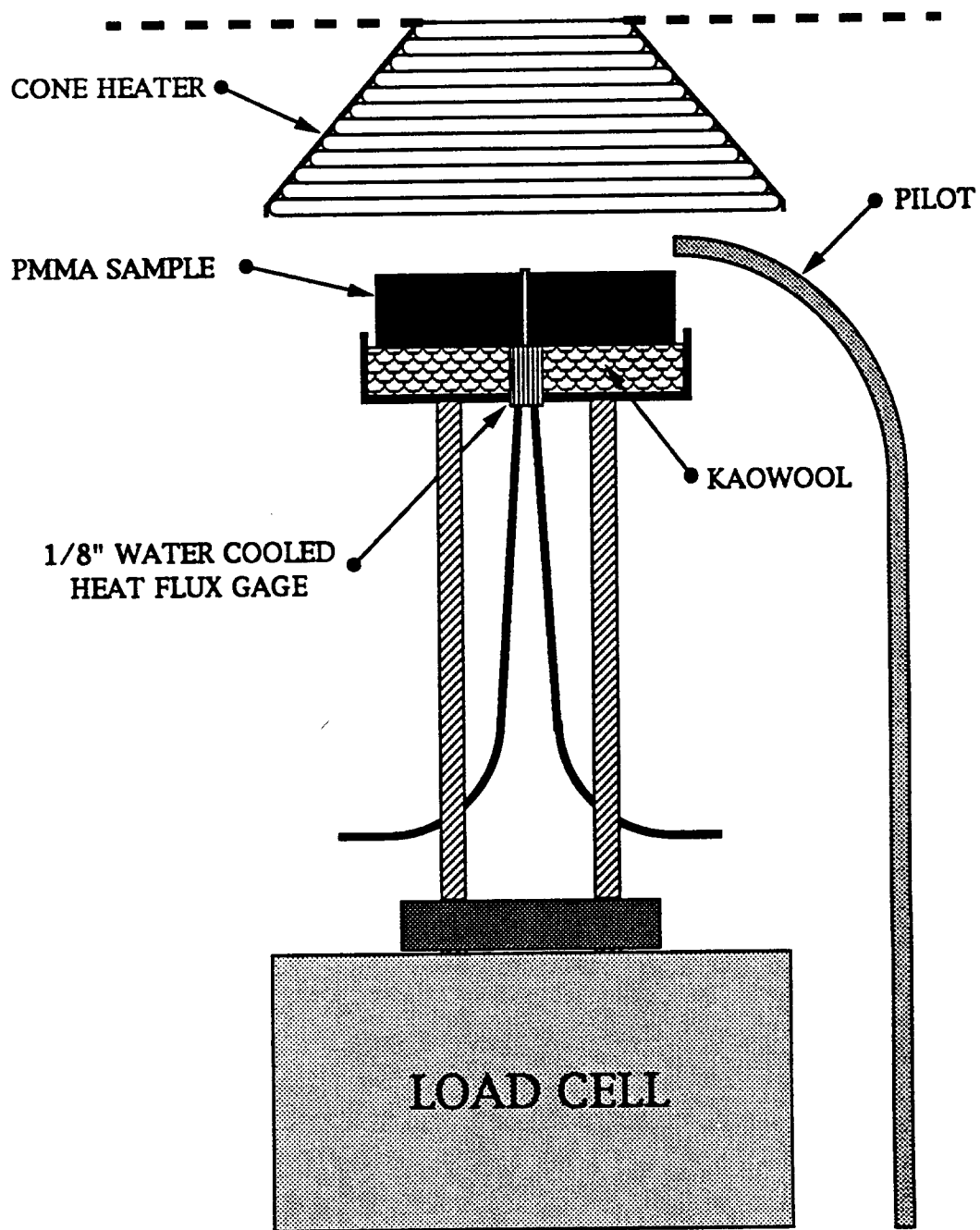
Figure 3.1. Schematic layout of burning rate apparatus

Labels in figure: CONE HEATER, PMMA SAMPLE, 1/8" WATER COOLED HEAT FLUX GAGE, PILOT, KAOWOOL, LOAD CELL
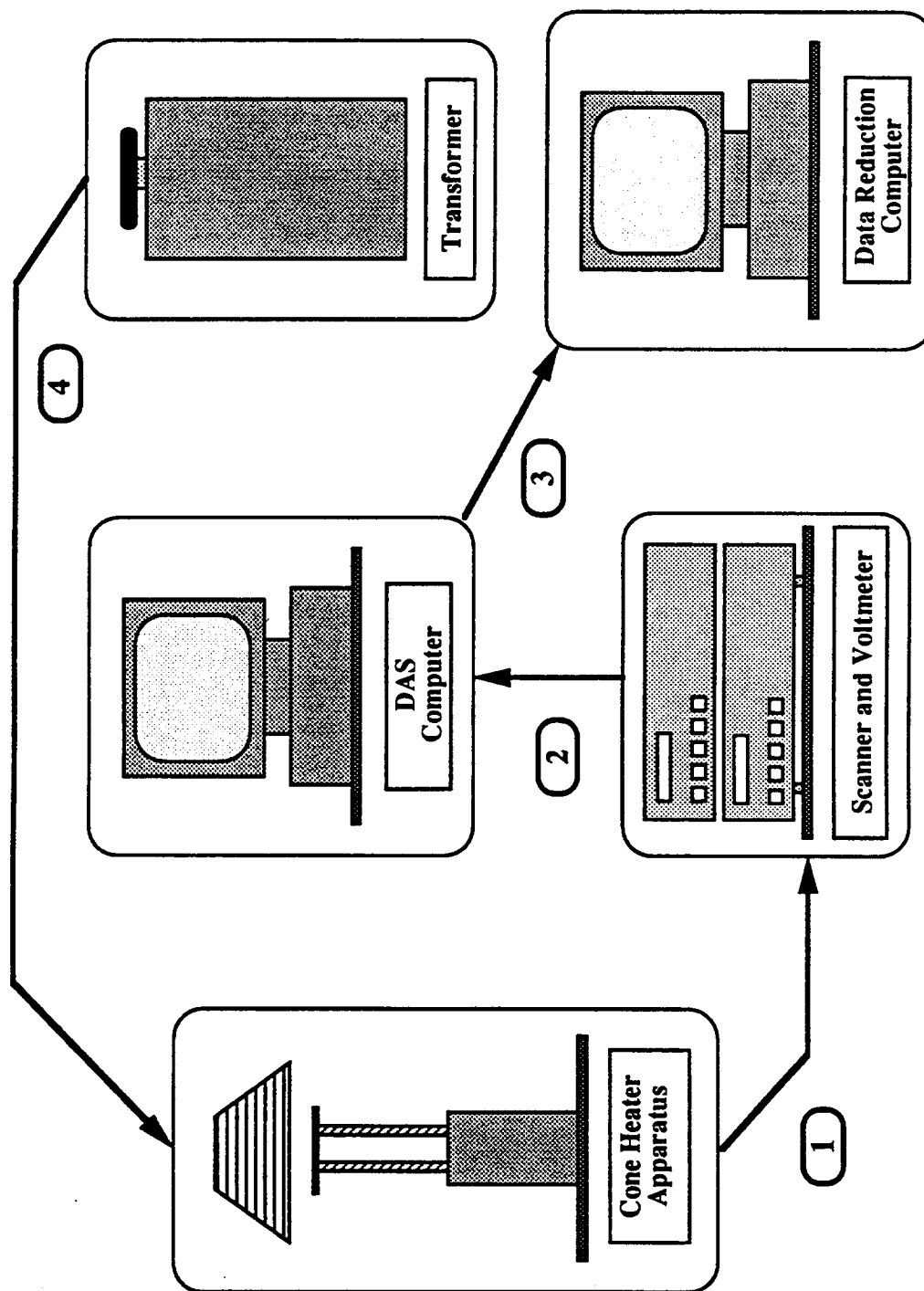
Figure 3.2. Schematic layout of experimental system

Transformer

Data Reduction Computer

DAS Computer

Scanner and Voltmeter

Cone Heater Apparatus

Figure 3.3. Experimental burning rate apparatus

highest fluxes (75 kW/m^2), ignition did not occur within the first ten seconds. Therefore no significant error in mass loss measurement resulted from the sliding of the load cell.

The temperature of the cone heater was measured by two thermocouples positioned within the coil. The temperatures were averaged in order to obtain a better estimate of the coil temperature. In order to maintain a constant incident heat flux ($\pm$ 2.5 kW/m^2) to the sample during the experiment, the temperature of the coil was kept steady ($\pm$ 5 °C). This was accomplished by manually varying the current to the coil using a 220 volt transformer. During the experiment, the average cone temperature was displayed on the screen every 2 seconds. As the temperature fluctuated due to flame impingement, the current to the coils were adjusted accordingly. A typical temperature variation of the coil is shown in Figure 3.4 for an incident flux of 46 kW/m^2.

In order to determine the initial incident heat flux to the sample, a Medtherm 1 inch thermopile type heat flux gage[1] was used. The heat flux gage was positioned such that it was the same distance below the center of the cone as would be the PMMA sample. Again, the incident heat flux was kept constant during the experiment by controlling the temperature of the cone.

A 1 inch methane flame was used as an ignition source for the PMMA. The pilot was located approximately 1/2 inch above the center edge of the PMMA. The configuration of the pilot is shown in Figure 3.1.

3.3   Flame Heat Flux
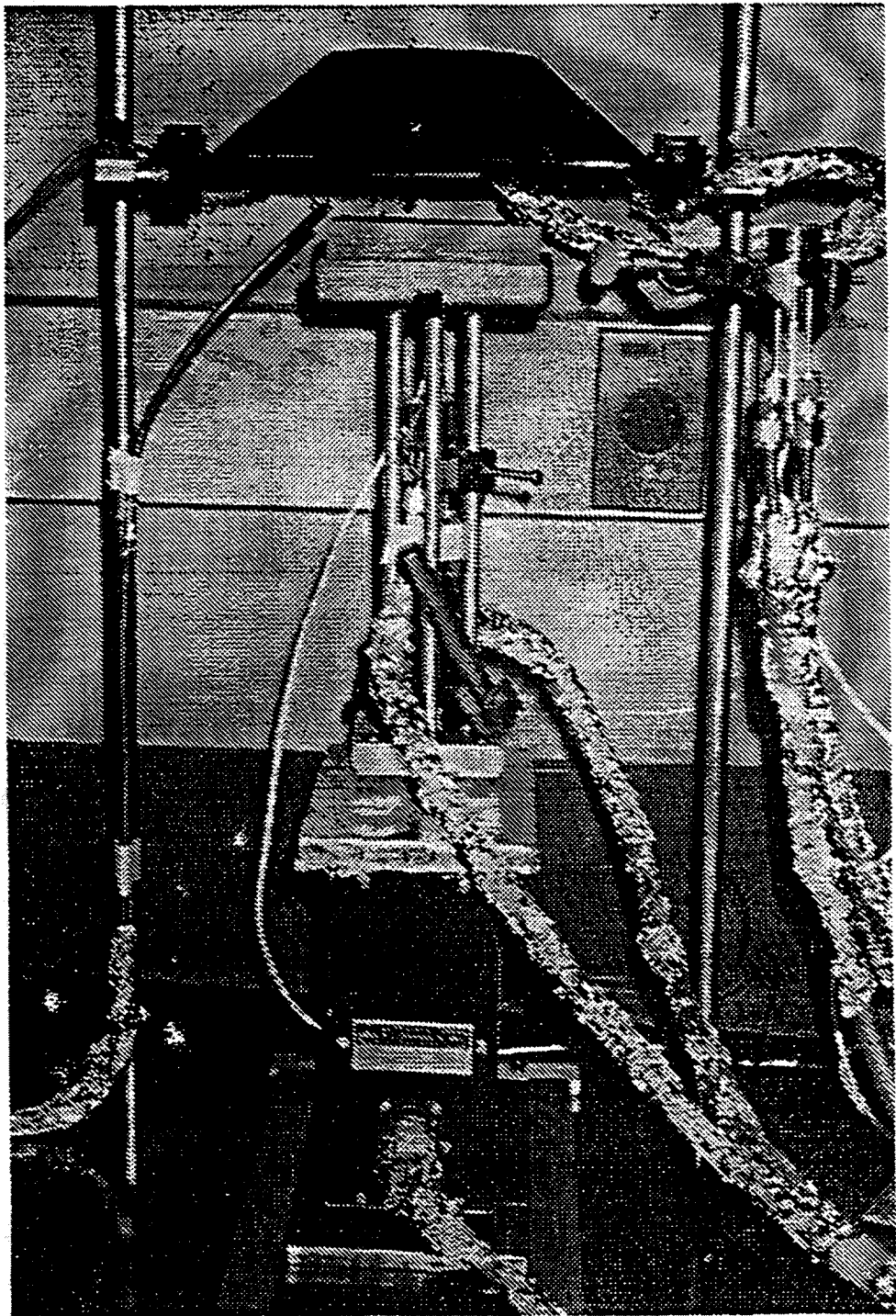
The flame plus external heat flux was measured during the experiment using a 1/8 inch Medtherm thermopile type heat flux gage[2] . The heat flux gage was initially cooled with water at room temperature. However, excessive condensation and re-evaporation of PMMA monomer occurred. It is believed that this gave positive and negative respective

---

[1] model number 64-5SB-20
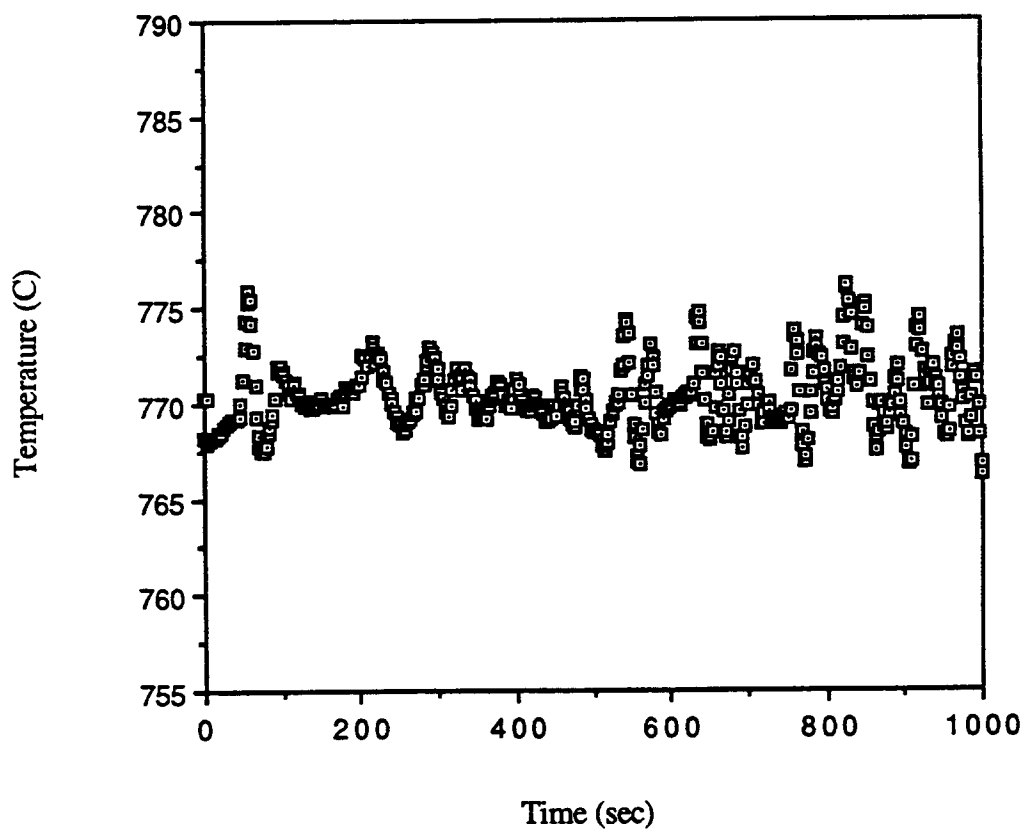[2] model number 8-1-10-4-0-36-20680K

Figure 3.4. Cone heater coil temperature variation for a 46 kW/m^2 irradiance

responses to the heat flux gage, independent of the incident heat flux. The temperature of the water was raised to 65 °C in order to increase the temperature of the heat flux gage high enough such that the vapors would not condensate on the sensor. This was done by circulating the water through a copper coil apparatus which was heated by a methane flame. Figure 3.5 shows the schematic layout of the water-coil heating system. However, 65 °C may not have been hot enough because some condensation and re-evaporation still occurred. It was found that insulating the gage on its sides during the experiments, using Kaowool, minimized extraneous results. In short, this measurement of heat flux was not easily accomplished. Therefore, the results presented are those from an analysis of data from tests where these effects were minimized. However, the experimental data for all of the PMMA tests are provided in Appendix B, C, D and F.

3.4 PMMA Sample

The sample was placed horizontally on a standard cone metal holder on a bed of Kaowool. Kaowool was used to insulate the back side of the sample to minimize heat loss. Black Polycast polymethylmethacrylate (PMMA) was chosen for these experiments because it burns evenly and does not char. Additionally, substantial work has previously been done using PMMA, therefore allowing a better comparison of the results. The black PMMA (100 mm x 100 mm x 25 mm thick) was constrained at the side edges by bonded cardboard. This enabled more uniform one-dimensional burning and eliminated side burning. The sample had a center hole that allowed freedom of movement between the heat flux gage and PMMA during continuous mass loss measurement of the sample. Although the heat flux gage did not move relative to the cone heater during the experiments, the PMMA expanded as it is heated and receded as the sample burned. The center hole was designed to minimize contact between the PMMA and the heat flux gage.

During some of the experiments, the surface temperature was measured using 0.003 inch type K thermocouples. The thermocouples were bonded to the PMMA surface using a soldering iron. The wires were melted into the PMMA such that the bead
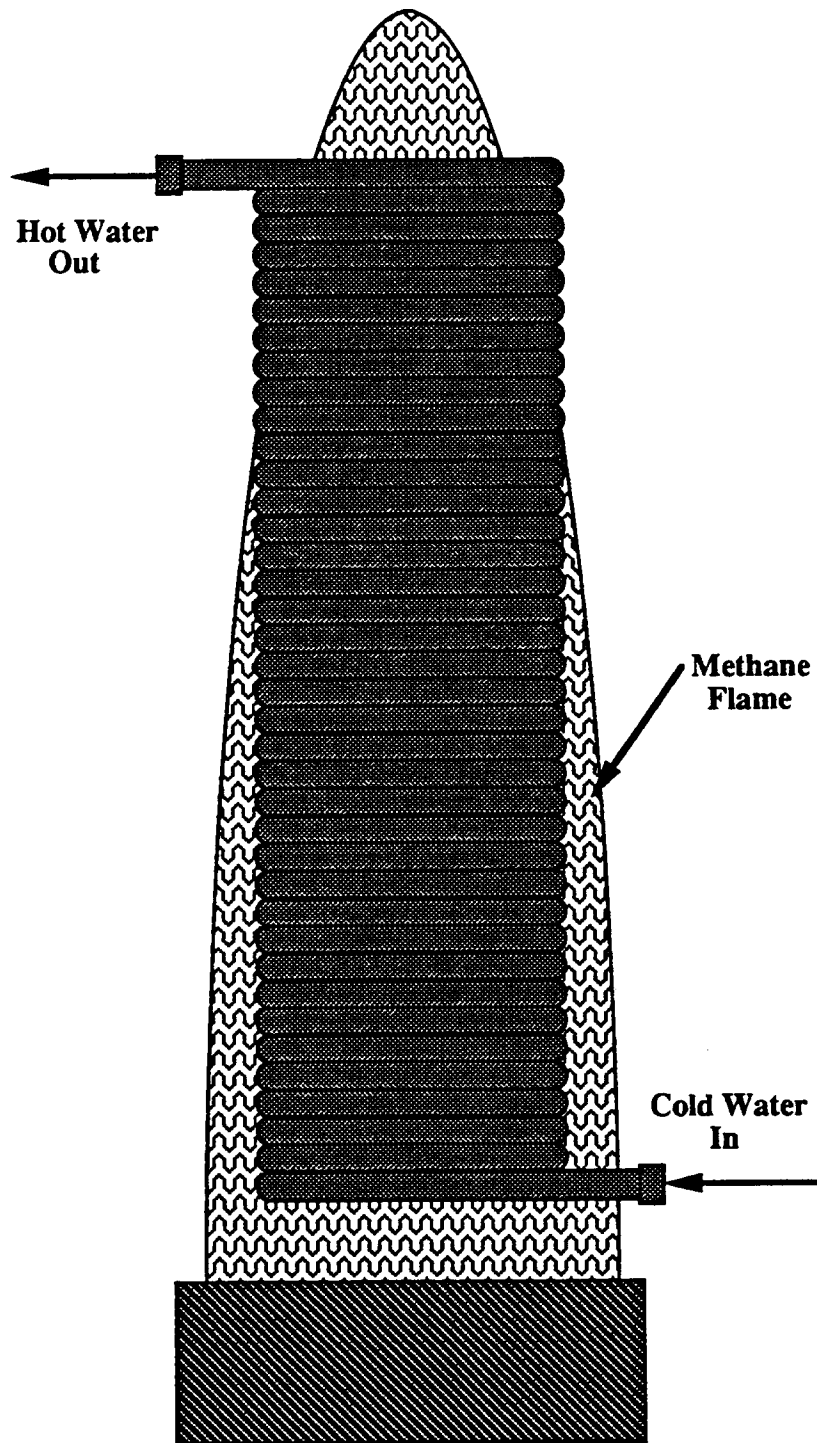
Hot Water Out

Methane Flame

Cold Water In

Figure 3.5. Water-coil heating system

of the thermocouple was flush with the PMMA surface. To minimize conduction losses in the wire, approximately 1/2 inch of the thermocouple wire to each side of the bead was bonded to the surface of the PMMA as well. All thermocouples used during these experiments were run through electronic ice point junctions.

3.5 Simulated Sample

A simulated sample was used to further identify the effect of flame radiation on burning rate. The simulated sample consisted of a 10 cm x 10 cm x 7.5 cm steel burner with a 9/16 inch center slot for the heat flux meter. The burner was filled with glass beads and methane was supplied through the bottom. Figure 3.6 shows the schematic of the methane burner. The glass beads maintained a steady, even flow of methane through the top surface. The flow rate of the methane gas was controlled by a regulator and calibrated flow meter.

3.6 Calibration

In most cases, such as the load cell, thermocouples and 1 inch heat flux gage, calibration was necessary before any experiments were conducted and only periodically once testing began. However, the 1/8 inch heat flux gage within the PMMA sample required calibration before and after each experiment. The methods used to calibrate each of the instruments are discussed.

3.6.1 Load Cell

The load cell was calibrated by first adjusting the weight of the sample holder and insulation to approximately zero. At this point, standard weights between 1 and 100 gram were added and the voltage readings recorded. The relationship between weight and voltage was found to be linear, with a calibration constant of 586.0 g/V. Because only mass loss rate is ultimately desired, the difference in mass is all that is needed. Therefore, small fluctuations in the zero weight did not affect the results. At the start of
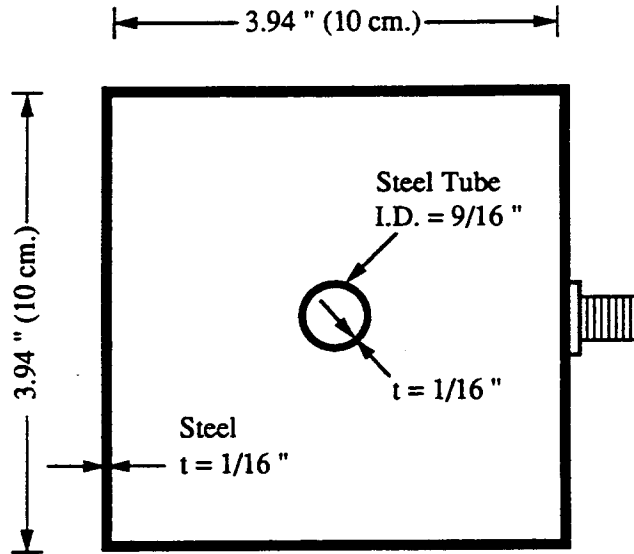
15

Figure 3.6. Schematic layout of methane burner simulated sample

each day, the load cell was rechecked for accuracy using 1 and 2 gram weights. Additionally, periodically the mass of the PMMA was recorded before and after testing and compared to that indicated by the load cell. No significant errors were found for the mass loss measurements.
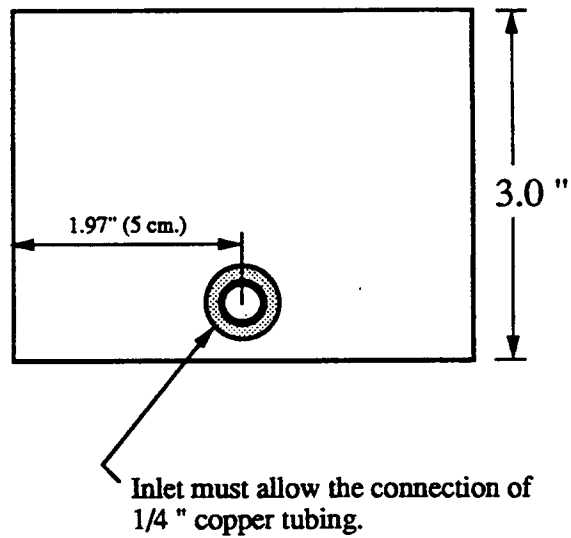
3.6.2 Heat Flux Gages

Both the 1 inch and 1/8 inch heat flux gages were initially calibrated using the standard NIST heat lamp calibration box. They were tested with water at room temperature and again with water at 46 °C. No notable differences in the calibration constants were observed. Calibration constants were found to be 5465 kW/m^2/V and 11360 kW/m^2/V for the 1 inch and 1/8 inch heat flux gages respectively. Although the water temperature did not affect the calibration constants, it did affect the zero reading. Unlike the mass loss, the heat flux measurement must be zero when there is no incident heat flux. The hot water resulted in an initial negative heat flux measurement due to convection between the sensor and the atmosphere. The heat flux measurement was calibrated to be zero, under no external irradiance, before each experiment in order to obtain consistent results. Besides the zero flux measurement, the 1 inch gage did not require calibration before each of the experiments because it was positioned such that it did not get disturbed or touched. However, the 1/8 inch gage, located within the PMMA, often became dirty and covered by melted PMMA. Therefore, this gage was calibrated before and after each test using the 1 inch gage as a standard. Differences between the 1/8 inch heat flux gage's measurement before and after each experiment were found to be within 5 to 10 percent.

3.6.3 Thermocouples

The thermocouples used to measure the coil temperature and surface temperature were calibrated before any testing began. This was done by placing them in an ice bath and also in boiling water for a prolonged period of time. Temperature readings were

found to be accurate within ± 2 °C. The thermocouples in the coil did not require additional calibration as the absolute temperature was not necessary. The thermocouples for the surface were calibrated against each other before each experiment.

Although the experiments yielded extraneous results for some tests, no major calibration errors were found. The 1/8 inch heat flux meter was found to have the greatest calibration error, but even this was small. Inconsistencies in the results are likely to be due to factors other than calibration errors.

4.1   Ignition

The experimental procedure consisted of irradiating the sample at a fixed external flux. This was done by positioning the 1 inch heat flux gage below the center of the cone such that the sensing element was level with the surface of the PMMA. Once the cone irradiance became constant, the heat flux gage was removed and the load cell, with the PMMA sample on it, was slid into position. Guide bars secured to the base of the apparatus maintained that the position of the sample was consistent between experiments. Initially, the surface of the PMMA was 1 inch below the base of the cone heater. This is consistent with the standard Cone [8] test method. A non-contacting pilot flame at the edge triggered ignition. In some cases, flashing occurred on the surface before a flame was sustained. However, in this study the time to ignition is defined as the time at which a continuous flame is supported on the PMMA surface. Since a heat flux gage was positioned in the sample, the onset of ignition is determined from the net surface heat flux. From the data, the time at which the net surface heat flux initially increases due to the flame is taken as the ignition time (see Figure 4.4). This method provided a time accurate to within ± 2 seconds.

In some cases, a fine wire Type K thermocouple (0.003 inch diameter) was used to measure the surface temperature up to the onset of burning. It was mounted on the PMMA by heating the thermocouple wire such that it recessed into the surface. A typical result of the surface temperature during the pre-heating period is shown in Figure 4.1 for an external flux of 19 kW/m^2. Ignition is indicated by the sudden increase and the subsequent plateau which indicates the effect of the added flame heat flux. The temperature at the onset of the "jump" is defined as the ignition temperature (T_{ig}) and at the onset of the plateau is the vaporization temperature (T_v). Transient surface temperature results for other irradiances are provided in Appendix B. The mass loss rate
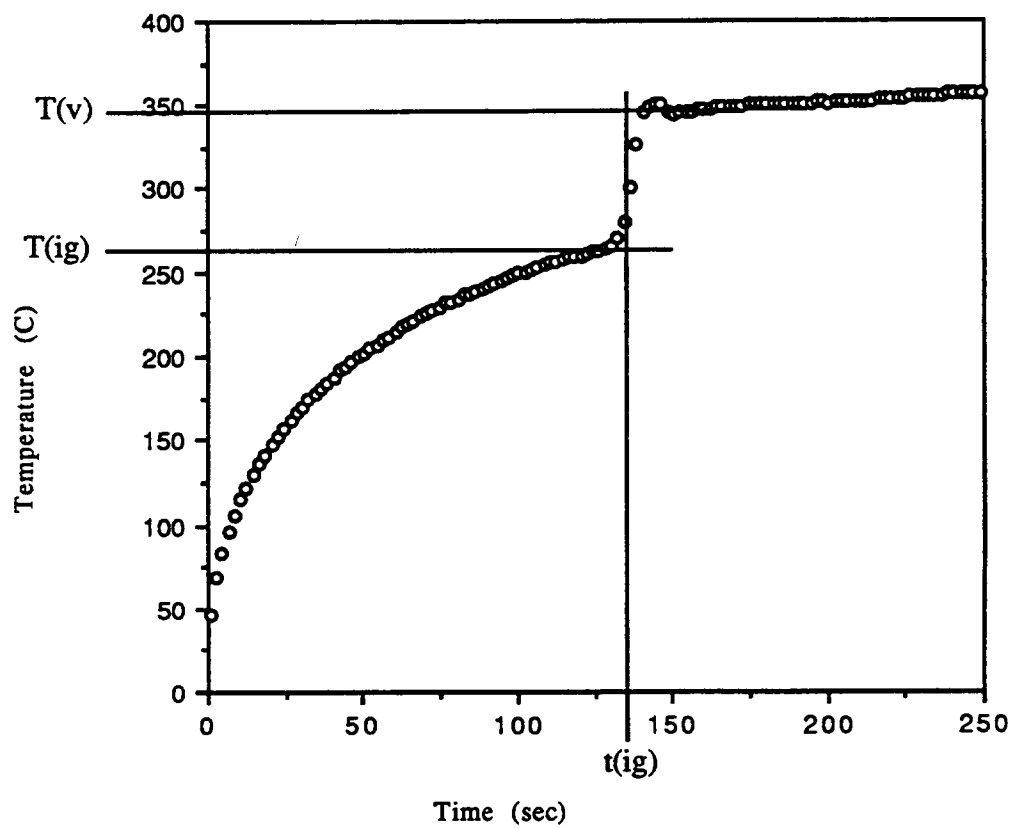
Figure 4.1. Surface temperature of black PMMA as a function of time with a 19 kW/m² external heat flux

is more appropriately related to temperature, e.g. in Arrhenius form given by Vovelle et al. [15],

$$\dot{m}'' \sim e^{-E/RT} \qquad (4.1)$$

where E/R is a material constant. Alternatively, a model which uses a fixed vaporization temperature is adopted in this analysis. This assumption is valid for large burning rates. Figure 4.2 shows the results for T_{ig} and T_v expressed as functions of external incident radiant heat flux. The temperatures are found to increase with heat flux. Thompson and Drysdale [16] make a further distinction between flashpoint temperature (at flashing) and firepoint temperature (at sustained ignition) for T_{ig}. They report, for a horizontal orientation of PMMA, a flashpoint of approximately 265 °C and a fire point of 300°C for external heat fluxes of 13 to 35 kW/m². These are consistent with the ignition temperatures found in this study for the same range of heat flux, but this fine of a discrimination is not made in the present analysis.

4.2 Mass Loss Rate

The transient mass loss rate is found from a 5-point least squares fit of the mass loss data. The mass loss rate at some time t_i is given as,

$$\dot{m}_i'' = \frac{5 \sum_{n=i-2}^{i+2} (m_n t_n) - \sum_{n=i-2}^{i+2} (m_n) \sum_{n=i-2}^{i+2} (t_n)}{5 \sum_{n=i-2}^{i+2} (t_n)^2 - \left(\sum_{n=i-2}^{i+2} (t_n) \right)^2} \qquad (4.2)$$

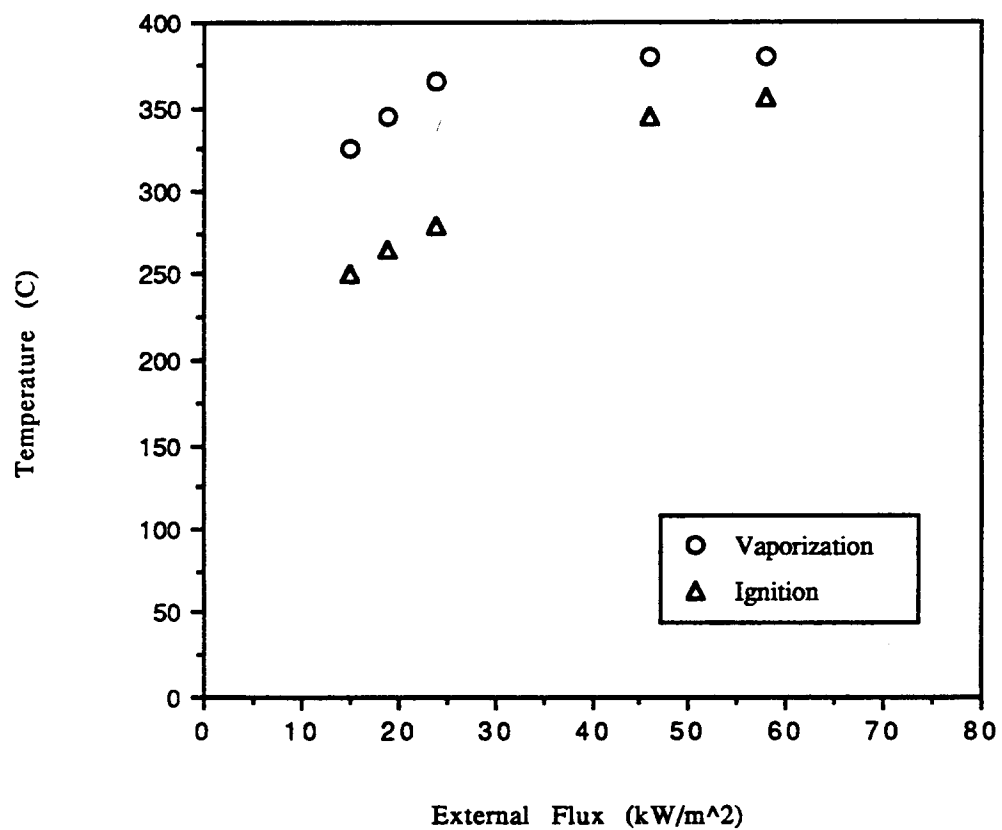where,   i   is a given measured data point,

Figure 4.2. Ignition and vaporization temperature of black PMMA as a function of external heat flux

	m	is the mass at i,
and,	t	is the time at i.

Data points were recorded every 2 seconds for the duration of the experiment. Although a higher point least squares fit would have reduced the fluctuation in the mass loss rate curve, a greater error would have resulted during the transient period because of the rapidly changing mass loss rate.

4.2.1 Flaming PMMA

Figures 4.3 and 4.4 depict the mass loss rate and net surface heat flux measured by the sensor, respectively, for an external radiant flux of 25 kW/m^2. The graph shows the time from which the PMMA was placed under the cone heater. The net surface heat flux in Figure 4.4 is the actual data measured by the 1/8 inch heat flux gage located in the center of the sample. These are representative results taken over 0 to 75 kW/m^2. Results for other irradiances may be found in Appendix C and D.

Figure 4.5 shows a burning sample which illustrates the typical elongated column flame that protrudes through the top of the cone heater. The flame length to effective diameter (sample face) ratio is of the order of 4. This is significant in estimating the mean beam length for typical flames under the cone heater.

The increase in heat flux in Figure 4.4 initially before ignition is due to convective heating. At ignition (~ 90 sec), there is a sharp rise in the burning rate and in the heat flux. The initial flame heat flux appears to be approximately 22 kW/m^2. As described later, this value is believed to be low, possibly due to the deposition of condensable monomer on the heat flux sensor. Condensation can add heat to the sensor, but the initial deposition may shield it. Subsequent evaporation of the monomer could also reduce the heat flux. These processes undoubtedly affected the accuracy of this measurement. Additionally, since the heat flux gage does not move relative to the cone, while the PMMA does, the measurement of the heat flux to the surface of the sample may be

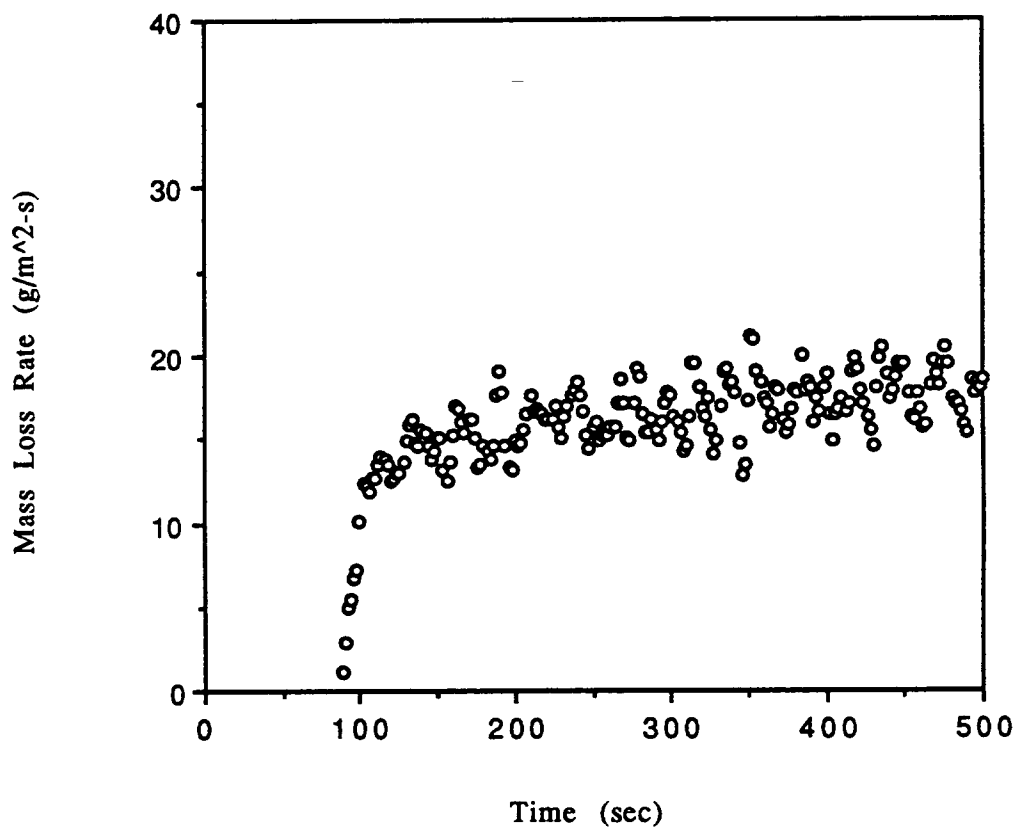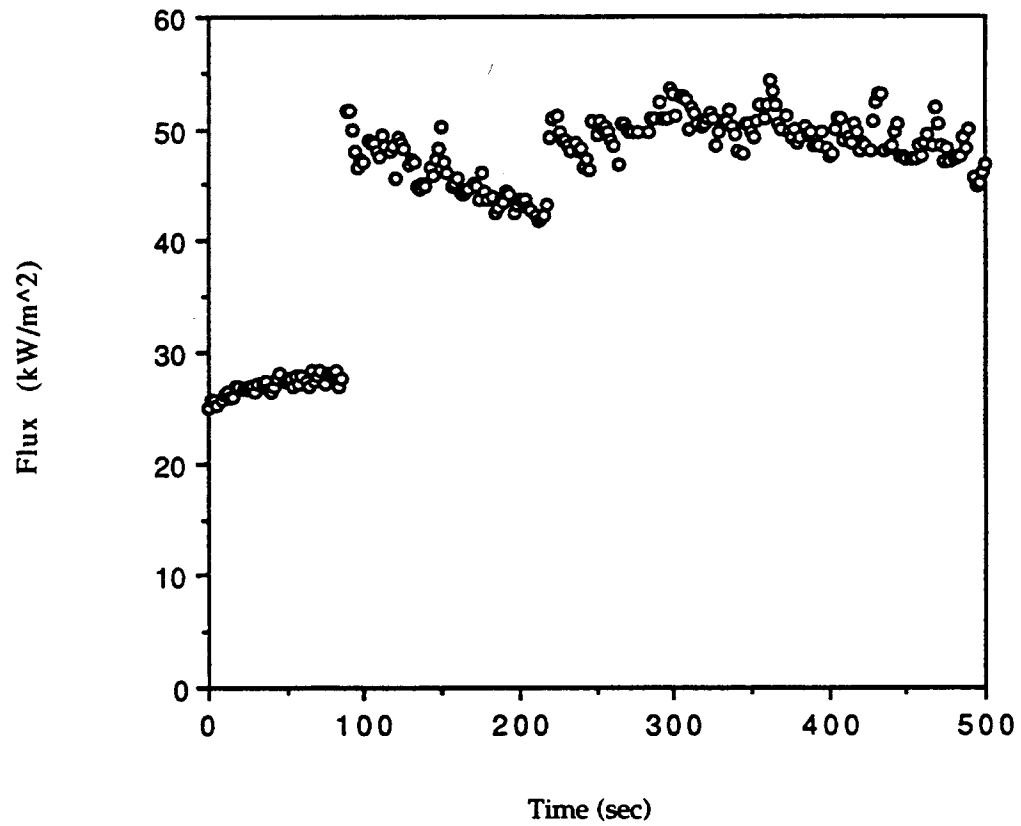**Figure 4.3.** Transient mass loss rate of black PMMA with a 25 kW/m^2 external heat flux

24

Figure 4.4. Total incident heat flux measured by sensor of black PMMA with a 25 kW/m² external heat flux
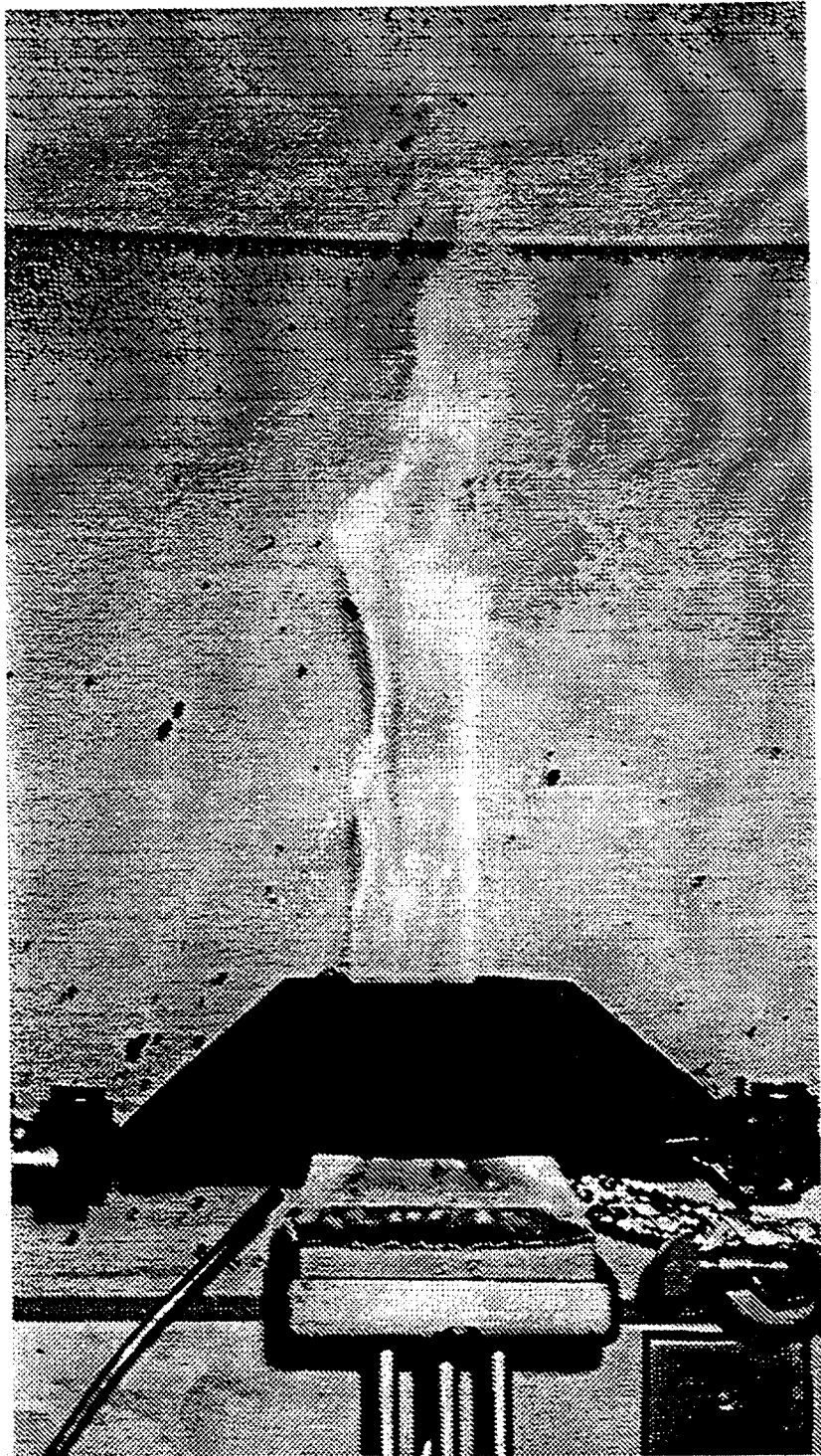
25

Figure 4.5. Flaming PMMA sample

affected. The relationship between distance from the cone and incident heat flux was examined by lowering the heat flux gage 1 inch from its normal position, i.e. the thickness of the PMMA sample. This provided the range of fluxes the sample would actually be exposed to. It was found that when the surface of the PMMA is 1 inch below the standard location of the heat flux sensor, it is exposed to approximately 85 percent of the incident flux measured by the gage. However, because the burning reaches steady state well before the surface recedes this distance, it is likely that this change in irradiance is not a major factor affecting the burning rate and flux measurements. Even so, there are still several unknown problems evident in the flame heat flux measurements. The subsequent "jump" at about 225 seconds in Figure 4.4 is indicative of the anomalies experienced in this measurement. However, the heat flux gage was very robust, and despite deposition, it was within 10 percent of calibration following each test under external radiant heat transfer.

4.2.2 Non-flaming PMMA

Figures 4.6 and 4.7 depict mass loss and surface heat flux to the sensor, respectively, for nonflaming conditions at an external radiant heating of 21 kW/m^2. The five point running differentiation of the mass loss signal does not lead to a smooth mass loss curve at this low range. However, the nominal average value of 5 g/m^2-s at equilibrium is consistent with expected results [17]. Subtracting the initial radiant heat flux from the steady value in Figure 4.7 implies a maximum convective flux loss of 4 kW/m^2 (25 - 21) due to the sample heating. A vaporization temperature of 365 °C (Figure 4.2), assumed to be the local gas temperature, exposed to the heat flux gage at 65 °C, yields a convective heat transfer coefficient of approximately 13 W/m^2-K which is consistent with natural convection correlations. As seen in Figure 4.7, fluctuations in the net surface heat flux measurement are minor compared to the flaming results (Figure 4.4). However, no extensive study is done for the nonflaming case.
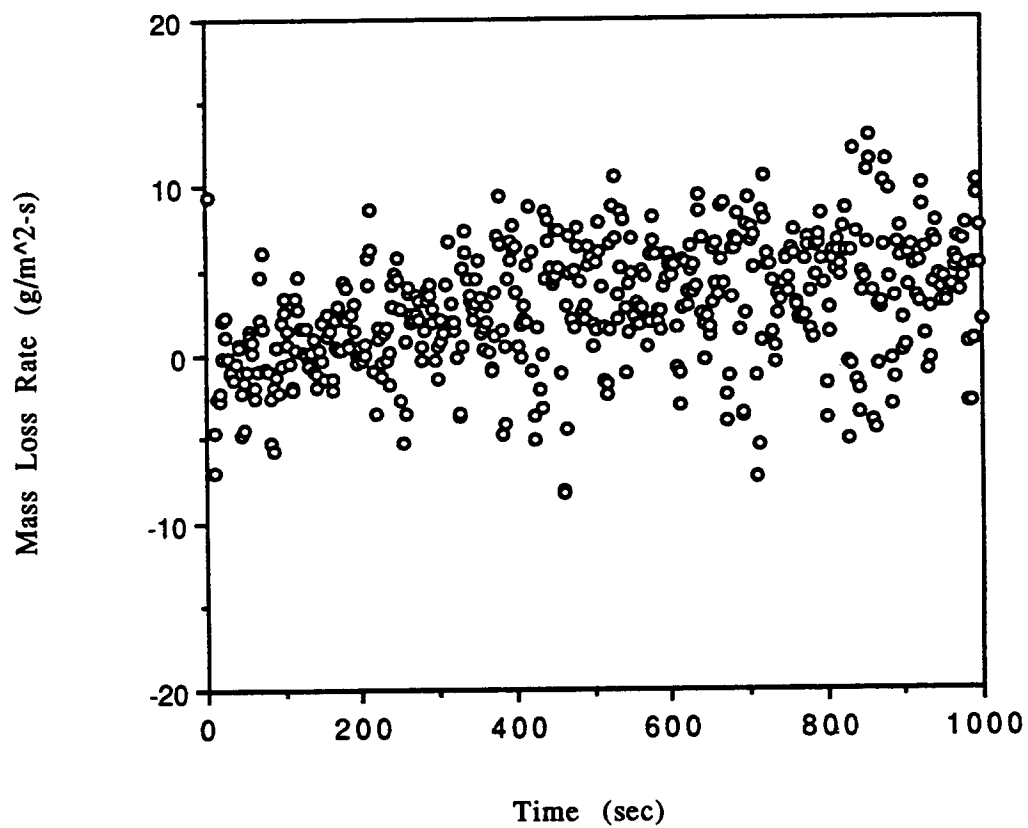
27

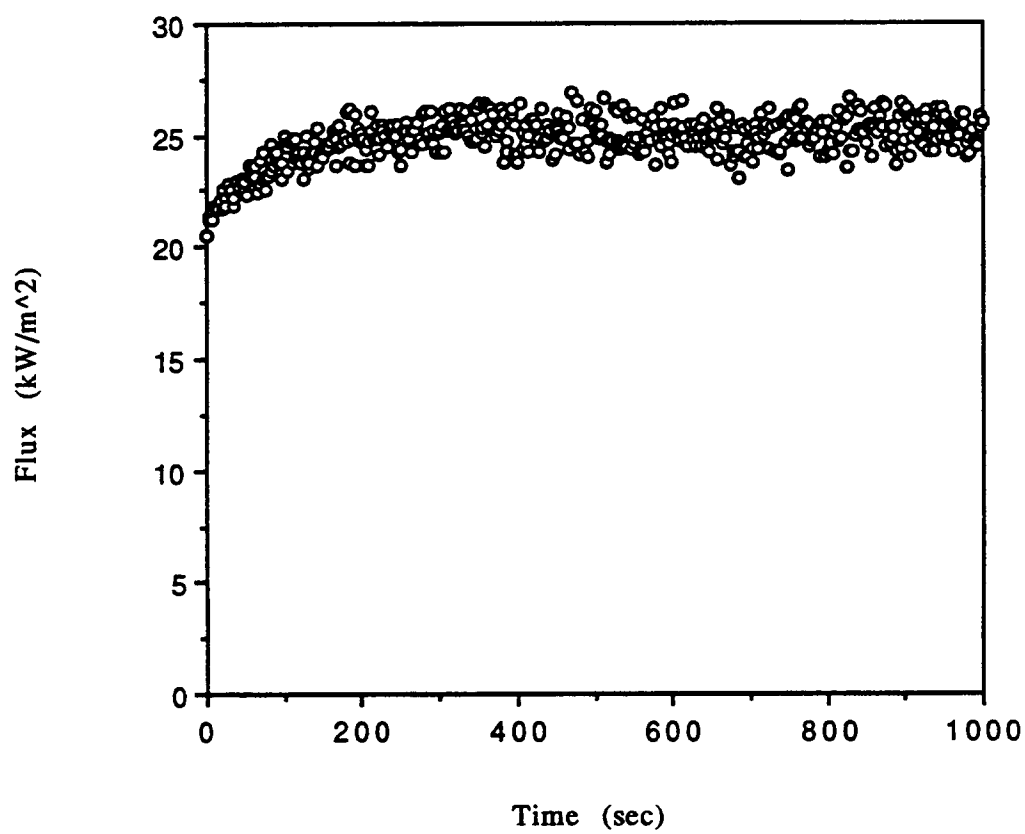**Figure 4.6.** Non-flaming transient mass loss rate of black PMMA with a 21 kW/m² external heat flux

28

Figure 4.7. Non-flaming total incident heat flux measured by sensor of black
PMMA with a 21 kW/m² external heat flux

29

4.3 Simulated Sample

A glass bead burner equal to the size of a PMMA sample was used to simulate a burning sample. Methane was used as the fuel and the center surface heat flux was measured with the heat flux gage. The methane burner was positioned beneath the cone heater apparatus exactly as the PMMA sample would be. It was exposed to a 50 kW/m^2 constant external flux to avoid problems with the flame heating up the coil, thus changing the surface heat flux. The simulated sample was not tested in the open because the cone apparatus tended to induce a specific air flow. Since the purpose of the methane burner was to simulate the PMMA burning, it was subjected to the same air flow conditions. No fouling problems with the heat flux sensor were observed for these tests. Figure 4.8 shows the steady state sensor heat flux measurements with an external cone exposure of of 50 kW/m^2. The results tend to show a constant flame heat flux above the external radiant flux. This is approximately 27 kW/m^2 over a range of energy release rates per unit area of 200 to 600 kW/m^2 consistent with the PMMA energy release rates. The energy release rates are determined from the methane flow rate, measured by a calibrated flow meter, and the heat of combustion of methane, taken as 50 kJ/g. It was also found that there were less fluctuations in the heat flux measurements for the higher energy release flames.

Heat flux measurements were also taken where the gas burner is lowered 1/2 inch below the tip of the sensor. This was intended to simulate the PMMA burning and receding below the sensor during the experiment. The measured flame heat flux was found to be approximately 15 kW/m^2 higher than when the sensor was flush with the surface. The fluctuations in the data did not vary as the energy release rates increased as they did in the first set of experiments. However, the results for this scenario also tended to show a constant flame heat flux. Results for these tests may be found in Appendix E. For the methane burner, despite the increased flame heights, due to increased burning rates, the flame heat flux is approximately constant. This is further explained later.
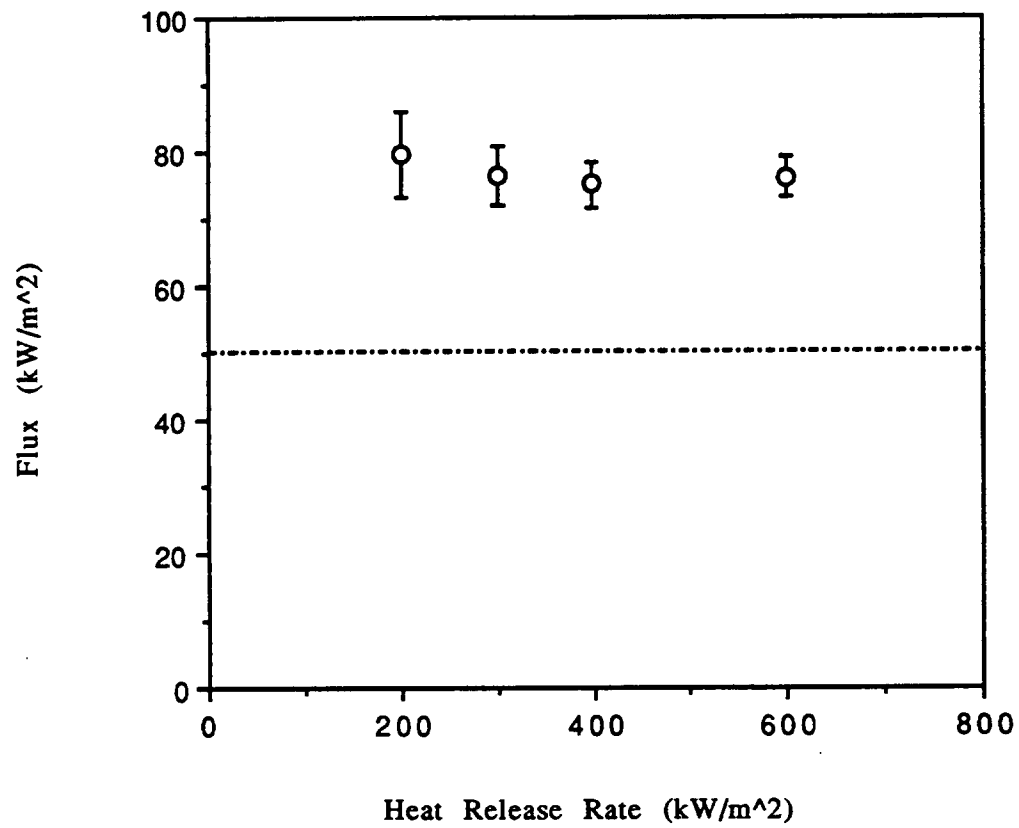
Figure 4.8. Steady state heat flux measured by sensor of methane gas burner with a 50 kW/m^2 external heat flux

The models used in the analyses are based on the presentation of Quintiere and Iqbal [3]. These use an integral model for one dimensional unsteady conduction and surface vaporization at a fixed temperature. The models are outlined below:

5.1   Preheating to Ignition

The governing equation is,

$$\frac{\partial T}{\partial t} = \alpha \frac{\partial^2 T}{\partial y^2} \qquad (5.1)$$

where,   T   is temperature,

                t   is time,

                y   is distance measured from the surface,

                α is the thermal diffusivity, $\frac{k}{\rho c}$,

                k   is the thermal conductivity,

                ρ is the density,

and   c   is the specific heat.

Figure 5.1 shows the heat and mass transfer processes for a thermoplastic type solid fuel. Properties are assumed constant. The equation is integrated from zero to delta where at $y = \delta$,

$$T = T_o, \qquad (5.2)$$

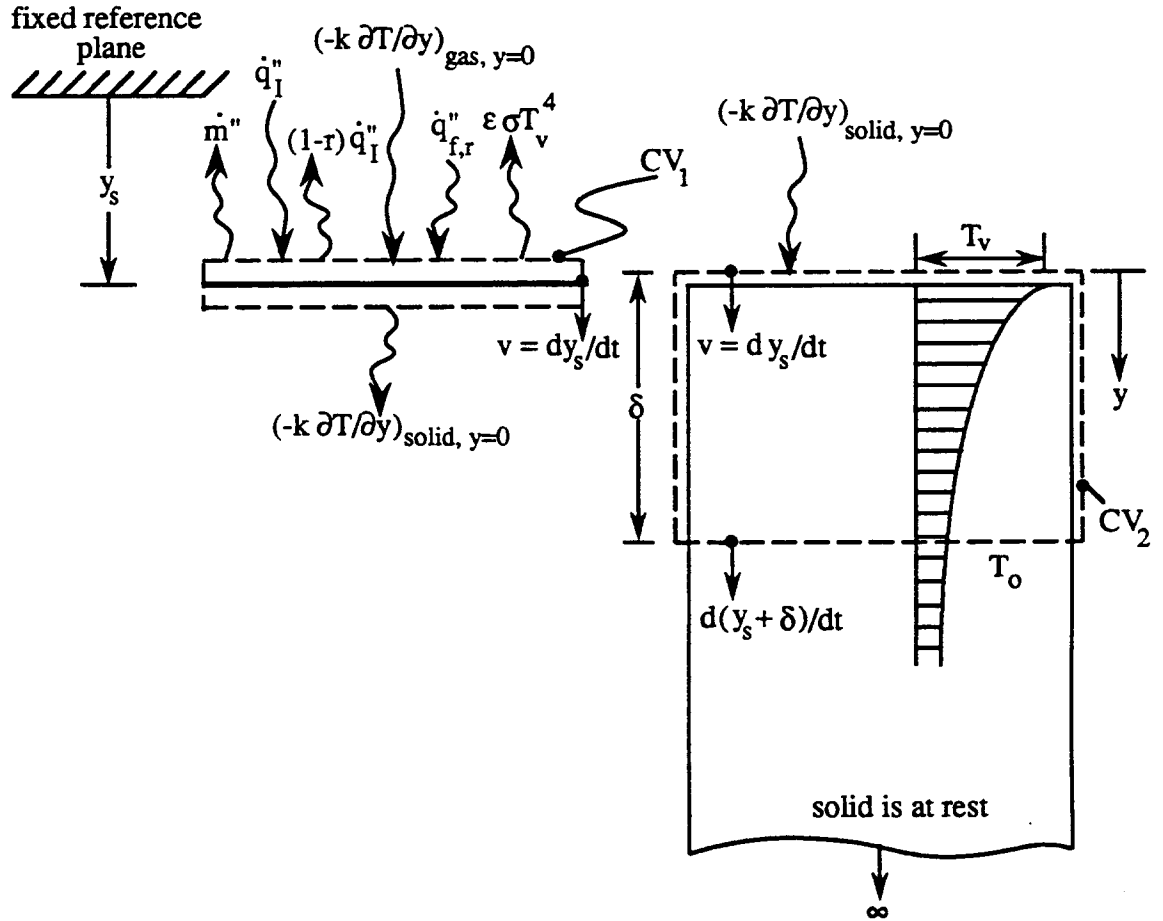and, $\frac{\partial T}{\partial y} = 0. \qquad (5.3)$

Figure 5.1. Heat and mass transfer processes for a thermoplastic type solid fuel. CV1 is around the vaporizing interface. CV2 is bounded by the interface and thermal penetration depth, δ.

33

At y = 0,

$$-k \frac{\partial T}{\partial y} = \dot{q}'' \equiv \varepsilon \dot{q}''_{ext} - h_c (T - T_o) - \varepsilon \sigma T^4 \qquad (5.4)$$

where, $\dot{q}''$ is the net surface heat flux during the pre-heat period,

ε is the surface emissivity and absorptivity,

h_c is the convective heat transfer coefficient,

$\dot{q}''_{ext}$ is the external incident radiative heat flux,

and σ is the Stefan-Boltzmann constant.

A quadratic profile is assumed such that the boundary conditions are satisfied:

$$T - T_o = \frac{\dot{q}'' \delta}{2 k} \left(1 - \frac{y}{\delta}\right)^2 \qquad (5.5)$$

Integrating Eq. (5.1) from 0 to δ and using the above boundary conditions, it can be shown that,

$$\frac{d}{dt}\left(\dot{q}'' \delta\right) = 6 \alpha \dot{q}'' \qquad (5.6)$$

If we assume $\dot{q}''$ is constant, which is a good assumption for large $\dot{q}''_{ext}$, then,

$$\delta \cong \sqrt{6 \alpha t}. \qquad (5.7)$$

It has been shown by Abu-Zaid and Atreya [18] that a more complete solution to the

above problem yields:

$$\delta = \sqrt{\frac{12\,\alpha\,t}{e_4}}$$ (5.8)

where e_4 was shown to vary between 1.6 at 15 kW/m^2 to 1.9 at 50 kW/m^2. The asymptote of e_4 is taken as 2.0, which yields the approximate result of Eq. (5.7). Since the present solution is approximate anyway, this accuracy can be sacrificed to simplify the solution methodology. But at very low heat fluxes, the error introduced will be greatest.

Substituting Eq. (5.7) into Eq. (5.5) at y = 0 gives:

$$T_{ig} - T_o = \frac{\dot{q}''\,\delta}{2\,k} = \frac{\dot{q}''}{2\,k}\sqrt{6\,\alpha\,t_{ig}}$$ (5.9)

or,

$$t_{ig} = \frac{2}{3}(k\,\rho\,c)\frac{(T_{ig} - T_o)^2}{(\dot{q}'')^2}.$$ (5.10)

Note that this algorithm also gives a means for computing the surface temperature over time. This is done implicitly by selecting T_s, computing the corresponding net heat flux, and using Eq. (5.10) to find the time. Moreover, this result allows a computation of the critical flux, $\dot{q}''_{cr}$, for ignition by extrapolating ignition data for $(t_{ig})^{-1/2}$ to zero. At this intercept,

$$\dot{q}''_{ext} = \frac{1}{\varepsilon}\left[h_c\,(T_{ig} - T_o) + \varepsilon\,\sigma\,T_{ig}^4\right] \equiv \dot{q}''_{cr}.$$ (5.11)

The critical flux is found from Eqns. (5.4) and (5.10). From this, the temperature at the critical flux is determined using Eq. (5.11). Eq. (5.10) is in contrast to the analytical fit to the exact solution offered by Janssens [19]:

$$\dot{q}_{ext}'' = \dot{q}_{cr}'' \left[1 + 0.73 \left(\frac{k \rho c}{h_c^2 \, t_{ig}} \right)^{0.547} \right] . \qquad (5.12)$$

5.2 Burning Rate

The governing equation for the burning rate problem follows from Eq. (5.1) which governs conduction below the moving vaporizing surface at a fixed vaporization temperature, T_v (Fig. 5.1). Hence at $y = 0$,

$$T = T_v \qquad (5.13)$$

and also,

$$- k \frac{\partial T}{\partial y} = \dot{q}'' - \dot{m}'' \Delta H_v \qquad (5.14)$$

where, $\dot{m}''$ is the mass loss rate per unit area,

                ΔH_v is the heat of vaporization,

and $\dot{q}''$ is the net surface heat flux.

Note that $\dot{q}''$ in Eq. (5.14) is different from that defined in Eq. (5.4).

$$\dot{q}'' = \varepsilon \, \dot{q}_{ext}'' + \dot{q}_{fl}'' - \varepsilon \, \sigma \, T_v^4 \qquad (5.15)$$

36

where $\dot{q}''_{fl}$ is the flame heat flux given as:

$$\dot{q}''_{fl} = \varepsilon\,\dot{q}''_{fl,r} + \dot{q}''_{fl,c} \,.$$

(5.16)

The flame incident radiant heat flux is $\dot{q}''_{fl,r}$ and the convective flux, from a stagnation film

flame model [1], can be shown as,

$$\dot{q}''_{fl,c} = \frac{h_c}{c_g}\left(\frac{\xi}{e^{\xi}-1}\right)\left[Y_{ox,\infty}(1-\chi_r)\frac{\Delta H_c}{r} - c_g\,(T_v - T_o)\right]$$

(5.17)

where, $\quad \xi = \dfrac{\dot{m}''\,c_g}{h_c}\,,$

$\left(\dfrac{\xi}{e^{\xi}-1}\right)$ is the mass transfer "blocking factor" that is one for $\dot{m}'' \rightarrow 0$,

$Y_{ox,\infty}$ is the ambient mass fraction of oxygen,

χ_r is the flame radiative fraction,

ΔH_c is the heat of combustion,

r is the stoichiometric fuel to oxygen mass ratio,

and, $\quad c_g$ is the gas phase specific heat at constant pressure.

Alternatively, this might be expressed as,

37

$$\dot{q}''_{fl,c} = h_c \left(\frac{\xi}{e^\xi - 1} \right) (T_{fl} - T_v) \qquad (5.18)$$

where T_{fl} is an effective flame temperature.

Assuming a quadratic profile,

$$\frac{T - T_o}{T_v - T_o} = \left(1 - \frac{y}{\delta} \right)^2 \qquad (5.19)$$

which satisfies Eqns. (5.2) and (5.13). Substituting this profile in Eq. (5.14) provides,

$$\dot{m}'' \Delta H_v = \dot{q}'' - \frac{2k}{\delta} (T_v - T_o) \qquad (5.20)$$

where the last term is the transient conduction heat loss into the solid. Integration of Eq. (5.1) over y as before and substituting Eq. (5.19) yields,

$$\frac{1}{3} \frac{d\delta}{dt} + \frac{\dot{m}''}{\rho} = \frac{2\alpha}{\delta} \qquad (5.21)$$

where at ignition, $T = T_v$ and $\delta = \sqrt{6 \alpha t_{ig}} = \delta_{ig}$.

Eqns. (5.20) and (5.21) describe the transient burning rate in terms of material properties and the thermal penetration depth. If the dependence of the burning rate on the blocking factor is ignored, or if the total flame heat flux is assumed to be constant, Eq. (5.21) may be solved exactly. It can be shown that,

$$t - t_{ig} = \frac{\delta_s^2}{6\,\alpha} \frac{\Delta H_v}{L} \left[\frac{\delta_{ig} - \delta}{\delta_s} - \ln\left(\frac{\delta_s - \delta}{\delta_s - \delta_{ig}} \right) \right] \qquad (5.22)$$

where, $\delta_s = \frac{2\,k}{c} \frac{L}{\dot{q}''}$, a steady value   (5.23)

and, $L = \Delta H_v + c\,(T_v - T_o)$, the heat of gasification.   (5.24)

It follows that the steady state mass flux is given as,

$$\dot{m}_s'' = \frac{\dot{q}''}{L} . \qquad (5.25)$$

Note, in addition to the flame heat flux, the properties required to obtain a solution are ε, ρ, c, k, T_v, (or T_{ig}), and ΔH_v (or L). These must be derivable in a convenient way consistent with the burning rate and ignition models.

5.3 Flame Heat Flux

The flame heat flux is described in Eq. (5.16) as the radiative plus convective heat flux from the flame to the surface. For the present experiments, both the steady mass loss measurements and the surface heat flux measurements are used to determine the total flame heat flux. However, these measurement do not account for absorption of the external flux by the flame. Additionally, it is desired to determine the affect of increased flame height, as a result of increased burning rate, on the total flame flux to the surface.

5.3.1 Radiative Heat Flux

The emissivity of a flame can be represented as,

$$\varepsilon_{fl} = 1 - e^{-\kappa \, l_m} \qquad\qquad (5.26)$$

where, κ is the absorption coefficient,

and, l_m is the mean beam length.

According to Orloff and deRis [20], κ and l_m can be computed from an algorithm for pool fires. By applying their algorithm, it is found than l_m/R (where R is the effective radius of the pool fire) is asymptotic at 1.3 for the present PMMA cone assembly. In this study, 2R equals 10 centimeters, the sample side dimension. Alternatively, if a homogeneous grey gas cylindrical flame is considered, $l_m = 0.65(2R)$ for a flame height greater than 4R [21] which is identical to the Orloff and deRis [20] algorithm. Their algorithm further gives $\kappa = 1.4$ m^{-1} which compares to 1.3 m^{-1} by measurement [22]. Using $\kappa = 1.4$ m^{-1} and $l_m = 0.065$ m, Eq. (5.26) yields a flame emissivity of approximately 0.09 for the cone PMMA assembly. It also indicates that this flame is very transparent (> 91%), and hence, most of the Cone heat radiation is expected to penetrate the flame and reach the surface. Moreover, for flame heights greater than 20 cm., the PMMA flame emissivity is approximately constant at 0.09. In all the burning rate measurements in the cone apparatus, the PMMA flame was atleast 20 cm. in height.

The incident flame radiative heat flux is,

$$\dot{q}''_{fl,r} = \varepsilon_{fl} \, \sigma \, T_{fl}^4 \qquad\qquad (5.27)$$

For $T_{fl} = 1400$ K [22], the radiative heat flux for all the burning conditions is estimated as 20 kW/m^2.

5.3.2 Convective Heat Flux

The convective heat flux (assuming a blocking factor of 1) can also be estimated by Eq. (5.17) considering,

$$h_c = 10 \text{ W/m}^2 \cdot \text{K} \qquad\qquad \Delta H_c / r = 13 \text{ kJ/g}$$

$$c_g = 1.0 \text{ J/g} \cdot \text{K} \qquad\qquad \chi_r = 0.4$$

$$Y_{ox,\infty} = 0.233$$

A maximum $\dot{q}''_{fl,c} = 15 \text{ kW/m}^2$ is found since blocking would reduce this value as the burning rate increases.

5.3.3 Total Flame Heat Flux

Realizing the surface emissivity, $\varepsilon \approx 1$, Eq. (5.16) suggests a constant total flame heat flux of 35 kW/m^2 at most. Although experimental results in Section 6.2 provide a similar value, it is the constancy of the flame heat flux for samples burning in the Cone Calorimeter which is significant. Additionally, the above analysis suggests that most materials are likely to have relatively transparent flames with respect to the external radiant heating.

The experimental results are analyzed and the models are applied. The accuracy of the models and their utility for deriving property data are examined for materials tested in the Cone Calorimeter. Properties derived from the literature [2] or by direct measurements are given below:

$$\rho = 1190 \text{ kg/m}^3 \qquad \text{(measured)}$$

$$k = 2.49 \times 10^{-7} \, T + 1.18 \times 10^{-4} \text{ kW/m·K}$$

$$c = 2.374 \times 10^{-3} \, T + 1.1 \text{ J/g·K}$$

$$\alpha = 8.81 \times 10^{-8} \text{ m}^2/\text{s}$$

where temperature (T) is in Kelvin.

6.1   Ignition

Kashiwagi and Omori [17] investigated piloted ignition of two different class PMMA samples (75 mm x 75 mm x 13 mm thick): one high molecular weight (MW), "thermally stable" material; and the other a low MW, "thermally unstable" material. The surface temperatures at piloted ignition ranged from 320 to 340 °C for the high MW PMMA, and 260 to 270 °C for the low MW samples irradiated between 10 to 20 kW/m² respectively. The low MW temperatures appear to be consistent with Thompson and Drysdale [16] and the present results.

Time to ignite as a function of external radiant flux is given in Figure 6.1. In order to better assess the present results, the standard NIST Cone [8] apparatus was also

used to test the black PMMA. Results from these tests may be found in Appendix F. The standard Cone differs from the one used in that the ignition source is an electric spark positioned above the center of the sample; as opposed to a pilot flame at the edge. The standard NIST Cone electric spark piloted apparatus gave longer ignition times than the flame piloted system. The location of the pilot is probably the reason. The results by Thompson and Drysdale [16] are just slightly higher than the present ignition times. Other results by Mikkola and Wickman [23] for black PMMA are consistent. Kashiwagi and Omori [17] measured an ignition time of 900 seconds for the high MW PMMA at approximately 9 kW/m². A minimum heat flux for piloted ignition of PMMA was not measured in this study, nor was one found in the literature. However, in the following section, a method for extrapolating a minimum heat flux for ignition is presented.

The lines in Figure 6.1 correspond to the application of Eq. (5.10) with the properties evaluated at a mean temperature with respect to T_{vap}. For the present data, it appears that better agreement is achieved for a decreasing ignition temperature as the external flux decreases. This is consistent with the data of Figure 4.2.

6.1.1   Ignition Temperature and Thermal Inertia

Figure 6.2 shows the present ignition data for the black PMMA as a linear function of external heat flux. Fitting the data below 40 kW/m² to a straight line gives an intercept of approximately 4 kW/m² for the critical heat flux. Values are chosen in this range as to provide an asymptotic fit of the data with the external heat flux close to the critical heat flux. Again, Figure 6.1 suggests that the experimental ignition results better agree with the theoretical results at the lower external heat fluxes. Additionally, because the ignition times are longer in this range, the relative experimental error is smaller than that at shorter ignition times. Solving Eq. (5.11) for T_{ig} with T_o = 22 °C, h_c = 10 W/m²-K, and ε = 0.95 gives T_{ig} = 180 °C. This is lower than the measured ignition temperature of black PMMA, but the application of this model with the calculated ignition
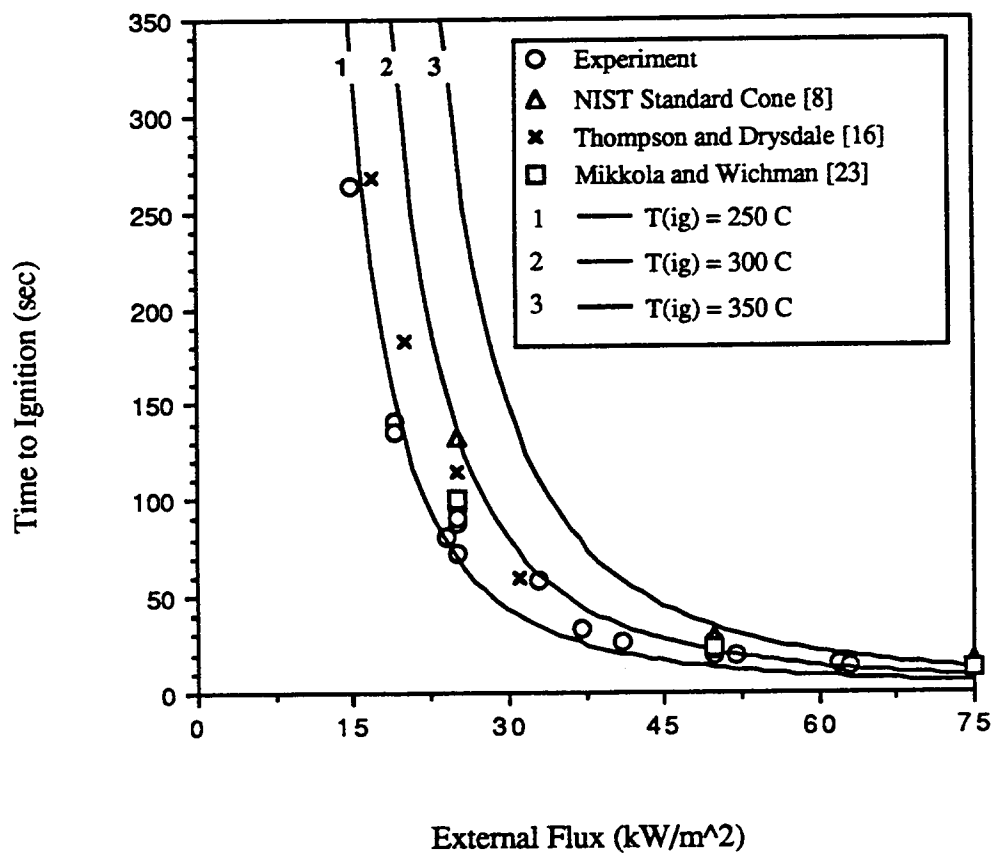
Figure 6.1. Calculated and measured ignition time of black PMMA as a function of external heat flux
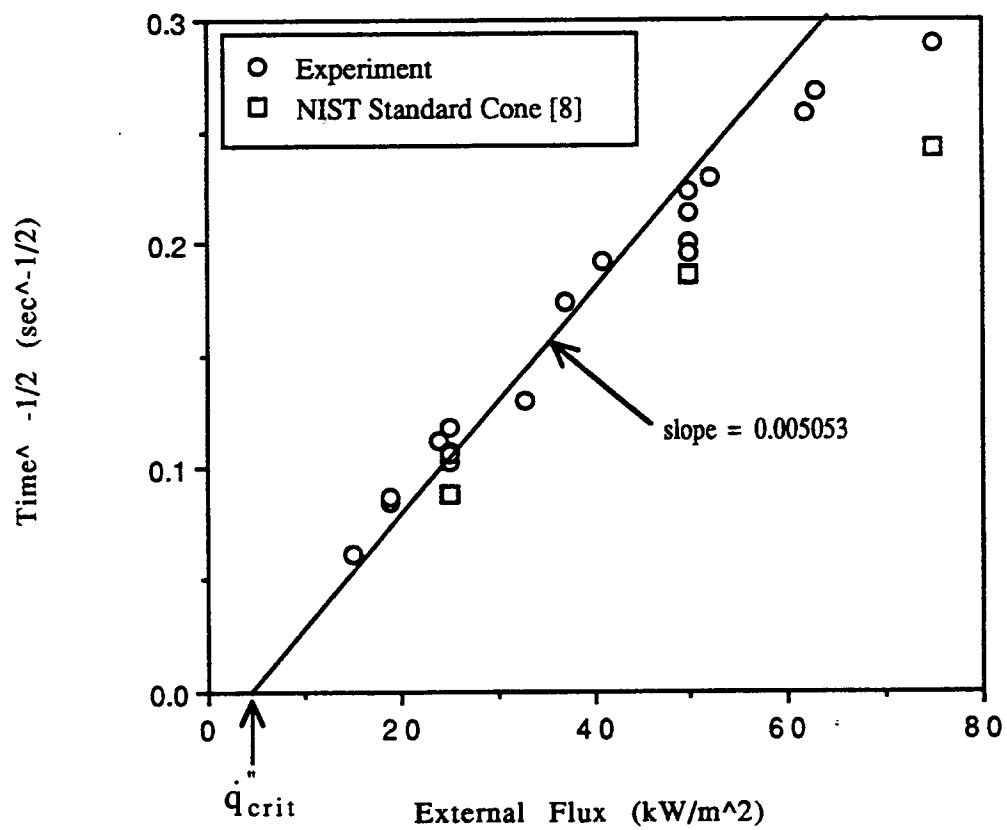
Figure 6.2. Ignition data for black PMMA

temperature will proceed to assess its overall effect. Based on the slope of the line in Figure 6.1, the thermal inertia is estimated as follows:

From Eqns. (5.4) and (5.10),

$$t_{ig}^{-\frac{1}{2}} = \left[\frac{\varepsilon}{\sqrt{\frac{2}{3} k \rho c} \, (T_{ig} - T_o)} \right] \dot{q}_{ext}'' - \left[\frac{h_c (T_{ig} - T_o) + \varepsilon \sigma T_{ig}^4}{\sqrt{\frac{2}{3} k \rho c} \, (T_{ig} - T_o)} \right]. \tag{6.1}$$

From Eq. (6.1) and the slope of the fit line in Figure 6.2,

$$\left[\frac{\varepsilon}{\sqrt{\frac{2}{3} k \rho c} \, (T_{ig} - T_o)} \right] = 0.005053.$$

Solving for the thermal inertia,

$$k \rho c = 2.12 \frac{kJ^2}{m^4 \cdot s \cdot K^2}.$$

Because $\rho = 1190 \ kg/m^3$ and assuming $\alpha = 8.81 \times 10^{-8} \ m^2/s$, a constant that can be independently determined, the thermal conductivity and specific heat are found,

$$k = 0.432 \times 10^{-3} \frac{kW}{m \cdot K}$$

and,

$$c = 4.12 \frac{kJ}{kg \cdot K}.$$

This gives a prescription for determining k and c provided α is known. The determination of α is still needed, but for most solids, it varies slightly with temperature, and does not vary greatly for non-metals.

6.2 Burning Rate

Since PMMA approximates a vaporizing solid, Eq. (5.25) is applied to the steady state data. The results are plotted in Figure 6.3 against the external radiant heat flux. The data from our apparatus and the NIST Cone Calorimeter are consistent for the black PMMA. However, the results of Tewarson and Pion [24] are markedly different for clear PMMA because they used a different type of PMMA (Rohm & Hass) compared to the type of PMMA used in the present analysis (Polycast). If the flame heat flux is constant, then,

$$\dot{m}'' L = \dot{q}''_{ext} + \dot{q}''_{fl} - \varepsilon \sigma T_v^4 \tag{6.2}$$

or,

$$\dot{m}'' = \left(\frac{1}{L}\right) \dot{q}''_{ext} + \frac{\left(\dot{q}''_{fl} - \varepsilon \sigma T_v^4\right)}{L} \tag{6.3}$$

6.2.1 Effective Heat of Gasification and Total Flame Heat Flux

From Eq. (6.3) and the slope and intercept of the present data in Figure 6.3,

$$\left(\frac{1}{L}\right) = 0.361 \frac{g}{kJ}$$
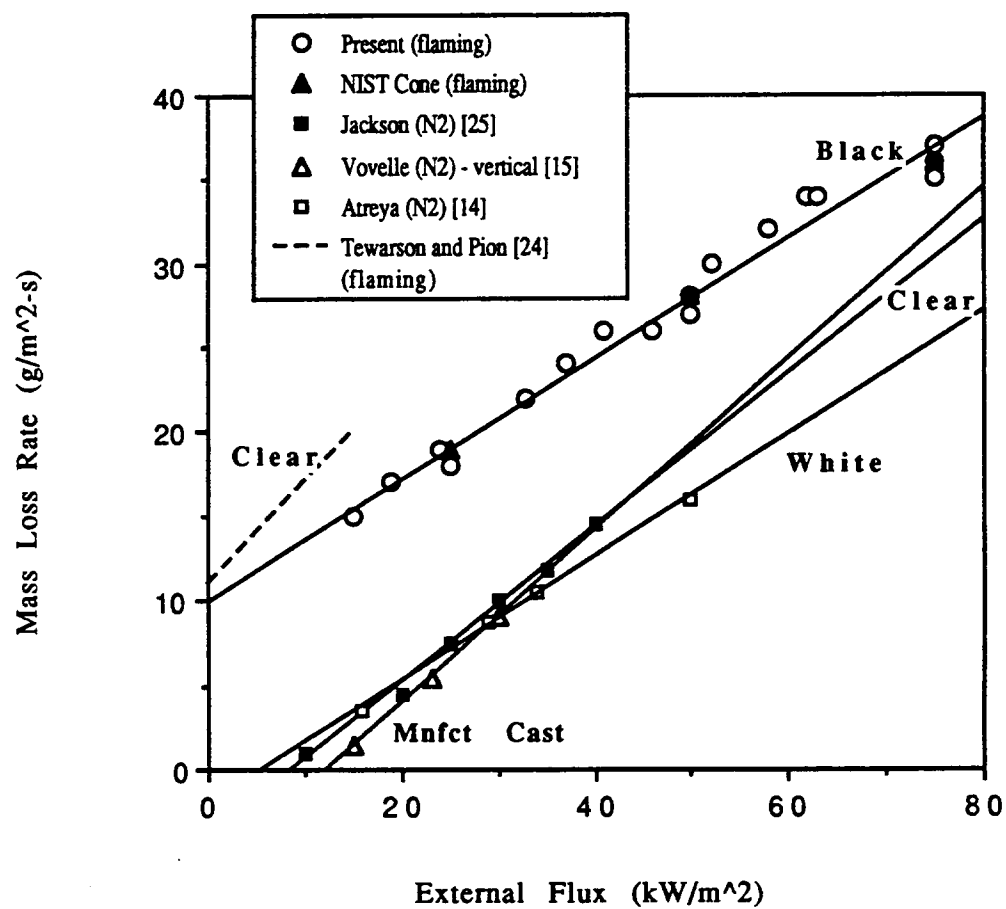
or,

$$L = 2.77 \frac{kJ}{g},$$

Figure 6.3. Steady state mass loss rate as a function of external heat flux for flaming and non-flaming PMMA

48

and,

$$\frac{\dot{q}_{fl}'' - \varepsilon \sigma T_v^4}{L} = 10.0 \frac{g}{m^2 \cdot s} \ .$$

For an average vaporization temperature, T_v, of 370 $^\circ$ C based on the measured surface temperatures of black PMMA at ignition, and the emissivity of the PMMA, ε, taken as 0.95, the steady state average flame heat flux may be determined using the above equation.

$$\dot{q}_{fl}'' \approx 37 \frac{kW}{m^2} \ .$$

The heat of gasification corresponding to the Tewarson PMMA is 1.67 kJ/g. An examination of data from radiant heated PMMA in nitrogen are also shown in Figure 6.3. These correspond to Vovelle et al.[15], Jackson [25] for clear PMMA and Agrawal and Atreya [14] for white PMMA. Their L values are 2.2, 1.96 and 2.73 kJ/g in corresponding order. The wide disparity between the clear and pigmented PMMA samples must indicate a real difference due to composition. This is similar to the variations found by Kashiwagi and Omori for ignition properties [17].

6.2.2   Flame Plus External Heat Flux

Figure 6.4 shows the incident flame plus external heat flux to the PMMA surface plotted against the external heat flux. This was done two ways: (1) by sensor measurement, and (2) by calculation from the steady mass loss rate data and extrapolation of an effective heat of gasification. From Eqns. (5.15) and (5.18) applied to the sensor at the water temperature, T_w, the net heat flux to the sensor is,
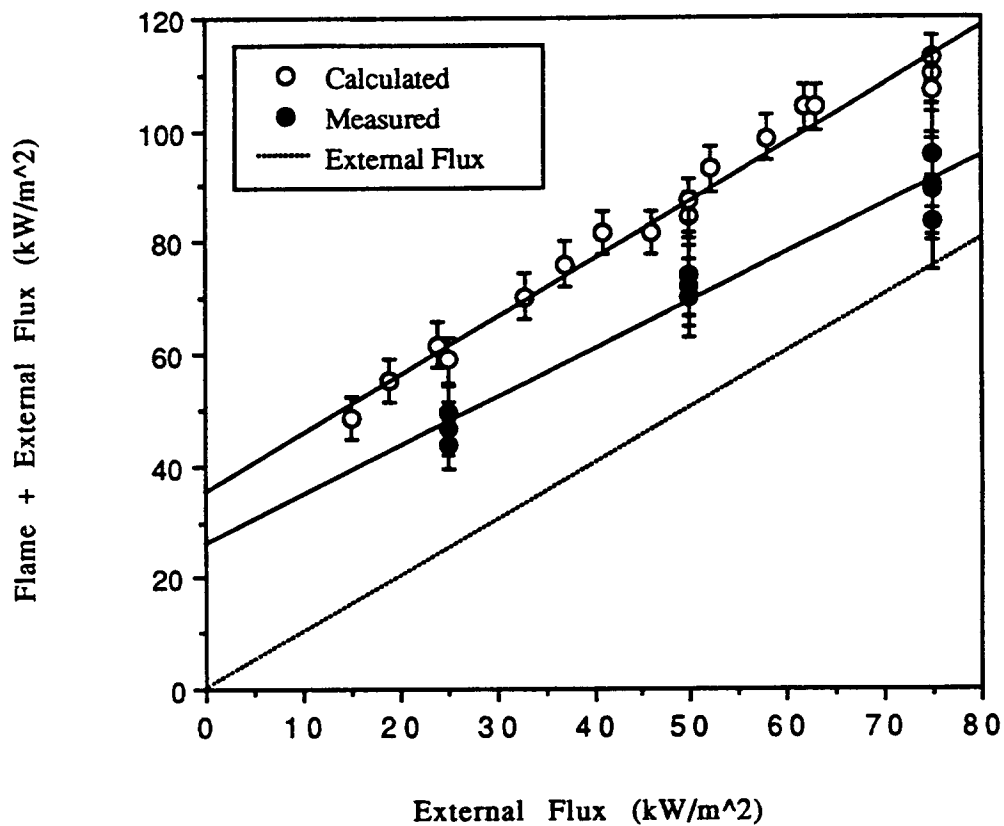
Figure 6.4. Calculated and measured flame plus external heat flux as a function of external heat flux for black PMMA

$$\dot{q}''_{sens} = \dot{q}''_{fl,r} + \dot{q}''_{ext} + h_c \left(\frac{\xi}{e^{\xi} - 1} \right) (T_{fl} - T_w) - \sigma T_w^4 \qquad (6.4)$$

or,

$$\dot{q}''_{sens} = \dot{q}''_{fl,r} + \dot{q}''_{ext} + h_c \left(\frac{\xi}{e^{\xi} - 1} \right) ((T_{fl} - T_v) + (T_v - T_w)) - \sigma T_w^4 . \qquad (6.5)$$

The flame and external flux to the PMMA surface measured by the sensor is,

$$\dot{q}''_{fl} + \dot{q}''_{ext} = \dot{q}''_{sens} - h_c \left(\frac{\xi}{e^{\xi} - 1} \right) (T_v - T_w) + \sigma T_w^4 . \qquad (6.6)$$

The "corrected" sensor flux is the total flame plus external flux incident to the center of the PMMA surface at temperature T_v. The present best data with indicated variability is plotted as shown in Figure 6.4. The calculated values come from applying Eq. (5.25), which becomes,

$$\dot{q}''_{fl} + \dot{q}''_{ext} = \dot{m}''_s L + \varepsilon \sigma T_v^4 , \qquad (6.7)$$

with L = 2.77 kJ/g and T_v corresponding to the ignition temperature extrapolated in Section 6.1. This gives the average flame plus external heat flux to the PMMA surface. It is higher than the sensor value either because the center has a lower flux than the calculated average flux, or because the sensor has a systematic error. The calculated results yield a constant value for the average flame heat flux of approximately 37 kW/m².

6.2.3 Transient Mass Loss Rate

Based on the result of the average flame heat flux found above, Figures 6.5, 6.6 and 6.7 show a comparison of calculated mass loss rates compared to data for 25, 50, 75 kW/m². The mass loss rates are calculated using Eqns. (5.20), (5.22), and the derived properties:

$$T_{ig} = T_v = 180\ ^\circ C \qquad\qquad k = 0.432 \times 10^{-3}\ \frac{kW}{m \cdot K}$$

$$\rho = 1190\ \frac{kg}{m^3} \qquad\qquad c = 4.12\ \frac{kJ}{kg \cdot K}$$

$$L = 2.77\ \frac{kJ}{g}$$

The predictions are, at worst, 20 percent different from the measured transient burning rate. Figure 6.8 shows the variations in the calculation if the more directly measured (literature) values [2] of T_v, T_{ig}, k and c are used to calculate the mass loss rate, i.e.,

$$T_{ig} = 275 - 360\ ^\circ C \qquad\qquad T_v = 365 - 385\ ^\circ C$$

$$k = 0.235 \times 10^{-3}\ \frac{kW}{m \cdot K} \qquad\qquad c = 2.22\ \frac{kJ}{kg \cdot K}$$

52

Figure 6.5. Calculated transient mass loss rates of black PMMA with a 25 kW/m^2 external heat flux
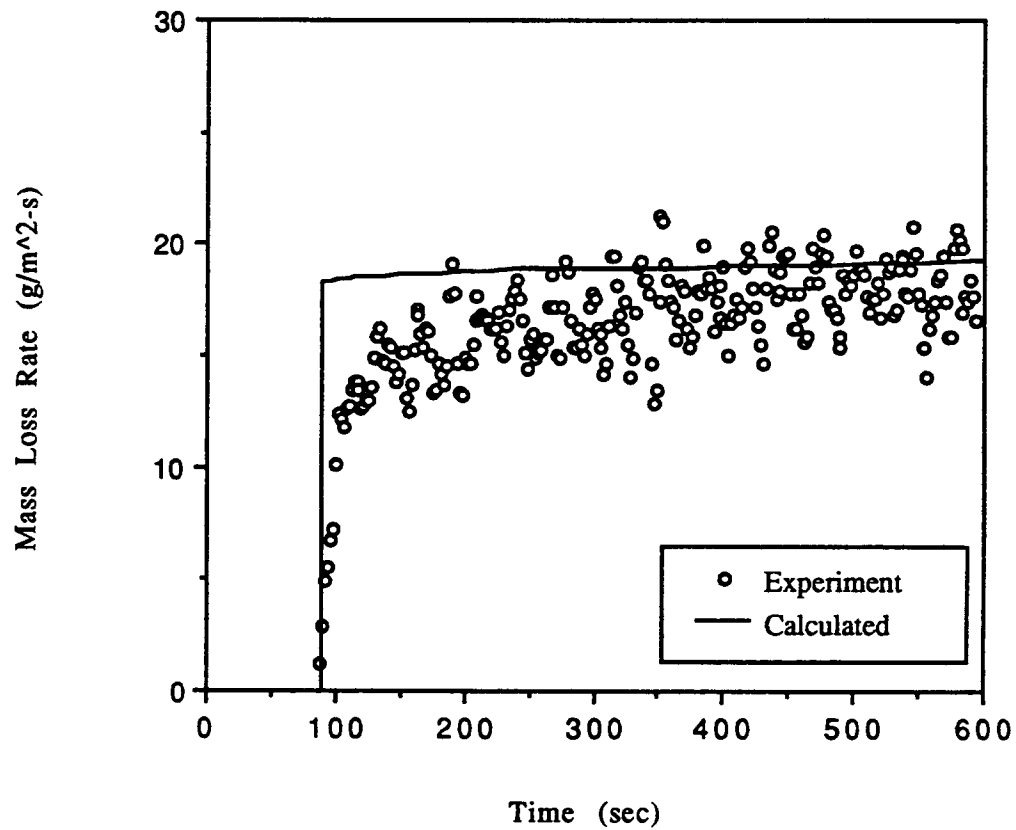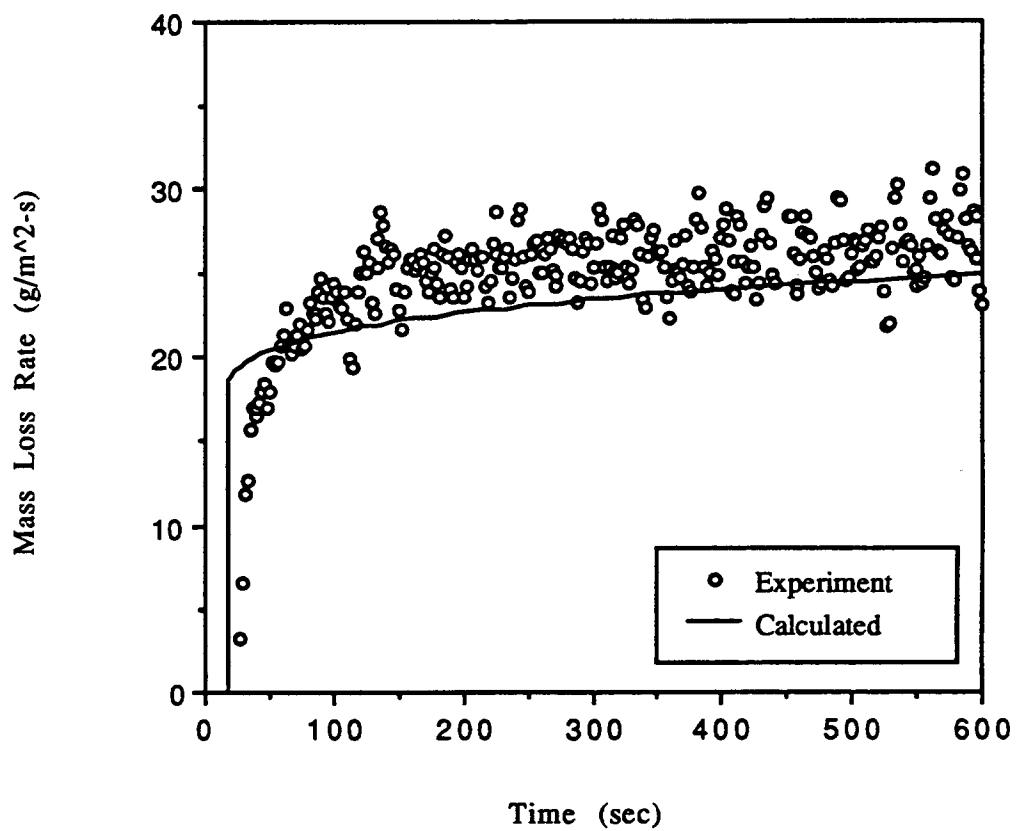
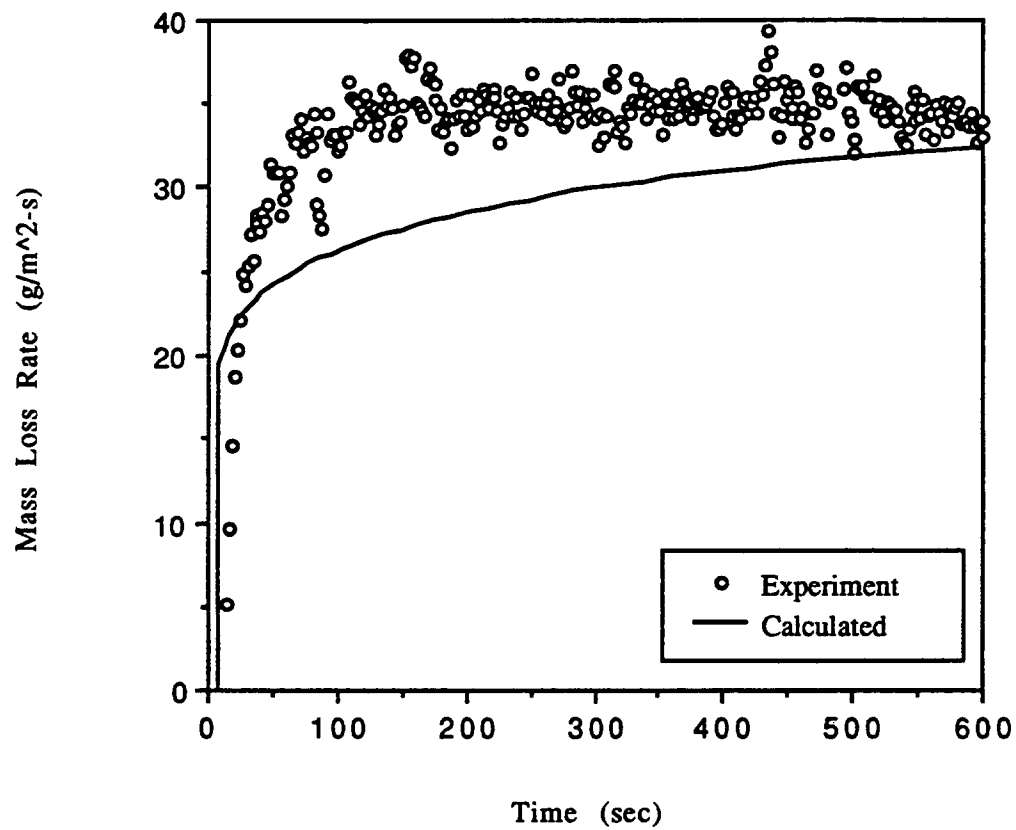**Figure 6.6.** Calculated transient mass loss rates of black PMMA with a 50 kW/m² external heat flux

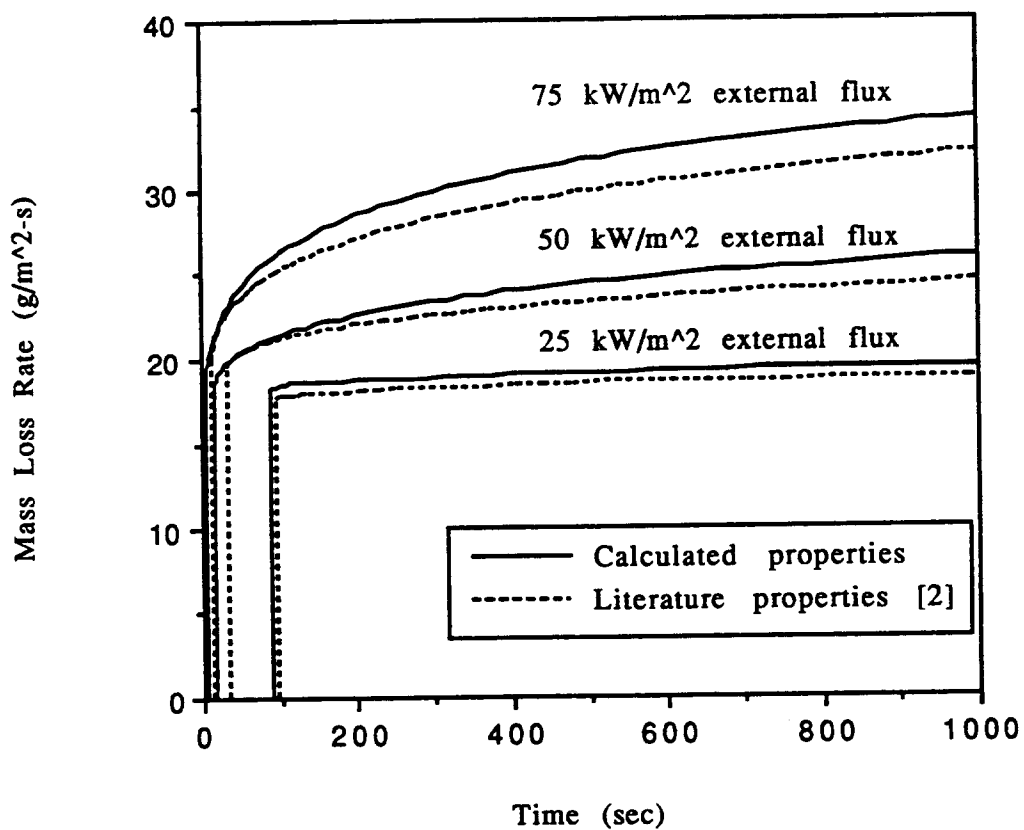**Figure 6.7.** Calculated transient mass loss rates of black PMMA with a 75 kW/m^2 external heat flux

Figure 6.8. Calculated transient mass loss rates of black PMMA using calculated and literature material property values

56

A modeling prescription has been developed which can use Cone Calorimeter data to derive useful properties needed to predict ignition and transient burning rates for thermoplastic-like materials. The level of accuracy has been demonstrated for PMMA. The low critical flux of PMMA may have given poorer results for the thermal inertia and ignition temperature than would be expected for materials with higher critical fluxes. This is because the ignition model is more accurate at higher fluxes. However, the simplicity of the ignition model is advantageous, and can be used with greater accuracy at higher heat fluxes to infer the critical flux for ignition without direct measurement.

The flame heat flux for samples in the Cone Calorimeter appears to be constant for a given material due to the flame configuration. This was found to be true for both the theoretical (Section 5.3) and experimental (Sections 4.3 and 6.2) results. For black PMMA, the flame heat flux is approximately 37 kW/m^2.

It appears that all PMMA's are not alike, and pigmented samples may have higher heat of gasification values than clear samples. The black Polycast PMMA used in the present experiments yielded different results from the Rohm & Hass PMMA used by Tewarson and Pion [24] and Jackson [25]. Likewise, the cast PMMA used by Vovelle [15] yielded different results than the Polycast PMMA. This could be due to molecular structure of the sample, as well as the pigmentation.

The heat flux measurement in the flame had many problems due to deposition of the vaporized PMMA. These have not been totally resolved, and appear to be associated with the nature of the phenomena and not necessarily the sensor. A higher temperature sensor may prove better.

For black PMMA, the extrapolation of the ignition temperature, thermal inertia and the heat of gasification yielded results quite different from literature values. However, using the calculated values in this model provided good results for the

prediction of burning rate compared to experimental data. An assessment of this testing prescription will be performed by evaluating several different thermoplastic samples. Mass loss data will be measured for the new materials in the same manner as the black PMMA. Flame heat flux will not be directly measured; rather, it will be inferred using the method prescribed in Section 6.2. Again, transient mass loss rate data will be calculated using the deduced material properties and compared to the experimental results. Once the methodology has been validated for thermoplastic materials, other materials, such as wood, will be examined.

NOMENCLATURE

c - specific heat

E/R - material constant (Eq. 4.1)

h_c - convective heat transfer coefficient

k - thermal conductivity

l - beam length

L - heat of gasification

m - mass

Q - power output

q - heat flow

r - stoichiometric oxygen to fuel mass ratio

T - temperature

t - time

y - space coordinate

$Y_{ox, \infty}$ - ambient oxygen mass fraction

α - thermal diffusivity

δ - thermal penetration depth

ΔH_v - heat of vaporization

ΔH_c - heat of combustion

ε - emissivity

κ - absorption-emission coefficient

ρ - density

σ - Stefan Boltzmann constant

ξ - variable (Eq. 5.17)

χ - heat fraction

Subscript

c - convective

cr - critical

e - external

fl - flame

f,c - flame convection

f,r - flame radiation

g - gas

ig - ignition

o - initial, ambient

m - mean

r - radiative

s - steady

sens - sensor

v - vaporization

w - water

Superscripts

$(\dot{\ })$ - per unit time

$(\ )''$ - per unit area

REFERENCES

1. Quintiere, J. G., "A Semi-Quantitative Model for the Burning of Solid Materials", National Institute of Standards and Technology, NIST-4840, June, 1992.

2. Steckler, K. D., Kashiwagi, T., Baum, H. R., and Kanemaru, K., "Analytical Model for Transient Gasification of Non-Charring Thermoplastic Materials", Fire Safety Science Proceedings of Third (International) Symposium, pp. 895-904, G. Cox and B. Landford, eds., Elsevier Applied Science, London, 1991.

3. Quintiere, J. G. and Iqbal, N., "A Burning Rate Model for Materials", accepted by Fire and Materials, July, 1993.

4. Delichatsios, M. M., Matthews, M. K., and Delichatsios, M. A., "Upward Fire Spread Code: Version 1: Non-Charring Fuels", FMRC J.I.ORO J2.BU, Factory Mutual Research, November, 1990.

5. Chen, Y., Delichatsios, M. A. and Motevalli, V., "Materials Pyrolysis Properties, Part I: An Integral Model for One-Dimensional Transient Pyrolysis of Charring and Non-Charring Materials", Combustion Science and Technology, Vol. 88, pp. 309-328, 1993.

6. Iqbal, N., "Burning Rate Model for Thermoplastic Materials", Department of Fire Protection Engineering, University of Maryland at College Park, May 1993.

7. Modak , A. and Croce, P., "Plastic Pool Fires", Combustion and Flames, Volume 30, 1977.

8. Standard Test Method for Heat and Visible Smoke Release Rates for Materials and Products Using Oxygen Depletion, (ASTM E 1354), American Society for Testing and Materials, Philadelphia, PA.

9. Wickstrom, U. and Goransson, U., "Prediction of Heat Release Rates of Surface Materials in Large-Scale Fire Tests Based on Cone Calorimeter Results", ASTM Journal of Testing and Evaluation, Vol. 15, No. 6, 1987.

10. Karlsson, B. "Modeling Fire Growth on Combustible Lining Materials in Enclosures", Report TVBB-1009, Lund University, Department of Fire Safety Engineering, Lund, Sweden, 1992.

11. Quintiere, J. G., "A Simulation Model for Fire Growth on Materials Subject to a Room-Corner Test", Fire Safety Journal, Vol. 18, 1992.

12. Quintiere, J. G., Haynes, G., and Rhodes, B. T., "Applications of a Model to Predict Flame Spread over Interior Finish Materials in a Compartment", International Conference for the Promotion of Advanced Fire Resistant Aircraft Interior Materials, FAA Technical Center, Atlantic City, NJ, March, 1993.

13. Mitler, H. E., "Algorithm for the Mass-Loss Rate of a Burning Wall", Fire Safety Science Proceedings, Second Internation Symposium, June 13-17, 1988, Tokyo, Japan, Hemisphere Pub. Corp., NY, ed. T. Wakamatsu, 1989.

14. Agrawal, S. and Atreya, A., "Wind-Aided Flame Spread over an Unsteady Vaporizing Solid", 24th Symposium (International) on Combustion, The Combustion Institute, Pittsburgh, PA, 1992.

15. Vovelle, C., Delfau, J.L., Reuillon, M., Bransier, J. and Laraqui, N., "Experimental and Numerical Study of the Thermal Degradation of PMMA", Combustion Science and Technology, Vol. 53, pp. 187-201, 1987.

16. Thompson, H. E. and Drysdale, D. D., "Effect of Sample Orientation on the Piloted Ignition of PMMA", pp. 35-42, INTERFLAM, 1990.

17. Kashiwagi, T. and Omori, A., "Effects of Thermal Stability and Melt Viscosity of Thermoplastics on Piloted Ignition", 22nd Symposium (International) on Combustion, The Combustion Institue, Pittsburgh, PA, 1988.

18. Abu-Zaid, M. and Atreya, A., "Effect of Water on Piloted Ignition of Cellulosic Materials", National Institute of Standards and Technology, NIST-GCR-89-561, February, 1989.

19. Janssens, M., "Fundamental Thermophysical Characteristics of Wood and their Role in Enclosure Fire Growth", Doctor of Philosophy Disertation, University of Gent, Belgium, September, 1991.

20. Orloff, L. and deRis, J., "Froude Modeling of Pool Fires", 19th Symposium (International) on Combustion, pp. 885-895, The Combustion Institute, Pittsburgh, PA, 1982.

21. Howell, J. and Siegel, R., Thermal Radiation Heat Transfer, 2nd Edition, Hemisphere Publishing Corporation, New York, 1981.

22. DeRis, J., "Fire Radiation - A Review", 17th Symposium (International) on Combustion, The Combustion Institute, Pittsburgh, PA, 1978.

23. Mikkola, E. and Wichman, I., "On the Thermal Ignition of Combustible Materials", Fire and Materials, Vol. 14, 1989.

24. Tewarson, A. and Pion, R. F., "Flammability of Plastics - I. Burning Intensity", Combustion and Flame, The Combustion Institute, 1976.

25. Jackson, J. L., "Direct Measurement of Heat of Gasification for Polymethylmethacrylate", National Institute of Standards and Technology, NISTIR 88-3809, September, 1986.

APPENDIX A

DATA ACQUISITION PROGRAM

```
10      OPTION BASE 1
20      DIM In$[100], Out(6)
21      P0=-5.115307103E-2
22      P1=2.485028007E+4
23      P2=-3.826622822E+5
24      P3=9.966105673E+7
25      P4=-1.082062357E+10
26      P5=6.039285524E+11
27      P6=-1.910899962E+13
28      P7=3.478234730E+14
29      P8=-3.399102821E+15
30      P9=1.382851398E+16
32      CALL Set_datacom
33      CLEAR 722
34      CLEAR 709
35      FOR I=1 TO 8
36        ON KEY I LABEL "         " GOSUB Beeper
37      NEXT I
38      OUTPUT 709;"F00 L05 I1"
39      OUTPUT 709;"00"
40      OUTPUT 722;"L1 RS1 D0 Z0 F1 R1 0.01STD SO1 10.0STI 6STN T4 SM004 -
        7STR RER Q"
41      OUTPUT 722;"X1"
42      Oncom=0
43      ON KEY 1 LABEL " COM   OFF" GOSUB Comonoff
44      ON KEY 4 LABEL " END   TEST" GOTO Endit
45      ON KEY 5 LABEL " START   TEST" GOTO Onward
46        !
47        !
48 Spin: !
49      GOTO Spin
50        !
51        !
52 Onward:  Ti0=TIMEDATE MOD 86400
53 Restart: !
54      TRIGGER 722
55      TI1=(TIMEDATE MOD 86400)-TI0
58      ENTER 722;In$
59      OUTPUT 722;"X1"
60      ENTER In$;Out(*)
61      IF Oncom=1 THEN
62      FOR I=2 TO 6 STEP 2
63        C(I)=Out(I)*(P6+Out(I)*(P7+Out(I)*(P8+Out(I)*P9)))
64        T(I)=P0+Out(I)*(P1+Out(I)*(P2+Out(I)*(P3+Out(I)*(P4+Out(I)*(P5+C(I))))))
65      NEXT I
66        OUTPUT 9 USING "DDDD.D,#";Ti1
69        OUTPUT 9;"    ";
70        OUTPUT 9 USING "DD.D,#";Out(1)*5465
71        OUTPUT 9;"    ";
72        ON ERROR GOTO Error
74        OUTPUT 9 USING "DDDD.D,#";T(2)-2.3
```

```
75      OUTPUT 9;"    ";
76      OUTPUT 9 USING "DDD.D,#";Out(3)*11360
77      OUTPUT 9;"    ";
78      OUTPUT 9 USING "DDD.D,#";T(4)
79      OUTPUT 9;"    ";
80      OUTPUT 9 USING "DDDD.DD,#";Out(5)*1000*(-0.58597)
81      OUTPUT 9;"    ";
82      OUTPUT 9 USING "DDDD.D";T(6) +0.4
83      ENDIF
84      PRINT USING "DDDD.D,#";Ti1
85      PRINT "   ";Out(*)
86      LOOP
87        EXIT IF (TIMEDATE MOD 86400)-Ti0>=Ti1+2
88      END LOOP
89      GOTO Restart
90 Comonoff: !
91      IF Oncom=0 THEN
92        Oncom=1
93        ON KEY 1 LABEL " COM   ON " GOSUB Comonoff
94      ELSE
95        Oncom=0
96        ON KEY 1 LABEL " COM   OFF " GOSUB Comonoff
97      ENDIF
98      RETURN
99 Beeper: !
100     BEEP
101     RETURN
102 Error: !
103     OUTPUT 9;"    ";
104     GOTO 75
106 Endit: !
107     ABORT 7
108     CLEAR 722
109     CLEAR 709
110     END
111     !
112 SUB Set_datacom
113     Sc=9
114     CONTROL Sc,0;1
115     CONTROL Sc,3;9600
124     CONTROL Sc,4;3
134     CONTROL Sc,5;0
144 SUBEND
```

APPENDIX B

PMMA IGNITION TIME and SURFACE TEMPERATURE

Test Number	External Flux (kW/m²)	Time to Ignite (sec)
t4	15	263
t1	19	141
t8	19	135
t5	24	81
t32	25	88
t33	25	95
t34	25	73
t35	25	90
t24	33	59
t9	37	33
t2	41	27
t22	46	not measured
t36	50	20
t37	50	25
t38	50	26
t39	50	22
t3	52	19
t23	58	not measured
t7	62	15
t10	63	14
t41	75	12
t42	75	12
t43	75	12
t44	75	13

Table B.1. Experimental ignition time for black PMMA

67

Test Number	External Flux (kW/m²)	Ignition Temperature (° C)	Vaporization Temperature (° C)
t4	15	250	325
t8	19	265	350
t5	24	280	365
t22	46	345	375
t23	58	355	380

Table B.2. Experimental ignition and vaporization temperatures for black PMMA
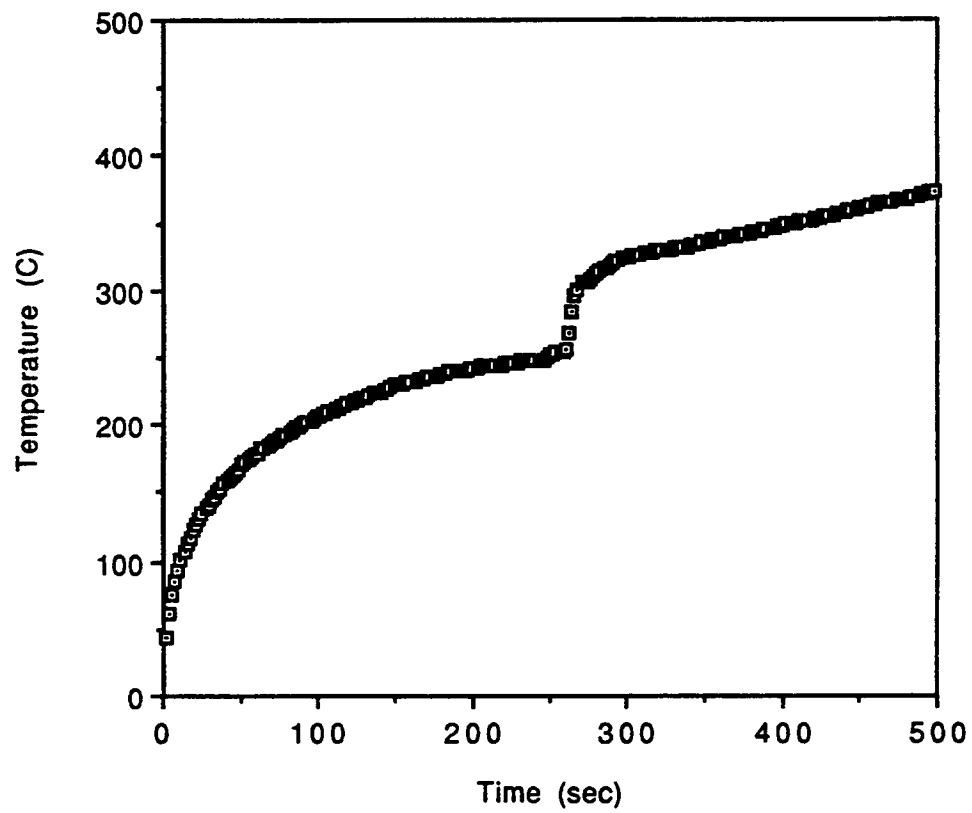
Figure B.1. Test number t4 - surface temperature results for black PMMA exposed to a 15 kW/m² external flux
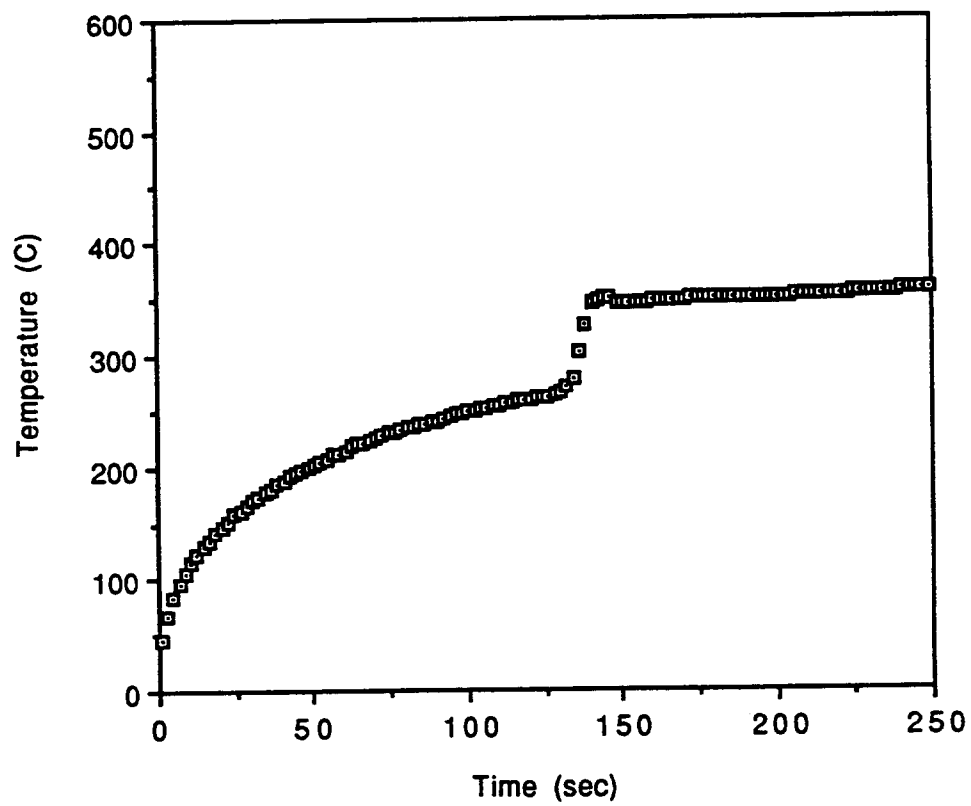
Figure B.2. Test number t8 - surface temperature results for black PMMA exposed to a
19 kW/m^2 external flux
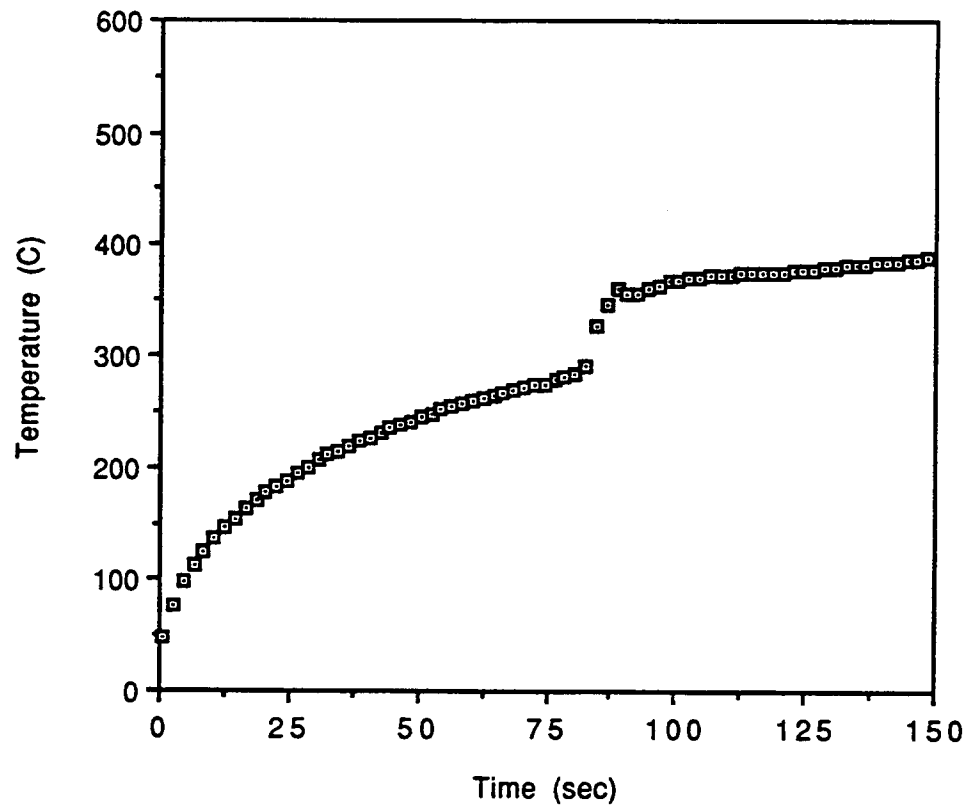
Figure B.3. Test number t5 - back side surface temperature results for black PMMA
exposed to a 24 kW/m² external flux
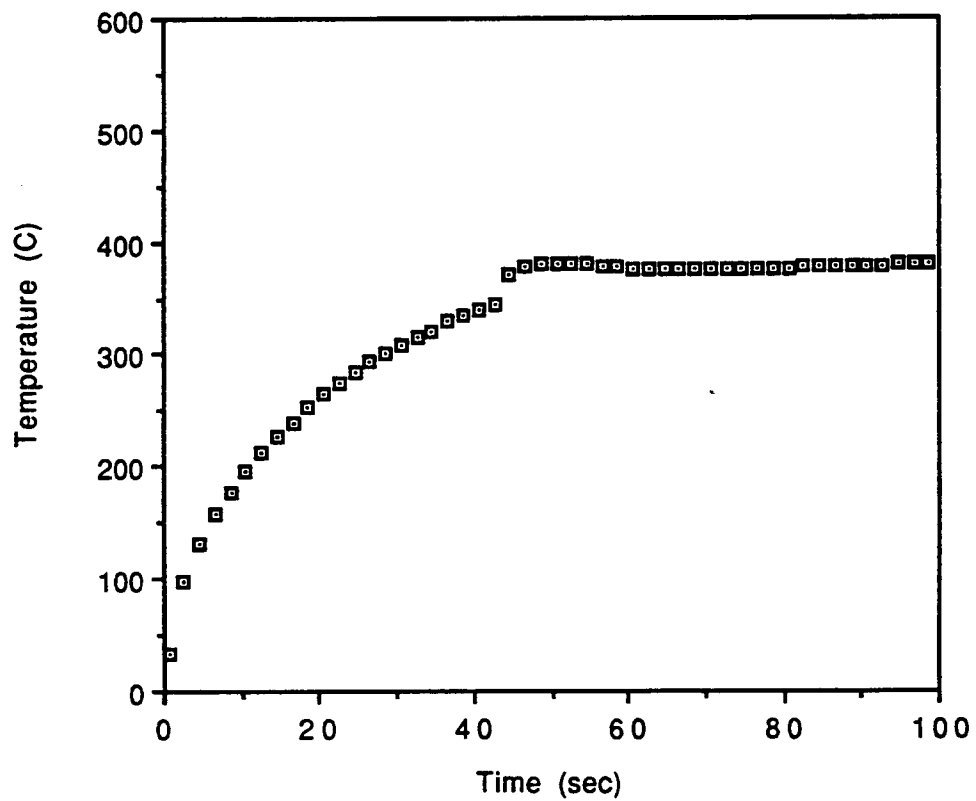
Figure B.4. Test number t22 - back side surface temperature results for black PMMA exposed to a 46 kW/m² external flux
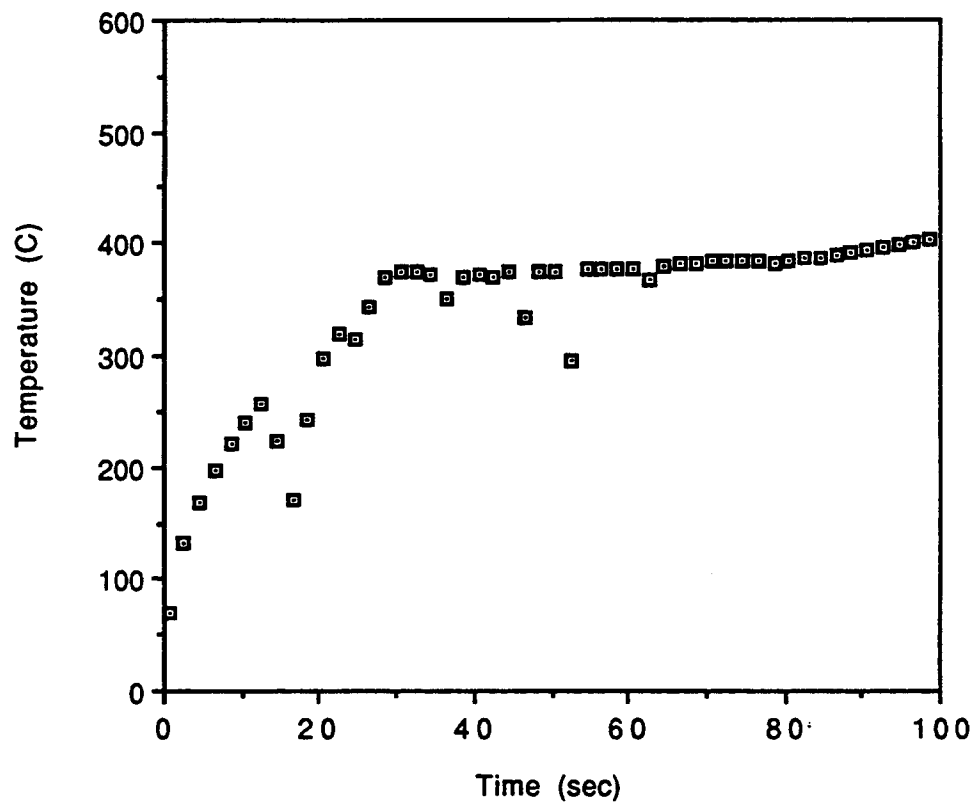
Figure B.5. Test number t23 - surface temperature results for black PMMA exposed to a 58 kW/m² external flux
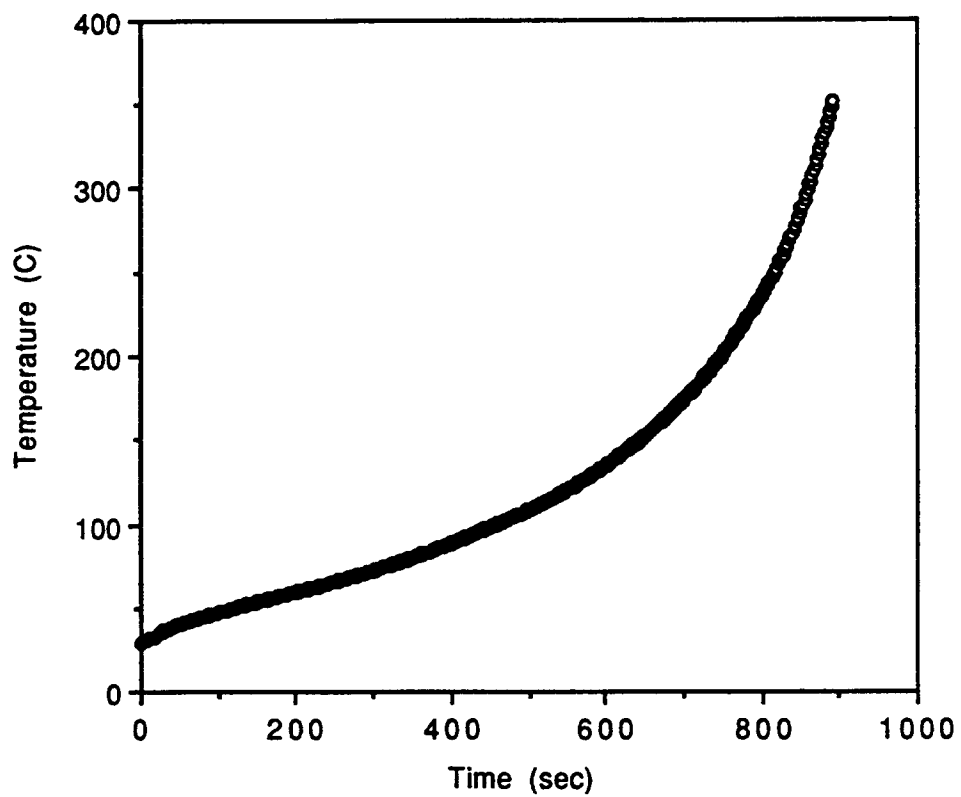
Figure B.6. Test number t10 - back side surface temperature results for black PMMA
exposed to a 63 kW/m² external flux

Test Number	External Flux (kW/m²)	Steady Mass Loss Rate (g/m² s)
t4	15	15
t1	19	17
t8	19	17
t5	24	19
t32	25	18
t33	25	18
t34	25	18
t35	25	18
t24	33	22
t9	37	24
t2	41	26
t22	46	26
t36	50	28
t37	50	27
t38	50	27
t39	50	28
t3	52	30
t23	58	32
t7	62	34
t10	63	34
t41	75	37
t42	75	36
t43	75	36
t44	75	35

Table C.1. Experimental steady mass loss rate for black PMMA
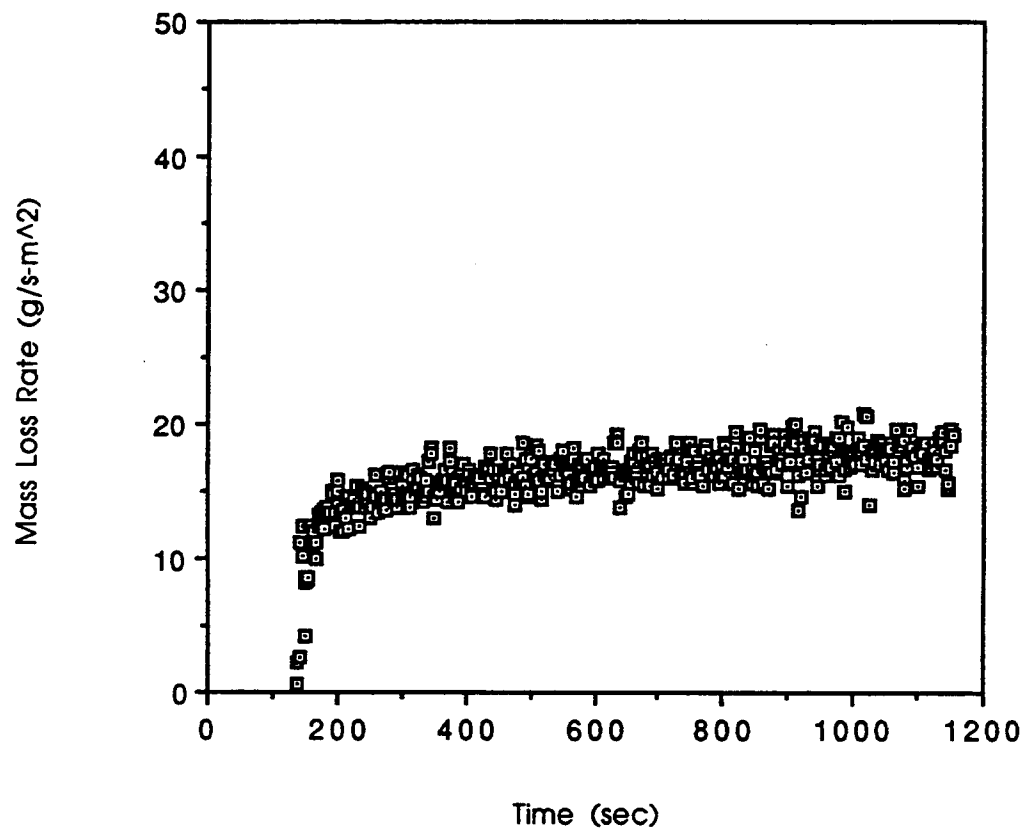
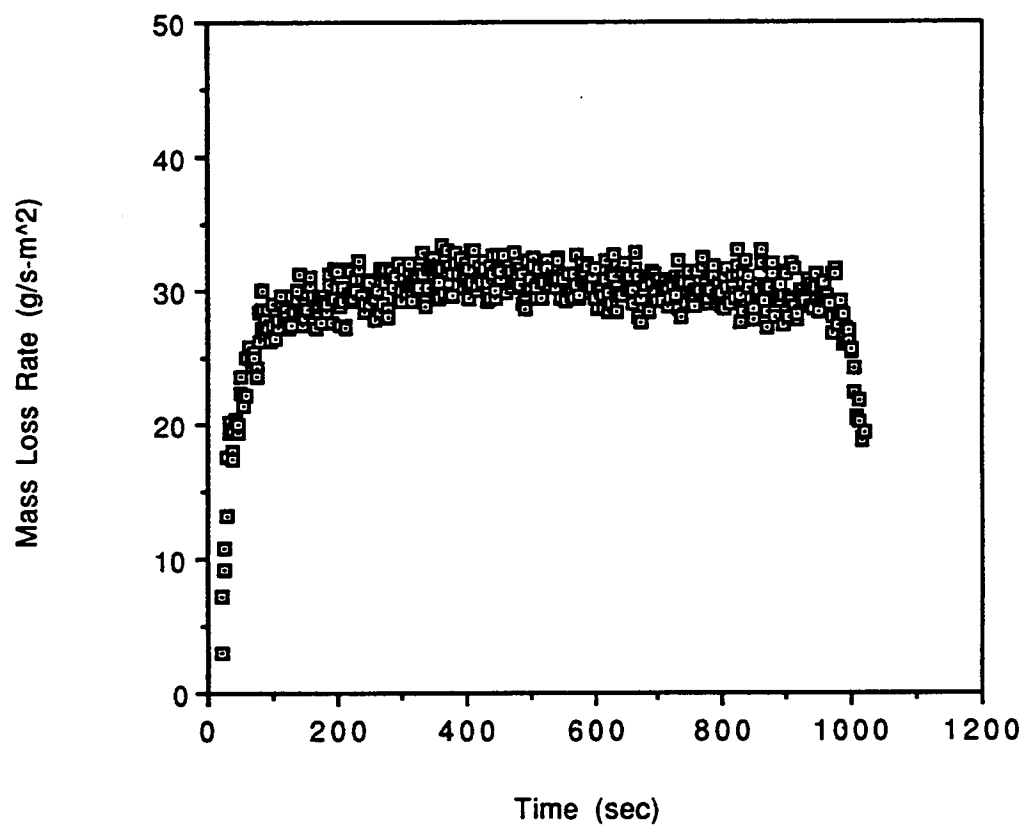Figure C.1. Test number t1 - transient mass loss rate for black PMMA exposed to a 19 kW/m2 external flux
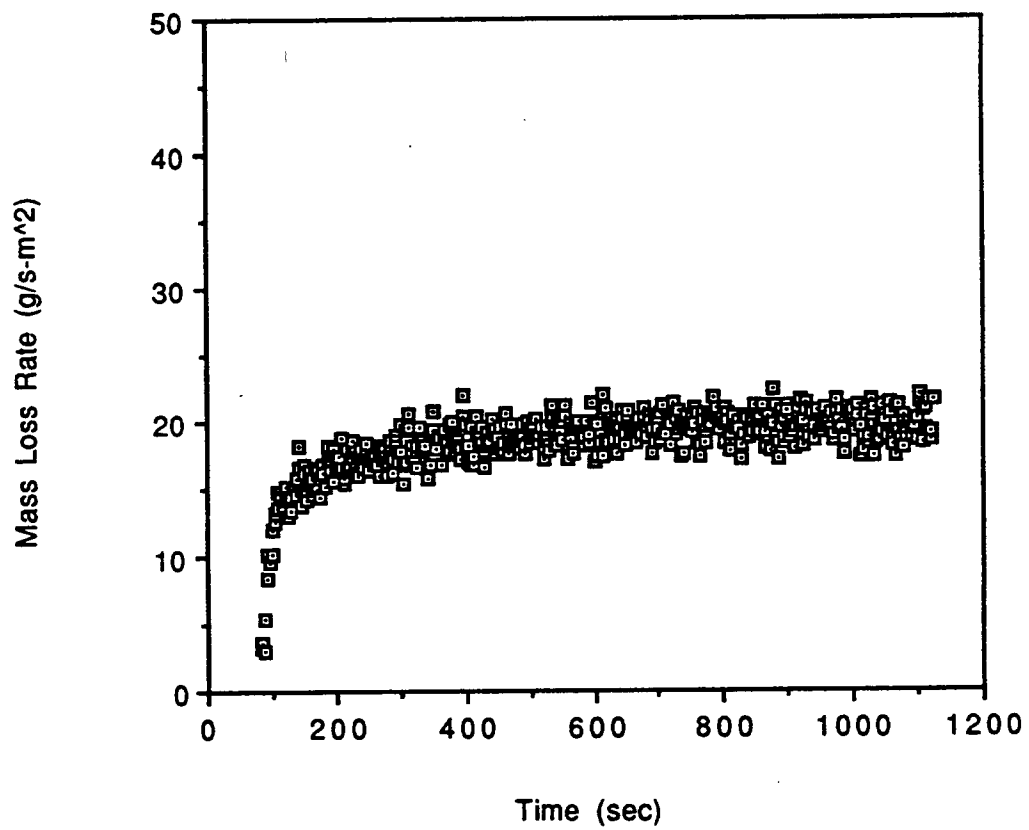
Figure C.2. Test number t5 - transient mass loss rate for black PMMA exposed to a 24 kW/m2 external flux
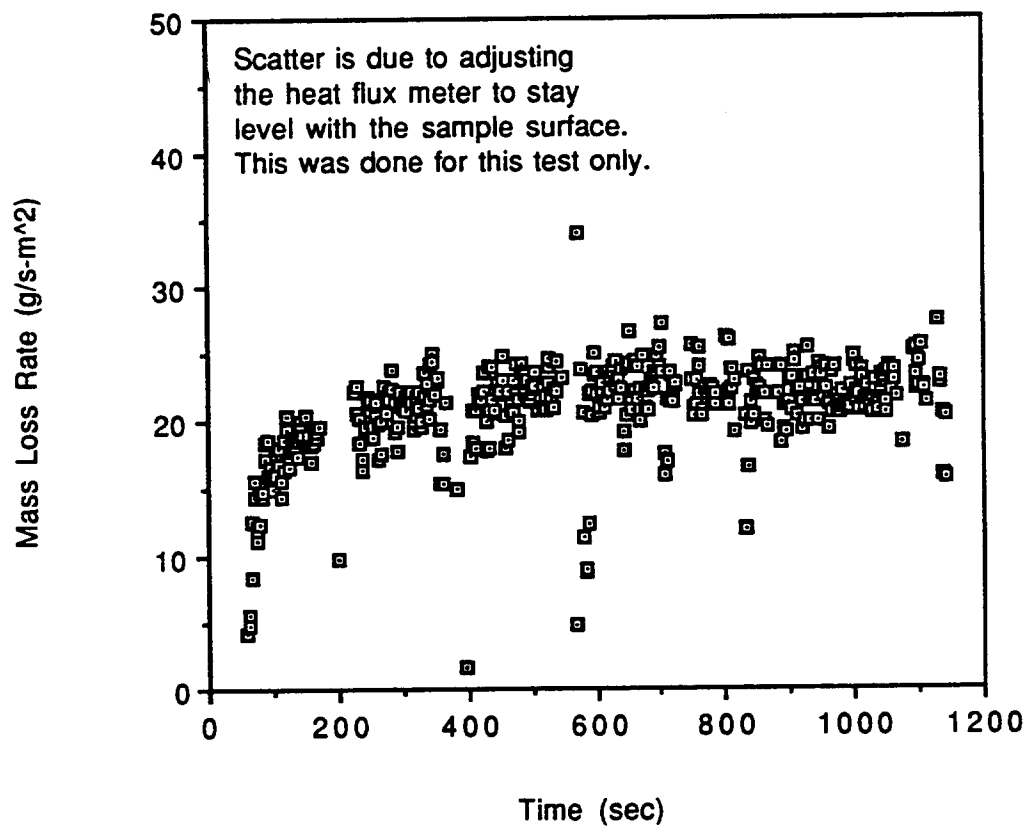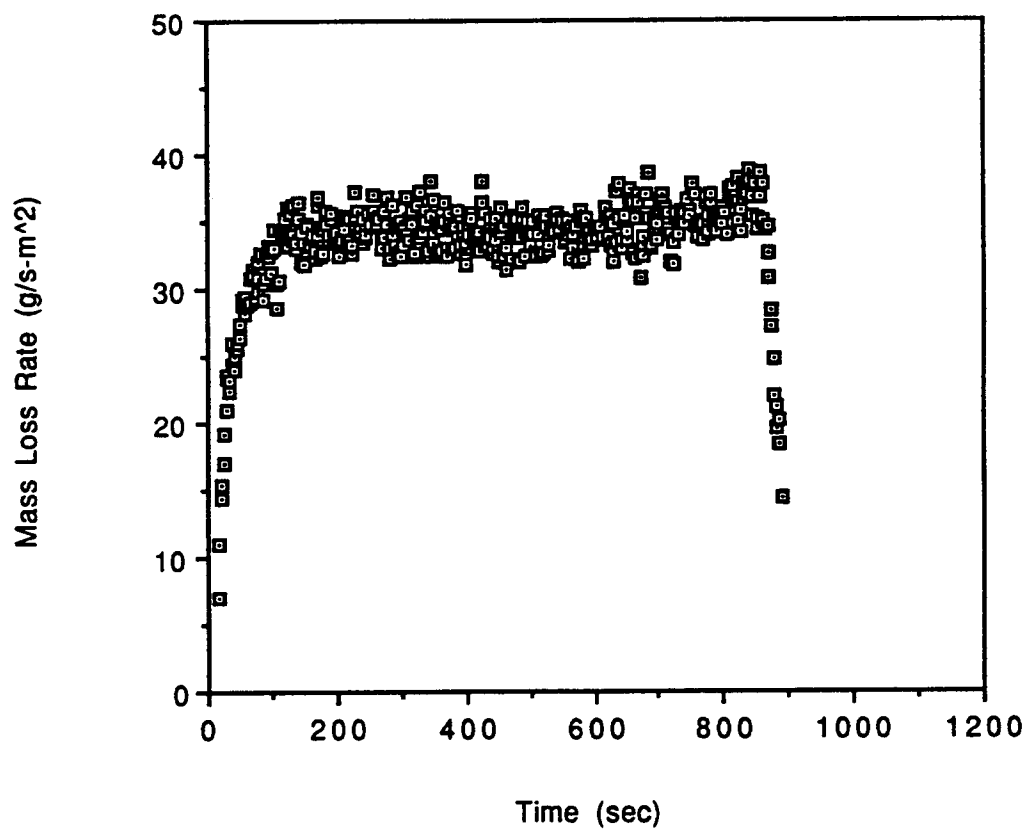
Figure C.3. Test number t24 - transient mass loss rate for black PMMA exposed to a 33 kW/m2 external flux
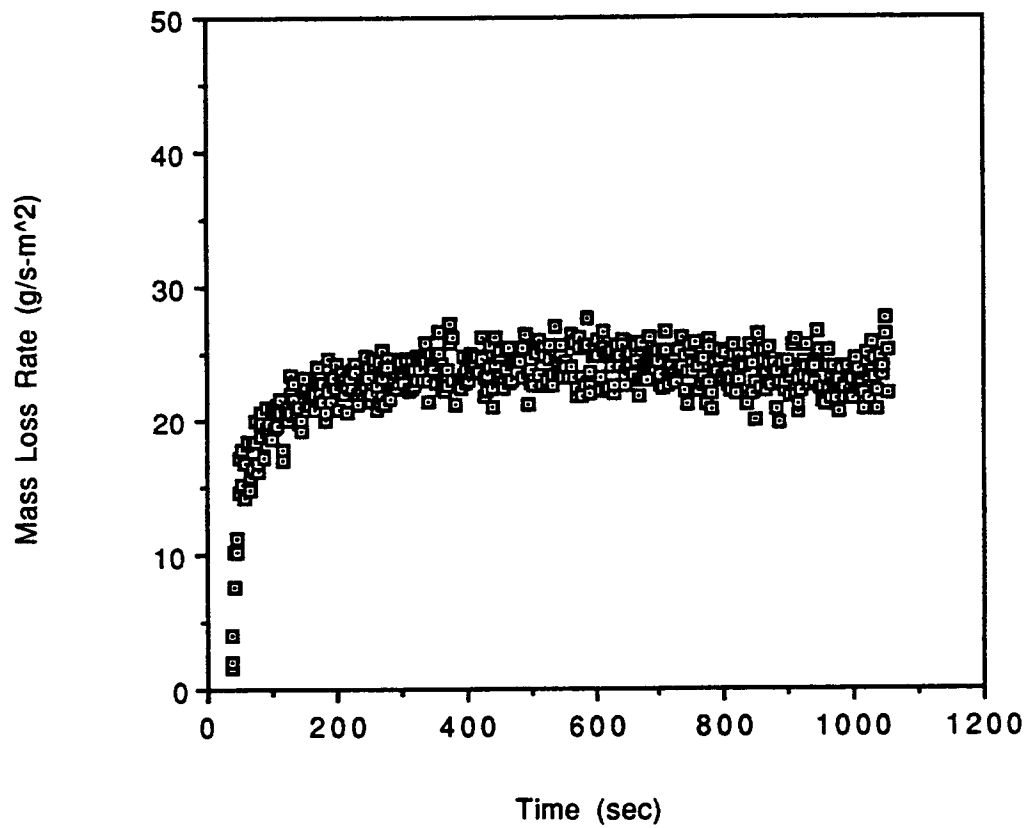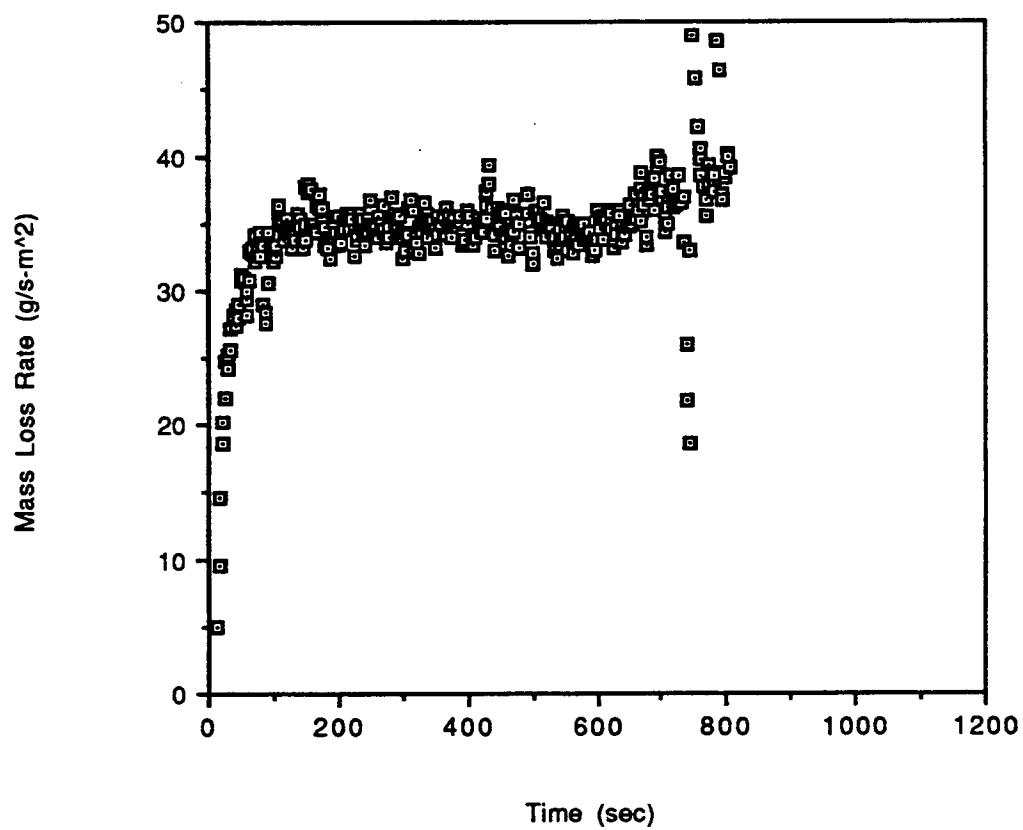
Figure C.4. Test number t9 - transient mass loss rate for black PMMA exposed to a
37 kW/m2 external flux
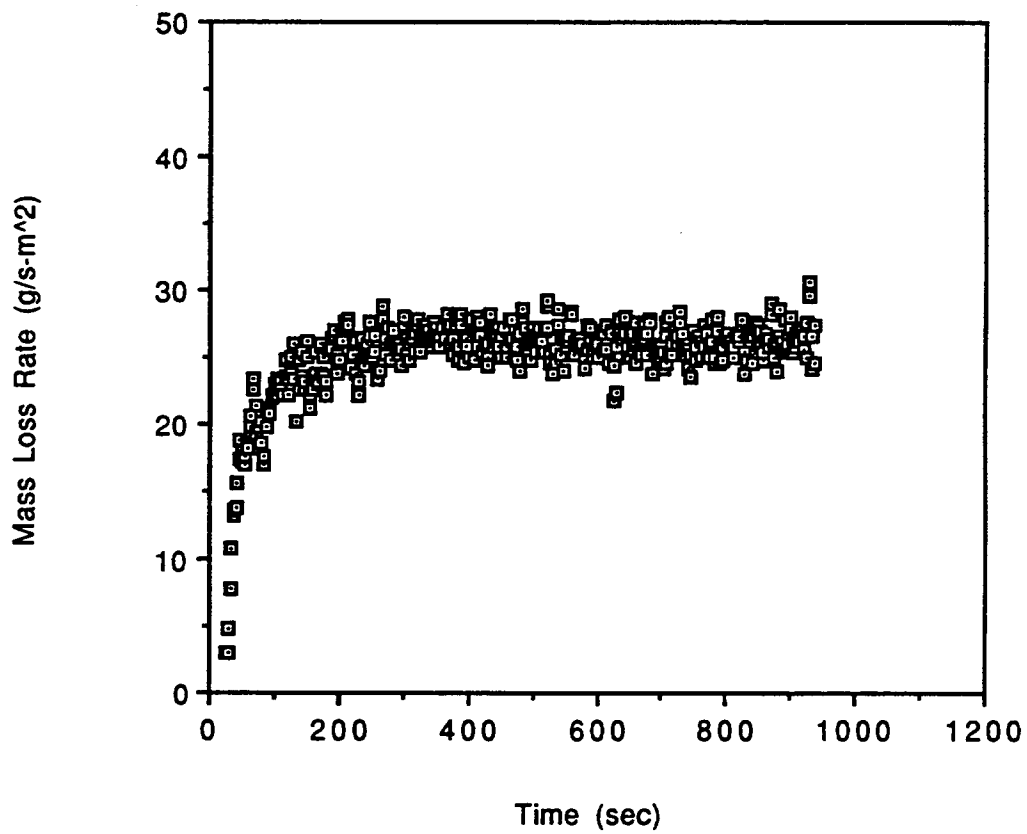
Figure C.5. Test number t2 - transient mass loss rate for black PMMA exposed to a
41 kW/m2 external flux
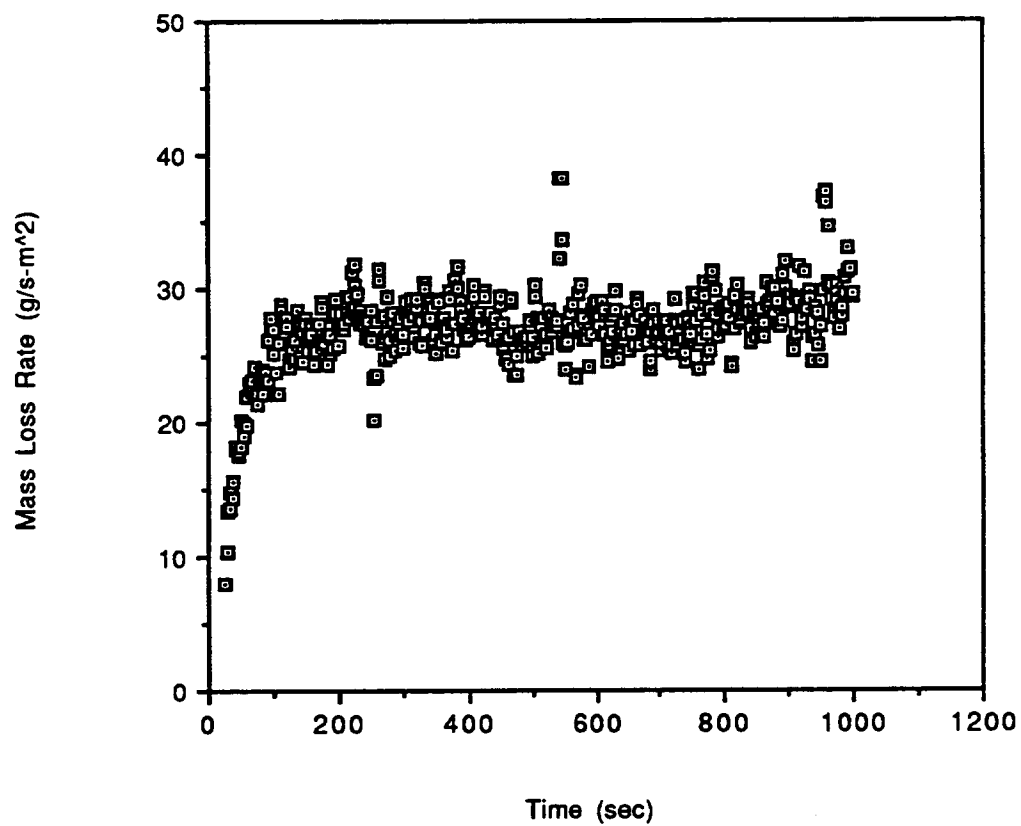
Figure C.6. Test number t37 - transient mass loss rate for black PMMA exposed to a
50 kW/m2 external flux

Figure C.7. Test number t3 - transient mass loss rate for black PMMA exposed to a
52 kW/m2 external flux

Figure C.8. Test number t10 - transient mass loss rate for black PMMA exposed to a 63 kW/m2 external flux

Figure C.9. Test number t44 - transient mass loss rate for black PMMA exposed to a 75 kW/m2 external flux

APPENDIX D

Test Number	External Flux (kW/m²)	Total Incident Flux (kW/m²)
t4	15	33
t1	19	48
t8	19	49
t5	24	60
t32	25	* 50
t33	25	* 47
t34	25	* 44
t35	25	* 47
t24	33	53
t9	37	60
t2	41	81
t22	46	not measured
t36	50	* 70
t37	50	* 72
t38	50	* 70
t39	50	* 74
t3	52	95
t23	58	not measured
t7	62	92
t10	63	73
t41	75	* 83
t42	75	* 90
t43	75	* 89
t44	75	* 95

Table D.1. Experimental total incident flux (as measured by the heat flux gage) for black PMMA. A * indicates that the measurement is used in the analysis.
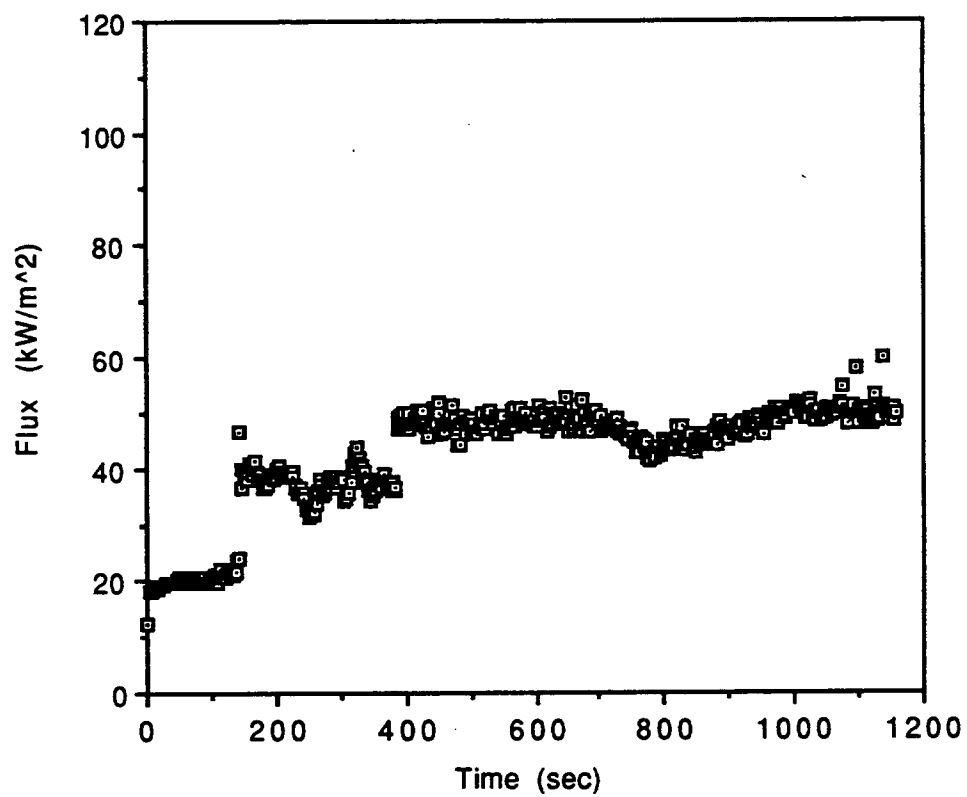
Figure D.1. Test number t1 - transient total incident flux measured by the heat flux gage for black PMMA exposed to a 19 kW/m² external flux
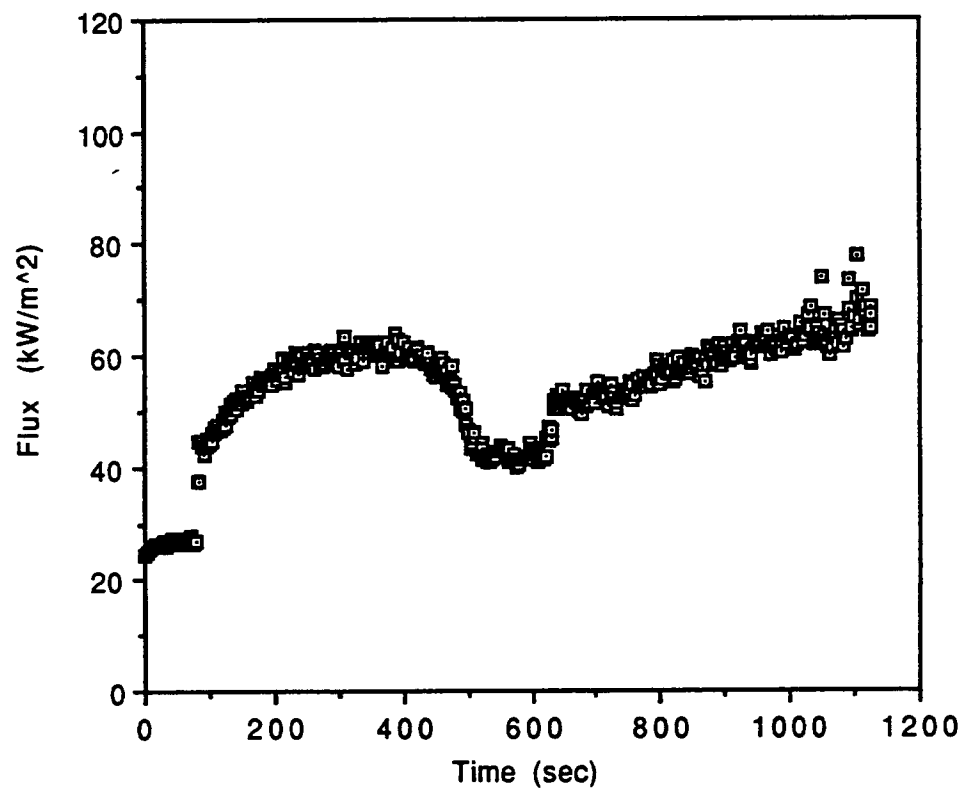
Figure D.2. Test number t5 - transient total incident flux measured by the heat flux gage
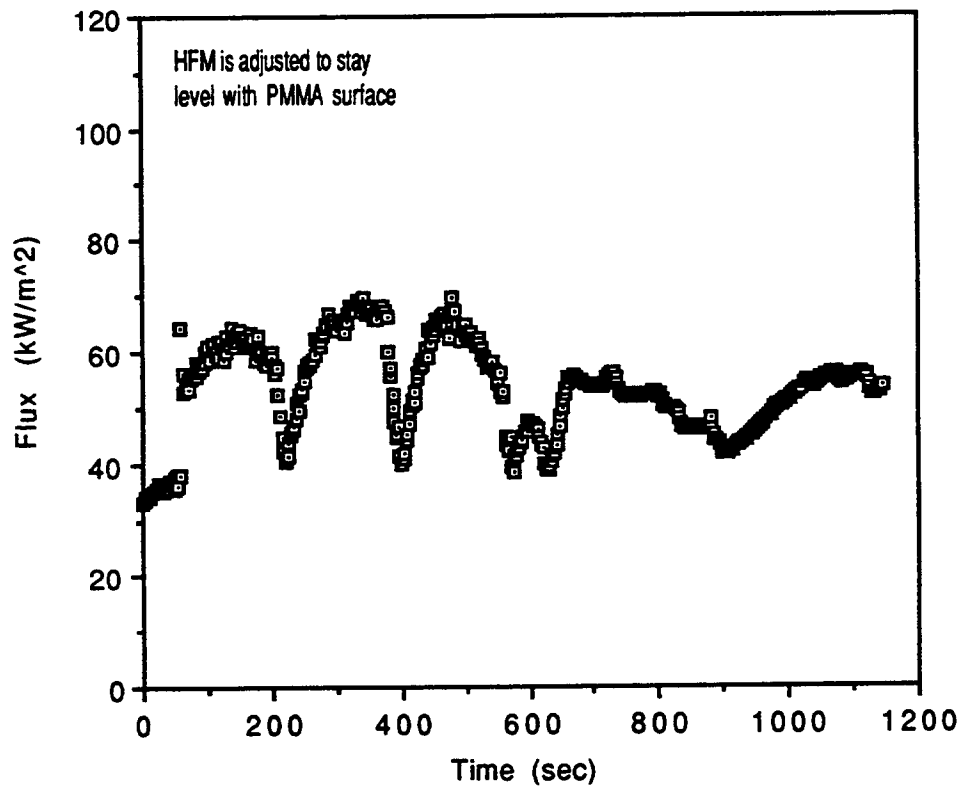for black PMMA exposed to a 24 kW/m² external flux

Figure D.3. Test number t24 - transient total incident flux measured by the heat flux gage
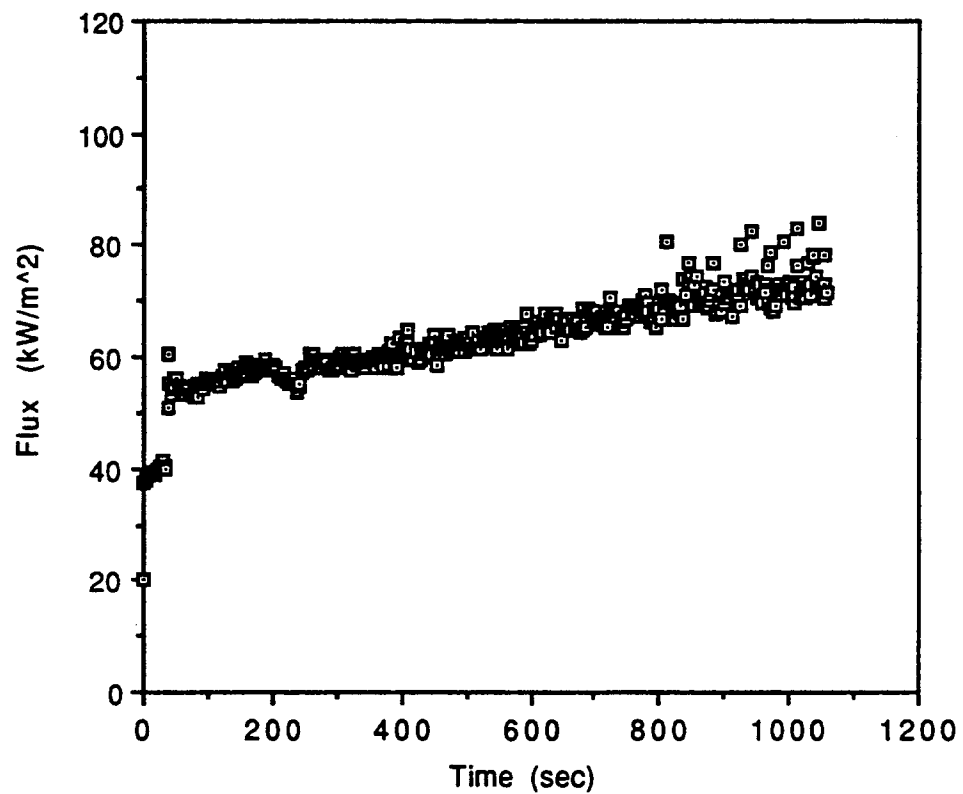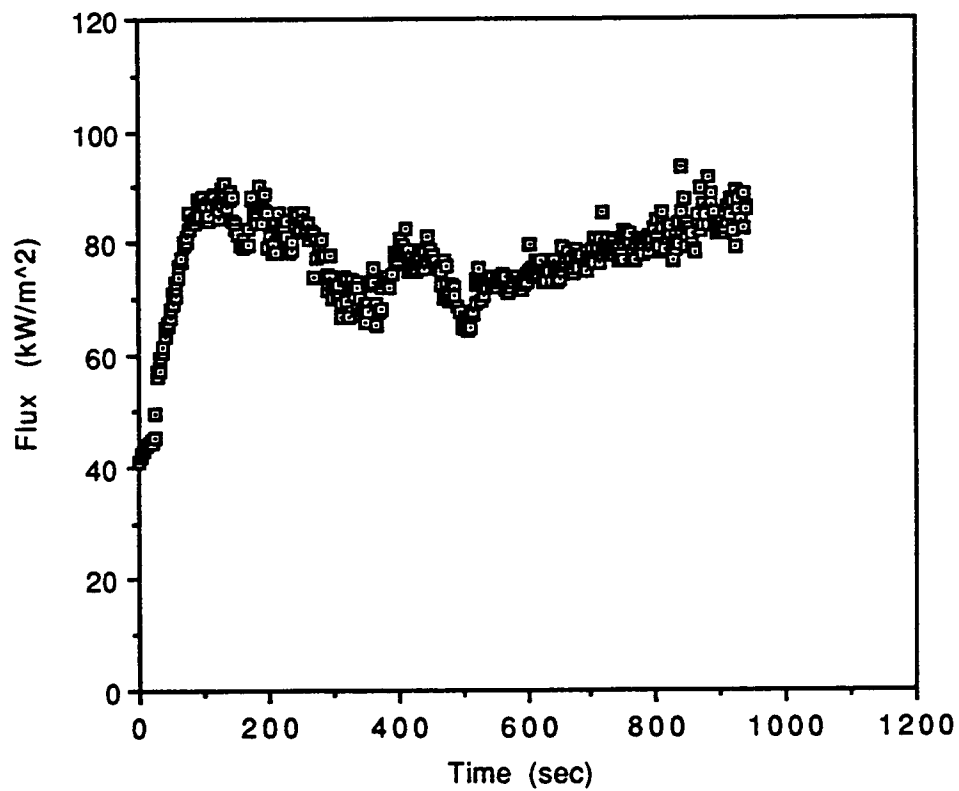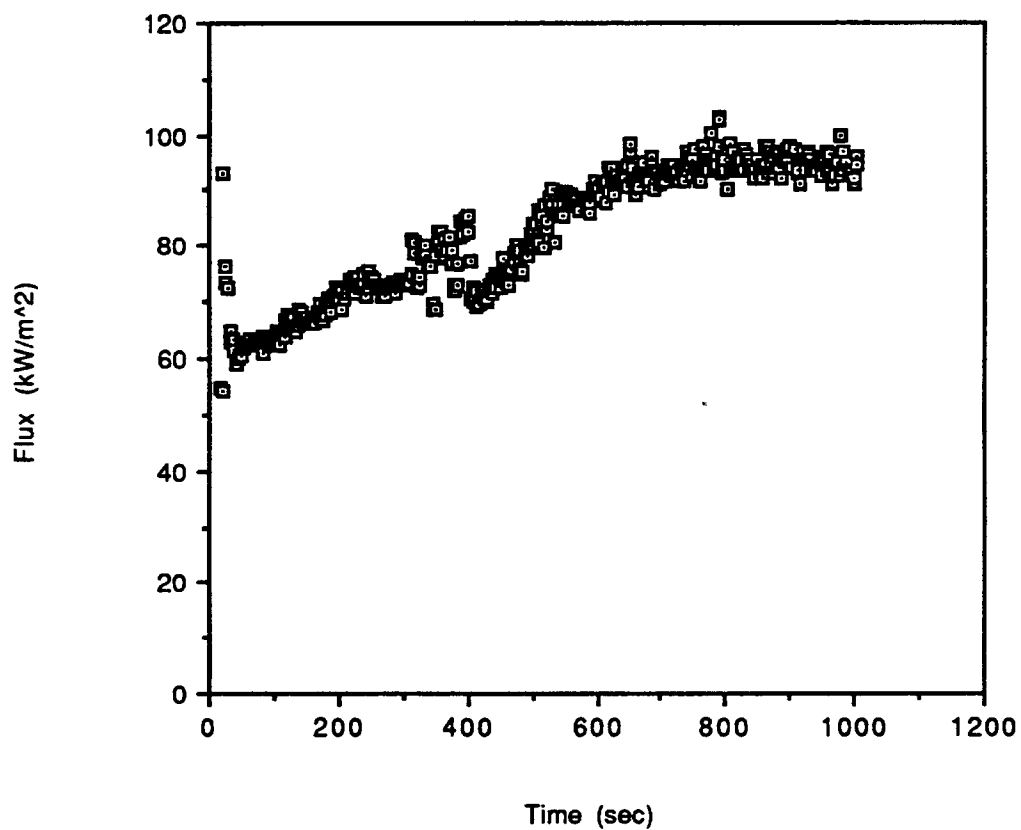for black PMMA exposed to a 33 kW/m² external flux

Figure D.4. Test number t9 - transient total incident flux measured by the heat flux gage
for black PMMA exposed to a 37 kW/m² external flux

Figure D.5. Test number t2 - transient total incident flux measured by the heat flux gage for black PMMA exposed to a 41 kW/m² external flux

Figure D.6. Test number t37 - transient total incident flux measured by the heat flux gage
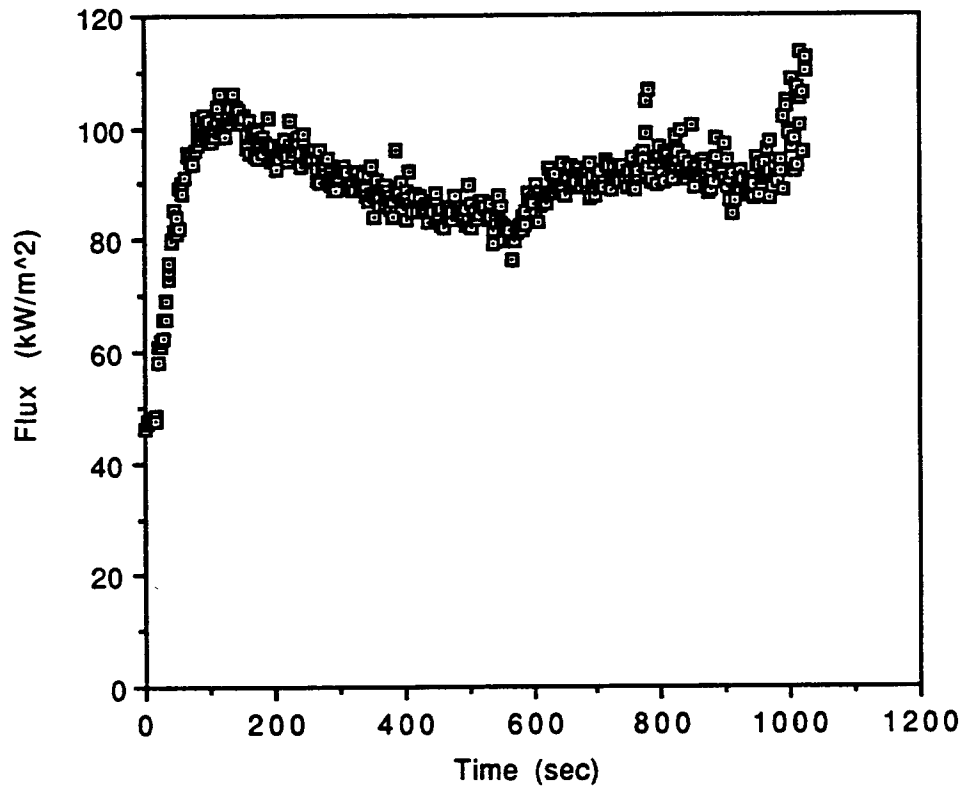for black PMMA exposed to a 50 kW/m² external flux

Figure D.7. Test number t3 - transient total incident flux measured by the heat flux gage for black PMMA exposed to a 52 kW/m² external flux
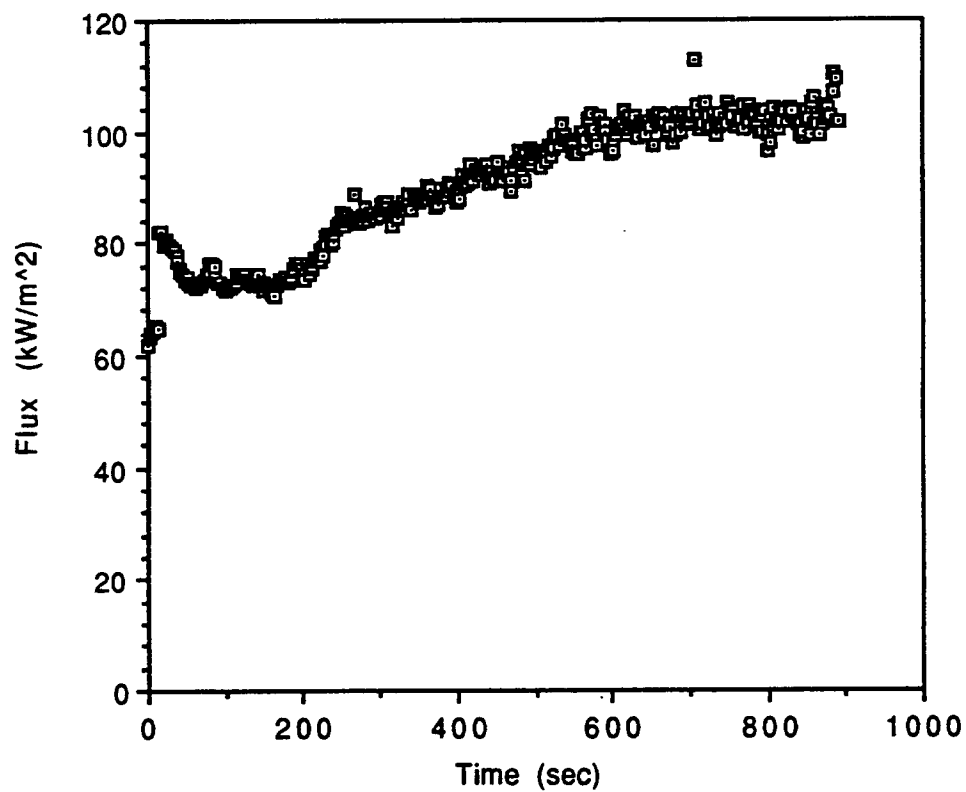
Figure D.8. Test number t10 - transient total incident flux measured by the heat flux gage
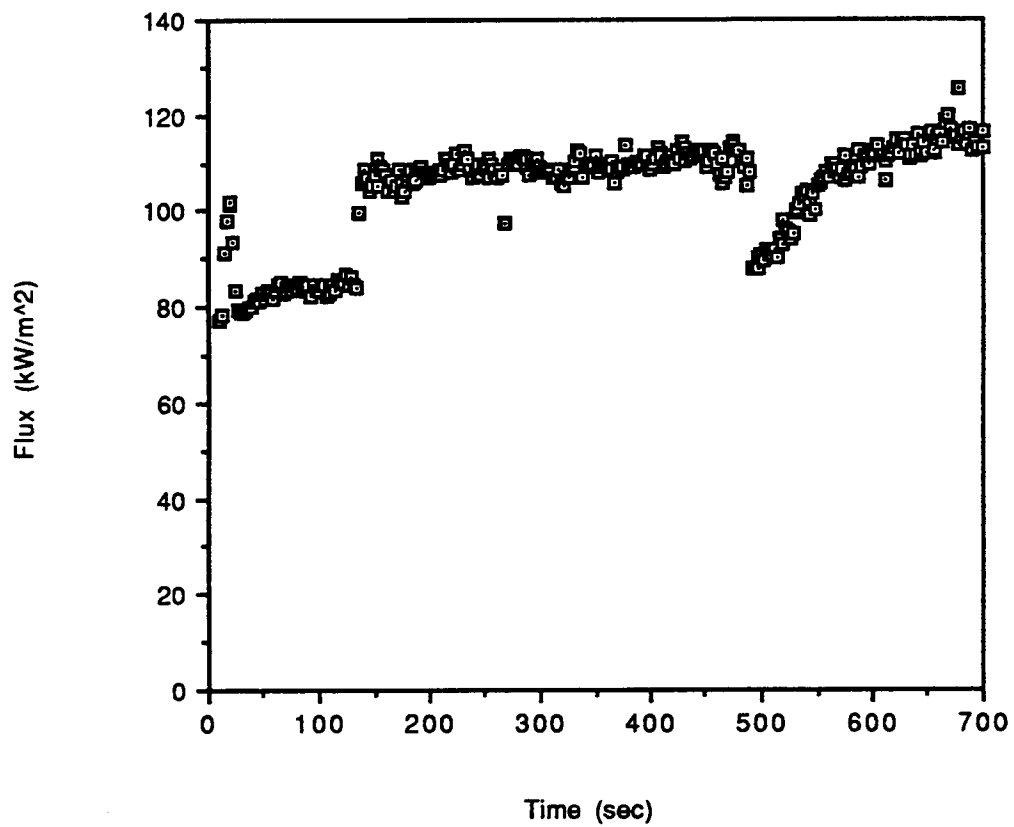for black PMMA exposed to a 63 kW/m² external flux

Figure D.9. Test number t44 - transient total incident flux measured by the heat flux gage for black PMMA exposed to a 75 kW/m² external flux

APPENDIX E

SIMULATED SAMPLE
INCIDENT HEAT FLUX

Test Number	External Flux (kW/m²)	H.R.R. (kW)	Incident Flux (kW/m²)
t12	49.8	2.0	79.6
t13	50.1	3.0	76.4
t14	50.2	4.0	75.1
t15	50.6	6.0	76.1

Table E.1. Simulated sample total incident heat flux as measured by the heat flux gage. Sensor is flush with the sample surface

Test Number	External Flux (kW/m²)	H.R.R. (kW)	Incident Flux (kW/m²)
t16	50.2	3.0	91.0
t17	50.3	4.0	95.1
t18	50.2	6.0	93.5
t19	50.1	7.0	91.5

Table E.2. Simulated sample total incident heat flux as measured by the heat flux gage. Sensor is 1/2 inch above the sample surface
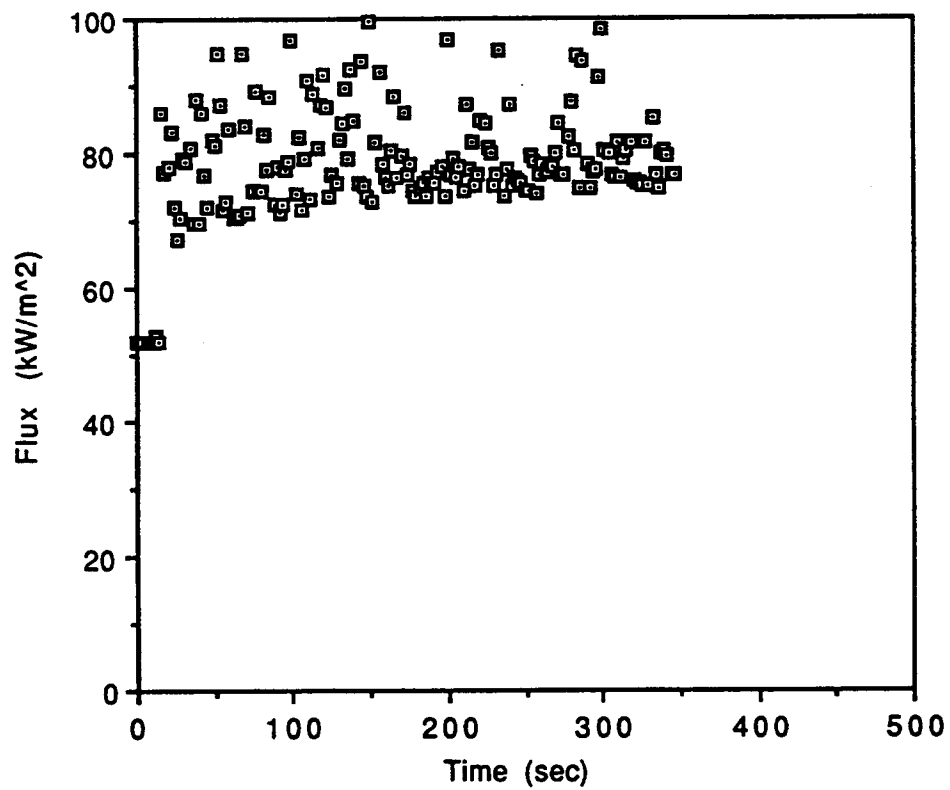
Figure E.1. Test number t12 - transient total incident flux for the methane burner with a 2.0 kW heat release rate exposed to a 50 kW/m² external flux.
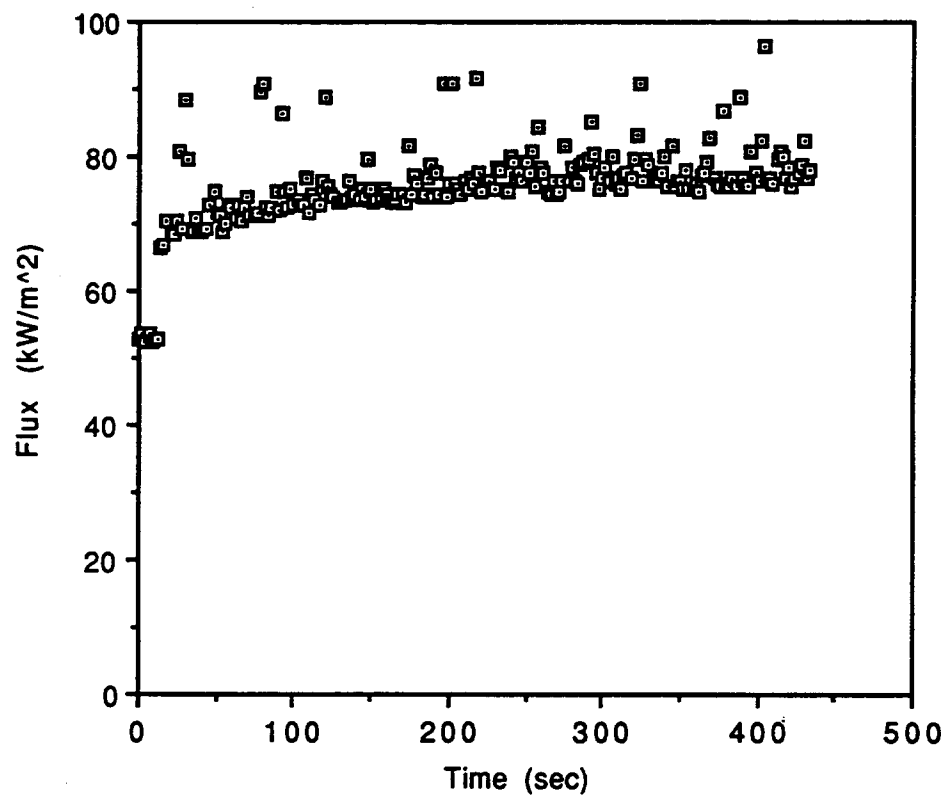
Figure E.2. Test number t13 - transient total incident flux for the methane burner with a 3.0 kW heat release rate exposed to a 50 kW/m² external flux.
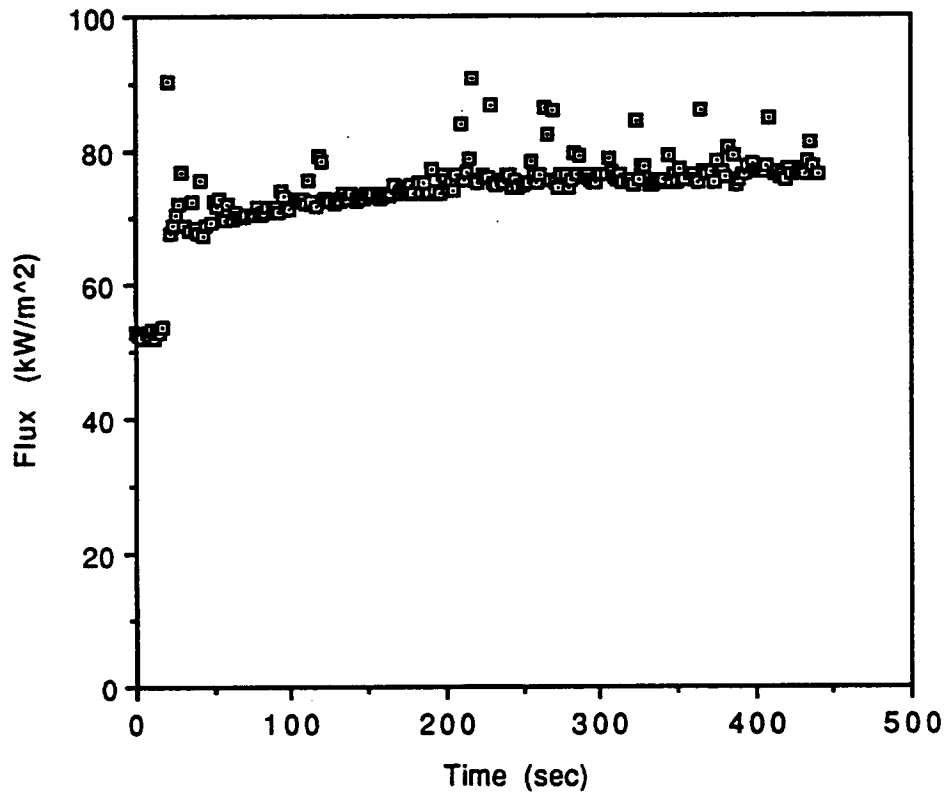
Figure E.3. Test number t14 - transient total incident flux for the methane burner with a 4.0 kW heat release rate exposed to a 50 kW/m² external flux.
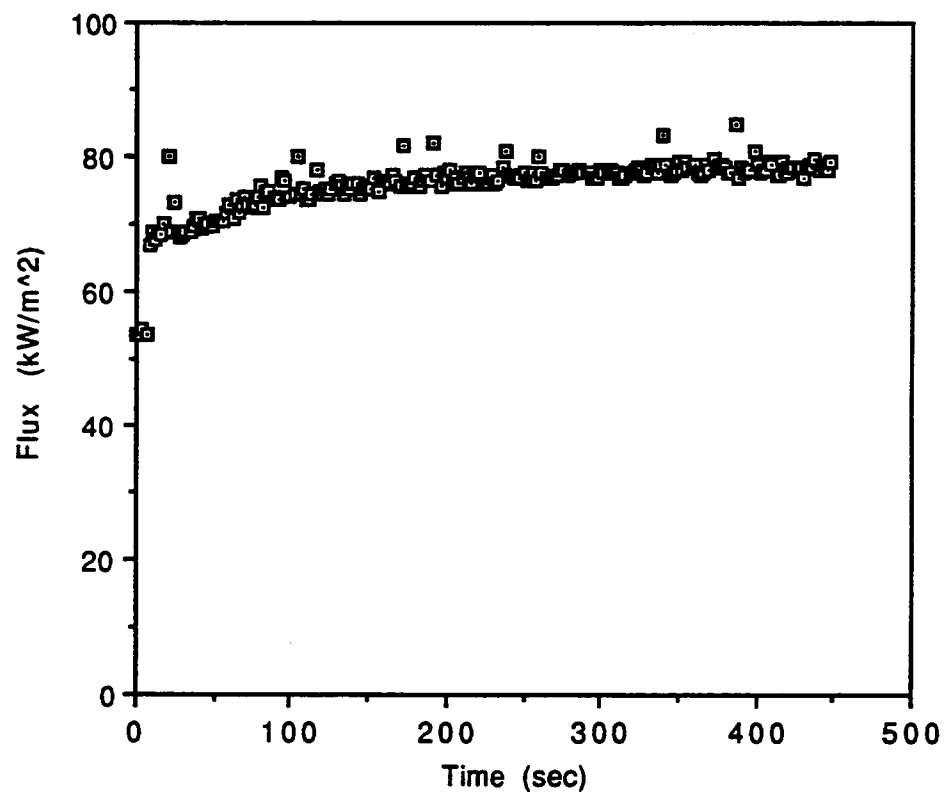
Figure E.4. Test number t15 - transient total incident flux for the methane burner with a 6.0 kW heat release rate exposed to a 50 kW/m² external flux.

Figure E.5. Test number t16 - transient total incident flux for the methane burner with a
3.0 kW heat release rate exposed to a 50 kW/m² external flux. The sensor
is 1/2 inch above the sample surface.

Figure E.6. Test number t17 - transient total incident flux for the methane burner with a 4.0 kW heat release rate exposed to a 50 kW/m² external flux. The sensor is 1/2 inch above the sample surface.

Figure E.7. Test number t18 - transient total incident flux for the methane burner with a 6.0 kW heat release rate exposed to a 50 kW/m² external flux. The sensor is 1/2 inch above the sample surface.
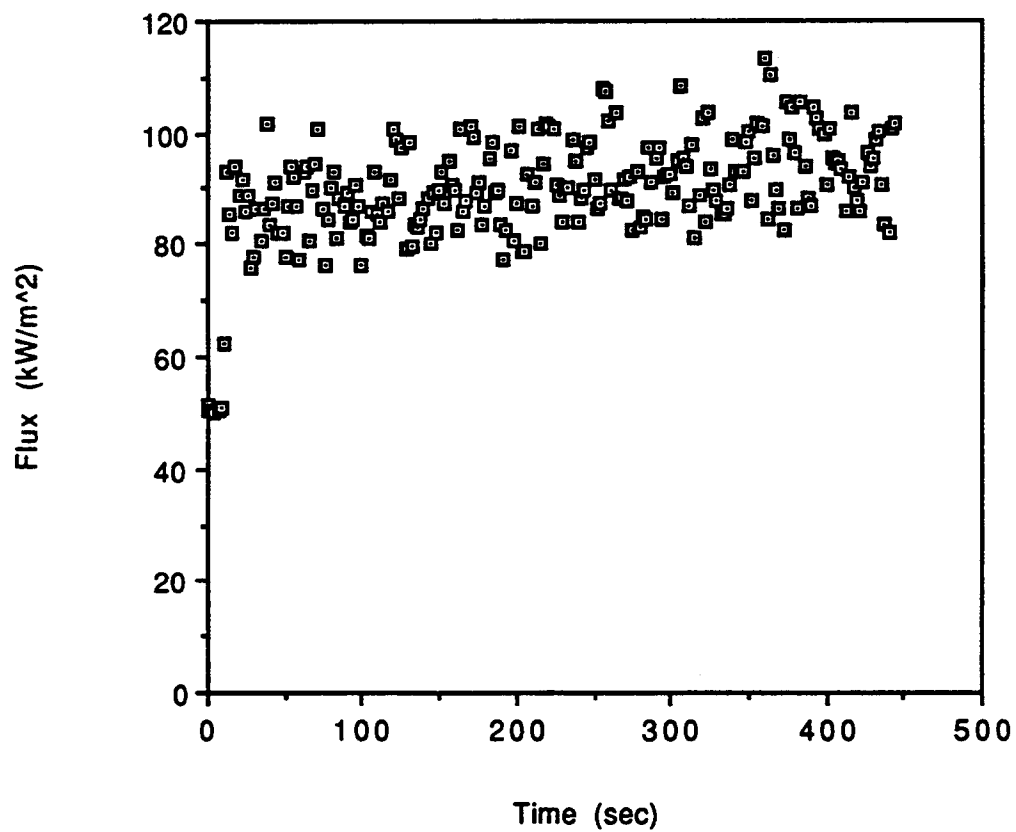
Figure E.8. Test number t19 - transient total incident flux for the methane burner with a
7.0 kW heat release rate exposed to a 50 kW/m^2 external flux. The sensor
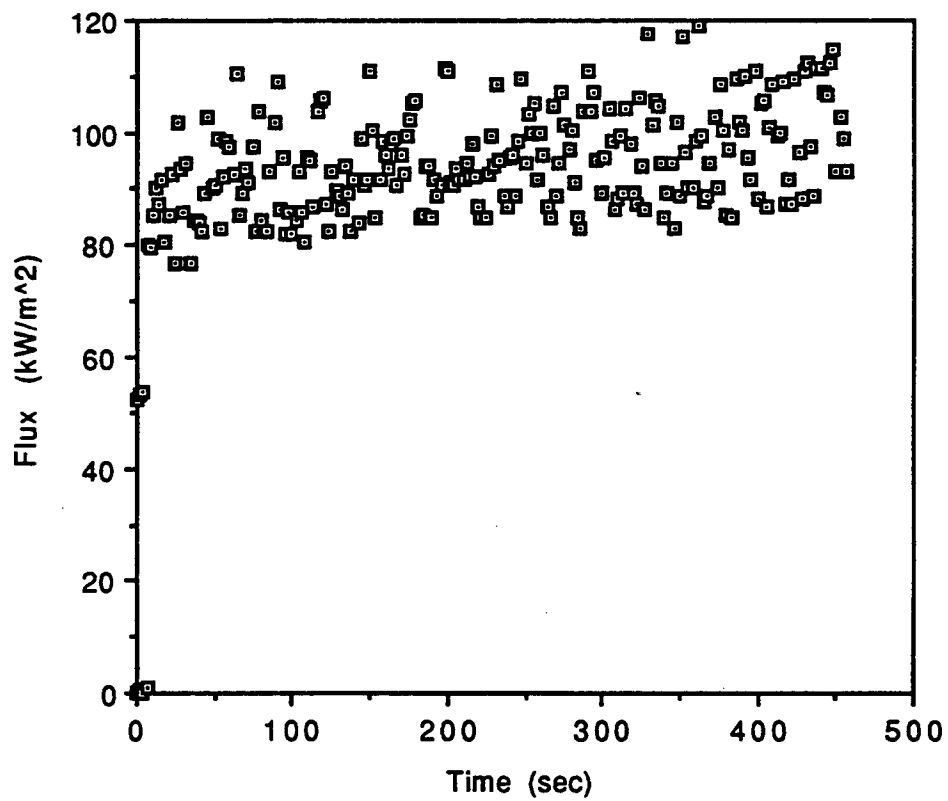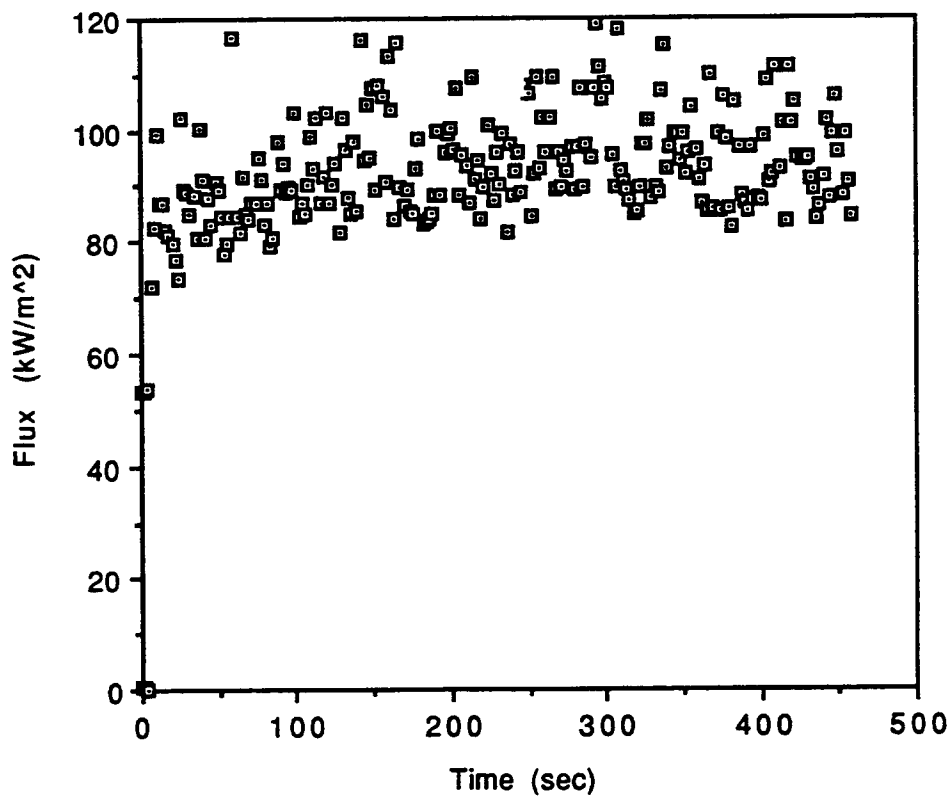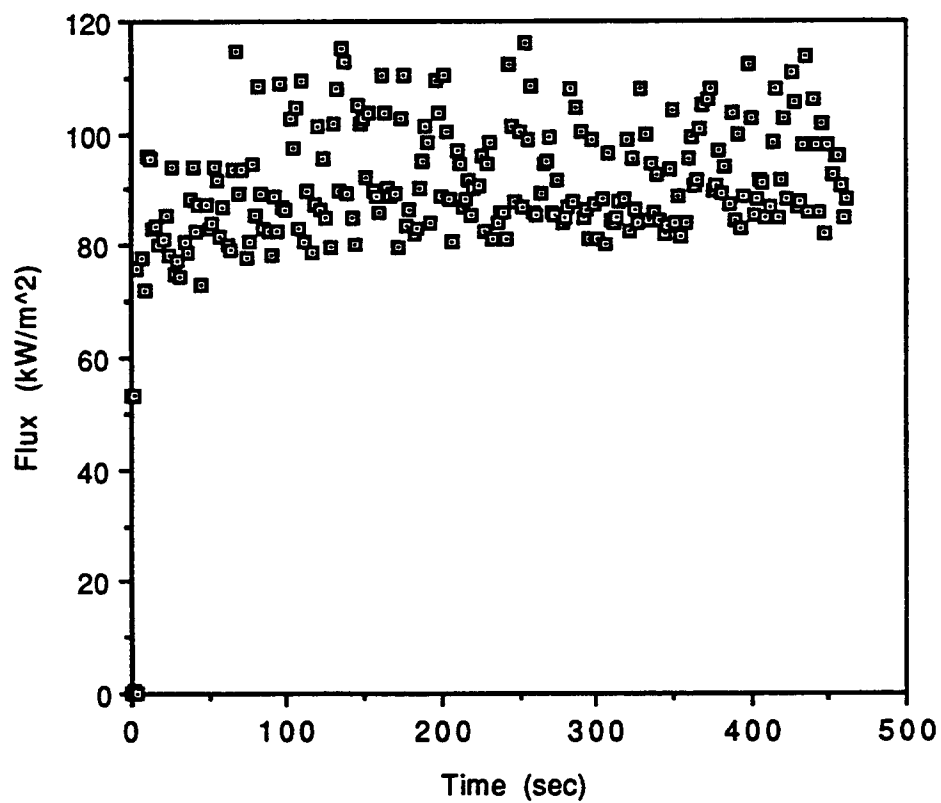is 1/2 inch above the sample surface.

APPENDIX F

SUMMARY TEST REPORT

Cone Calorimeter

Test Ref: T5920

Test Date: 08-09-1993
Date Received: 08-09-1993

DETAILS OF MATERIAL TESTED

Sponsor : National Institute of Standards & Technology

Material: PMMA

DETAILS OF TEST PROCEDURE USED

Heat Flux	: 25.1 kW/m²	Nominal Flow	: 24.0 l/s
Orifice Constant	: 0.044311	Heat per Unit Mole	: 12.98000 kJ/gO2
Heater Orientation	: Horizontal	Spark Ignitor Used	: Y
Grid Used	: N	Frame Used	: N

Conditioning : 50.0 RH @ 23.0°C
Specimen Thickness: 0.002540m

Test Conditions : 50.0 RH @ 0.0°C
Specimen Area : 0.010000 m²

TEST RESULTS

Initial Mass	: 298.9 g	Time of Peak RHR	: 1,075 s
Final Mass	: 0.0 g	Peak RHR	: 489.2 kW/m²
Mass Lost	: 30.01 kg/m²	Peak Mass Loss	: 20.14 g/s*m²
Ignition Time	: 132 s	Peak Extinction Area:	196.72 m²/kg
Flameout Time	: 1,926 s	Total Heat Released :	718.78 MJ/m²

Summary Data From Ignition

		Test Mean	60S	180S	300s
Heat Release	kW/m²	401.56	337.18	372.15	386.27
Mass Loss Rate	g/s*m²	18.47	13.73	15.44	16.07
Heat of Combustion	MJ/kg	23.95	24.56	24.11	24.03
Specific Ext. Area	m²/kg	111.57	101.19	113.16	116.47
Carbon Dioxide	kg/kg	2.53247	2.75183	2.58532	2.56514
Carbon Monoxide	kg/kg	0.00861	0.00615	0.00794	0.00842

OBSERVATIONS AND COMMENTS

Flaming out time 32 minute 7 second/1926 seconds. Cardboard
glued to side of PMMA--soot collected--spark ignited used
TUH is off--

Tested by : Lee, Jack
Officer   : Ohlemiller, Tom Dr.

109

T5920 PMMA   25mm   25 kW/m2

Cone Calorimeter

Test Ref: T5921

Test Date: 08-09-1993
Date Received: 08-09-1993

DETAILS OF MATERIAL TESTED

Sponsor : National Institute of Standards & Technology

Material: PMMA

DETAILS OF TEST PROCEDURE USED

Heat Flux	: 50.0 kW/m^2	Nominal Flow	: 24.0 l/s
Orifice Constant	: 0.044311	Heat per Unit Mole	: 12.98000 kJ/gO2
Heater Orientation	: Horizontal	Spark Ignitor Used	: Y
Grid Used	: N	Frame Used	: N

Conditioning : 50.0 RH @ 23.0°C
Specimen Thickness: 0.002540m

Test Conditions : 50.0 RH @ 0.0°C
Specimen Area : 0.010000 m^2

TEST RESULTS

Initial Mass	: 295.7 g	Time of Peak RHR	: 585 s
Final Mass	: 0.0 g	Peak RHR	: 746.3 kW/m^2
Mass Lost	: 29.73 kg/m^2	Peak Mass Loss	: 30.05 g/s*m^2
Ignition Time	: 29 s	Peak Extinction Area:	155.98 m^2/kg
Flameout Time	: 1,152 s	Total Heat Released :	716.02 MJ/m^2

Summary Data From Ignition

		Test Mean	60S	180S	300s
Heat Release	kW/m^2	642.21	530.53	583.08	605.51
Mass Loss Rate	g/s*m^2	27.89	20.35	23.47	24.65
Heat of Combustion	MJ/kg	24.08	26.07	24.85	24.57
Specific Ext. Area	m^2/kg	119.44	113.12	125.42	124.73
Carbon Dioxide	kg/kg	2.54311	2.90185	2.69888	2.64951
Carbon Monoxide	kg/kg	0.00761	0.00526	0.00729	0.00756

OBSERVATIONS AND COMMENTS

Flaming out time 19 minute 13 second/1152 seconds. Cardboard glued on side of PMMA. spark ignited used with pan holder and kao wool. TUH is off--Soot collected.

Tested by : Lee, Jack
Officer : Ohlemiller, Tom Dr.

T5921 PMMA 25mm 50 kW/m2

Heat release rate
Effective Heat of Combustion

Smoke specific extinction area in exhaust
- - Rate of Mass Loss

112
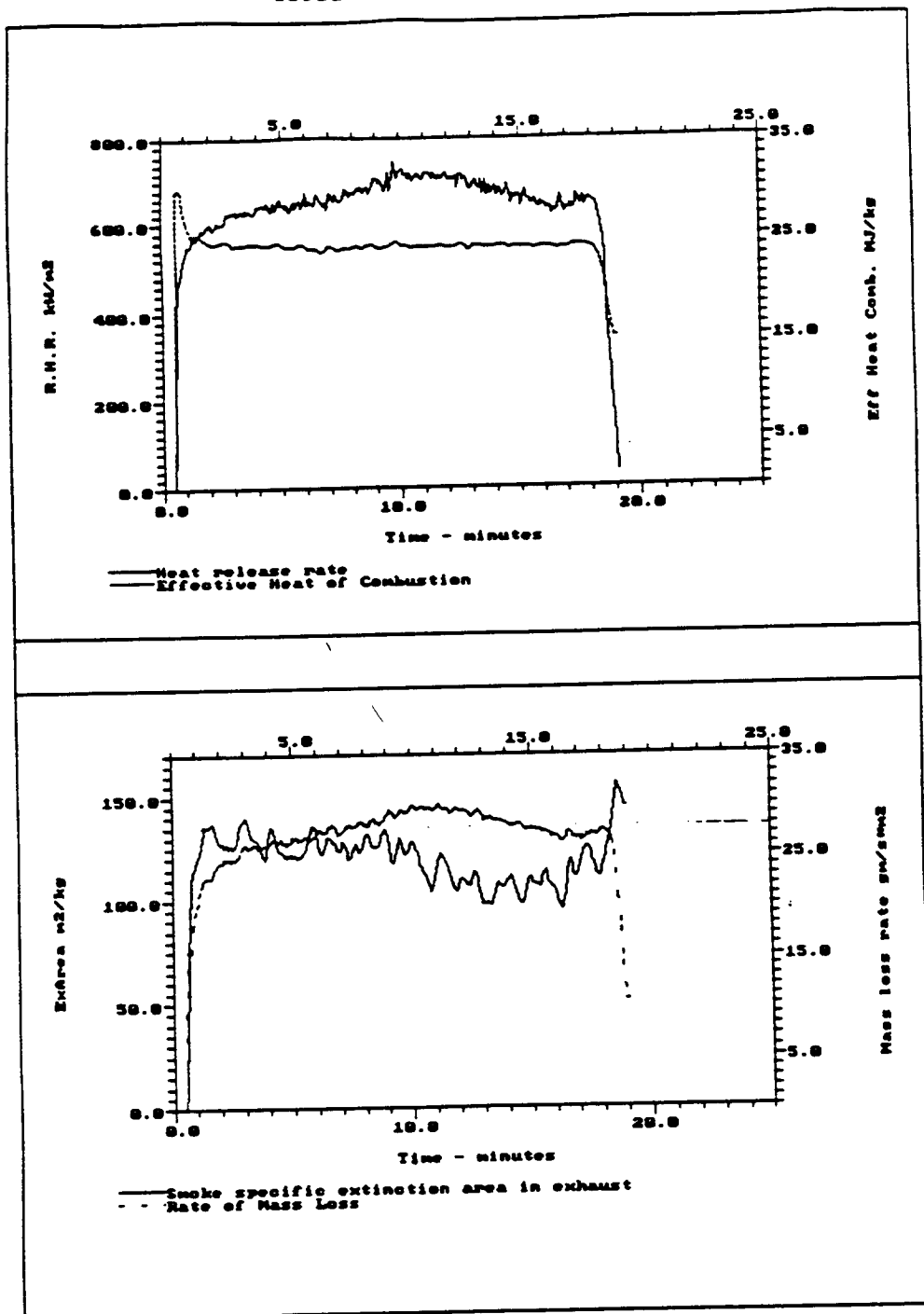
Cone Calorimeter

Test Ref: T5922

Test Date: 08-09-1993
Date Received: 08-09-1993

DETAILS OF MATERIAL TESTED

Sponsor : National Institute of Standards & Technology

Material: PMMA

DETAILS OF TEST PROCEDURE USED

Heat Flux	: 75.0 kW/m²	Nominal Flow	: 24.0 l/s
Orifice Constant	: 0.044311	Heat per Unit Mole	: 12.98000 kJ/gO2
Heater Orientation	: Horizontal	Spark Ignitor Used	: Y
Grid Used	: N	Frame Used	: N

Conditioning : 50.0 RH @ 23.0°C   Test Conditions : 50.0 RH @ 0.0°C
Specimen Thickness: 0.002540m   Specimen Area : 0.010000 m²

TEST RESULTS

Initial Mass	: 295.9 g	Time of Peak RHR	: 835 s
Final Mass	: 0.0 g	Peak RHR	: 989.1 kW/m²
Mass Lost	: 29.69 kg/m²	Peak Mass Loss	: 42.17 g/s*m²
Ignition Time	: 17 s	Peak Extinction Area:	197.02 m²/kg
Flameout Time	: 916 s	Total Heat Released :	710.99 MJ/m²

Summary Data From Ignition

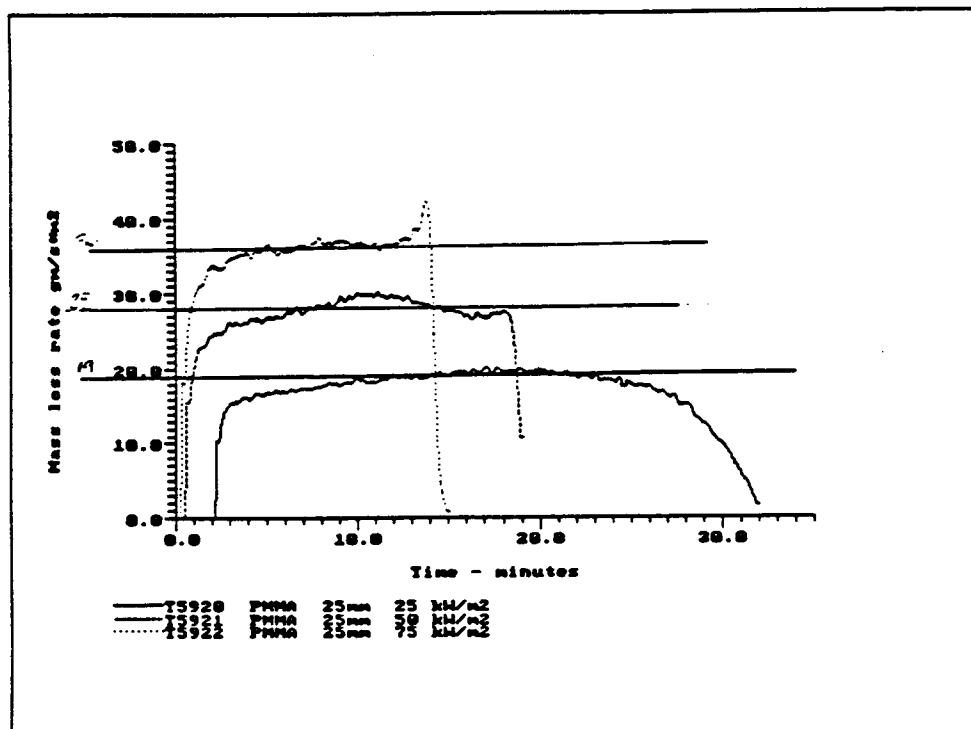|		Test Mean	60S	180S	300s
Heat Release	kW/m²	794.43	627.27	746.50	786.14
Mass Loss Rate	g/s*m²	35.93	26.43	31.05	32.84
Heat of Combustion	MJ/kg	23.95	23.73	24.04	23.94
Specific Ext. Area	m²/kg	121.08	123.24	130.57	129.51
Carbon Dioxide	kg/kg	2.53722	2.92647	2.67781	2.61532
Carbon Monoxide	kg/kg	0.00816	0.00568	0.00765	0.00803

OBSERVATIONS AND COMMENTS

    Flaming out time 15 minute 17 second/916 seconds. Cardboard glued to side of PMMA. Spark ignited used with pan holder. TUH is off--soot collected--
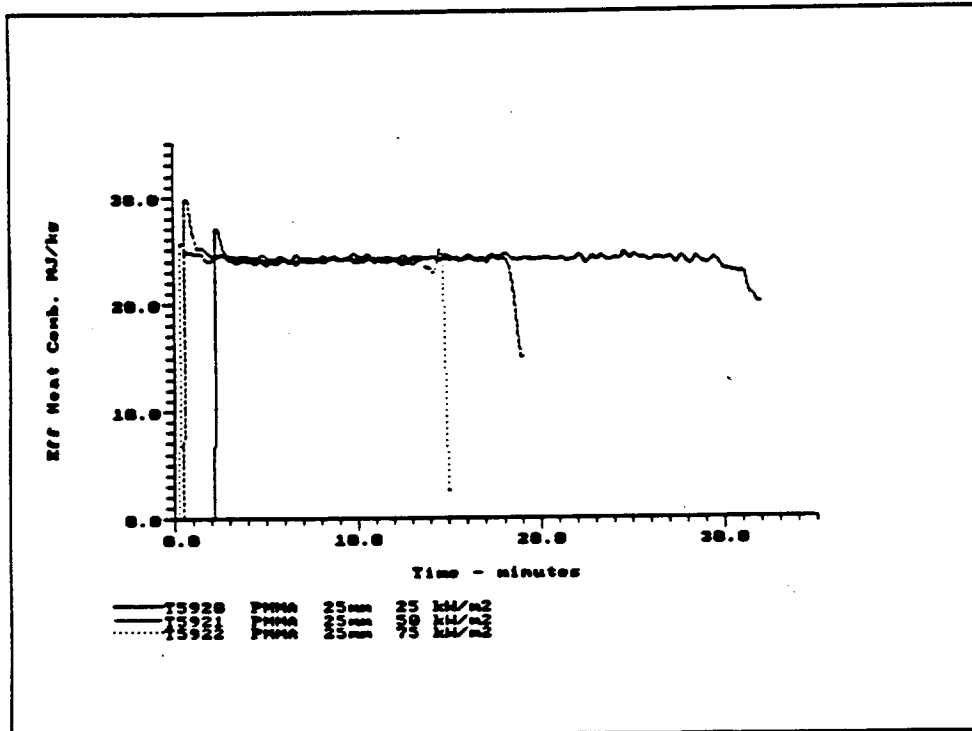
Tested by : Lee, Jack
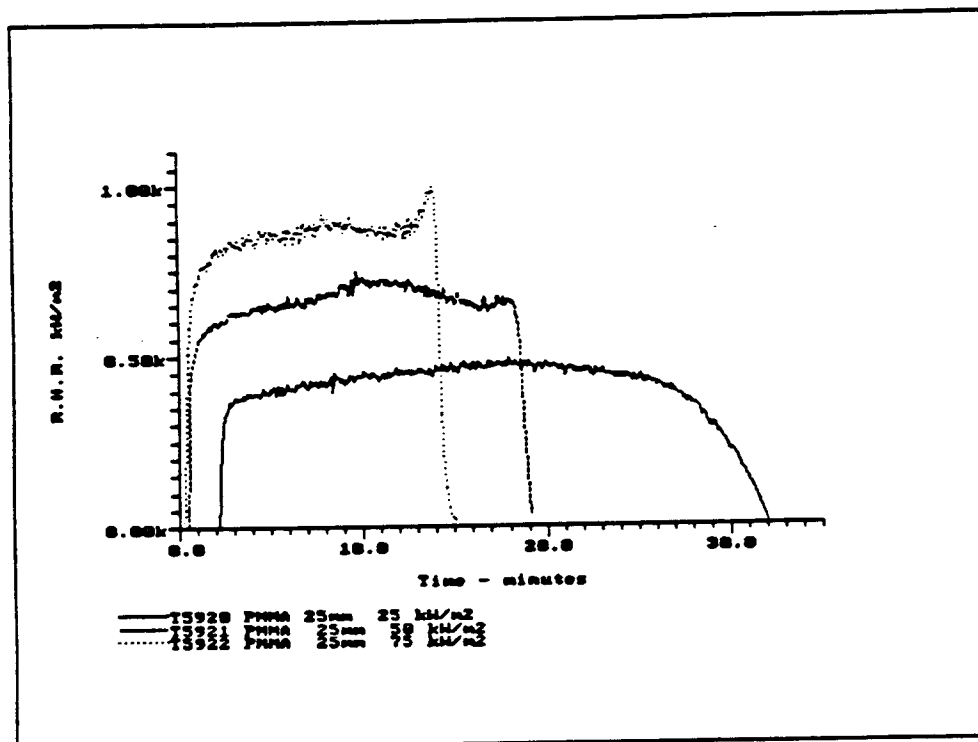**Officer : Ohlemiller, Tom Dr.**

T5922   PMMA   25mm   75 kW/m2

Heat release rate
Effective Heat of Combustion

Smoke specific extinction area in exhaust
Rate of Mass Loss

114

PMMA   25mm   25-50-75 kW/m2

PMMA   25mm   25-50-75 kW/m2

PMMA 25mm 25-50-75 kW/m2

NIST-114	**U.S. DEPARTMENT OF COMMERCE**	(ERB USE ONLY)	
(REV. 6-93)	NATIONAL INSTITUTE OF STANDARDS AND TECHNOLOGY	ERB CONTROL NUMBER	DIVISION
ADMAN 4.09			
	MANUSCRIPT REVIEW AND APPROVAL	PUBLICATION REPORT NUMBER	CATEGORY CODE
		NIST-GCR-95-664	

INSTRUCTIONS: ATTACH ORIGINAL OF THIS FORM TO ONE (1) COPY OF MANUSCRIPT AND SEND TO THE SECRETARY, APPROPRIATE EDITORIAL REVIEW BOARD	PUBLICATION DATE	NUMBER PRINTED PAGES
	December 1994	

TITLE AND SUBTITLE (CITE IN FULL)

Burning Rate and Flame Heat Flux for PMMA in the Cone Calorimeter

CONTRACT OR GRANT NUMBER	TYPE OF REPORT AND/OR PERIOD COVERED
Grant No. 60NA2D1266	Thesis May 1994

AUTHOR(S) (LAST NAME, FIRST INITIAL, SECOND INITIAL)	PERFORMING ORGANIZATION (CHECK (X) ONE BOX)
Brian T. Rhodes University of Maryland College Park, MD 20742	☐ NIST/GAITHERSBURG ☐ NIST/BOULDER ☐ JILA/BOULDER

LABORATORY AND DIVISION NAMES (FIRST NIST AUTHOR ONLY)

NIST/BFRL/Fire Science Division/Materials Fire Research Group

SPONSORING ORGANIZATION NAME AND COMPLETE ADDRESS (STREET, CITY, STATE, ZIP)

U.S. Department of Commerce
National Institute of Standards and Technology
Gaithersburg, MD 20899

PROPOSED FOR NIST PUBLICATION

☐ JOURNAL OF RESEARCH (NIST JRES)	☐ MONOGRAPH (NIST MN)	☐ LETTER CIRCULAR
☐ J. PHYS. & CHEM. REF. DATA (JPCRD)	☐ NATL. STD. REF. DATA SERIES (NIST NSRDS)	☐ BUILDING SCIENCE SERIES
☐ HANDBOOK (NIST HB)	☐ FEDERAL INF. PROCESS. STDS. (NIST FIPS)	☐ PRODUCT STANDARDS
☐ SPECIAL PUBLICATION (NIST SP)	☐ LIST OF PUBLICATIONS (NIST LP)	☐ OTHER _____
☐ TECHNICAL NOTE (NIST TN)	☐ NIST INTERAGENCY/INTERNAL REPORT (NISTIR)	

PROPOSED FOR NON-NIST PUBLICATION (CITE FULLY)	☐ U.S.	☐ FOREIGN	PUBLISHING MEDIUM
			☐ PAPER ☐ CD-ROM ☐ DISKETTE (SPECIFY) ☐ OTHER (SPECIFY)

SUPPLEMENTARY NOTES

ABSTRACT (A 2000-CHARACTER OR LESS FACTUAL SUMMARY OF MOST SIGNIFICANT INFORMATION. IF DOCUMENT INCLUDES A SIGNIFICANT BIBLIOGRAPHY OR LITERATURE SURVEY, CITE IT HERE. SPELL OUT ACRONYMS ON FIRST REFERENCE.) (CONTINUE ON SEPARATE PAGE, IF NECESSARY.)

Ignition and burning rate data are developed for thick (25 mm.) black Polycast PMMA in a Cone Calorimeter heating assembly. The objective is to establish a testing protocol that will lead to the prediction of ignition and burning rate from Cone data. This is done for a thermoplastic like PMMA. For black PMMA, ignition temperatures of 250 to 350°C and vaporization temperatures of approximately 325 to 380°C were measured over irradiance levels of 15 to 65 kW/m². The incident flame heat flux, for irradiation levels of 0 to 75kW/m², is found to be approximately 37 kW/m2 for black PMMA. Its constancy is shown due to the geometry of the Cone flame. Also, this flame is shown to be nearly transparent for Cone irradiance (>90%). The heat of gasification of the black PMMA used is found to be approximately 2.8 kJ/g; higher than other values reported for PMMA. This is believed to be due to differences in molecular structure or pigmentation effects and the types of PMMA tested. A burning rate model is demonstrated to yield good accuracy (>80%) in comparison to measured transient values.

KEY WORDS (MAXIMUM OF 9; 28 CHARACTERS AND SPACES EACH; SEPARATE WITH SEMICOLONS; ALPHABETIC ORDER; CAPITALIZE ONLY PROPER NAMES)

burning rate; cone calorimeters; flame heat flux; heat flux; ignition temperature; ignition time; polymethyl methacrylate

AVAILABILITY	NOTE TO AUTHOR(S): IF YOU DO NOT WISH THIS MANUSCRIPT ANNOUNCED BEFORE PUBLICATION, PLEASE CHECK HERE. ☐
☒ UNLIMITED ☐ FOR OFFICIAL DISTRIBUTION - DO NOT RELEASE TO NTIS ☐ ORDER FROM SUPERINTENDENT OF DOCUMENTS, U.S. GPO, WASHINGTON, DC 20402 ☒ ORDER FROM NTIS, SPRINGFIELD, VA 22161	

WORDPERFECT